METHOD AND MATERIAL DEVELOPMENT FOR THE DETECTION AND ANALYSIS OF CANCER CELLS

By

COLIN D. MEDLEY

A DISSERTATION PRESENTED TO THE GRADUATE SCHOOL
OF THE UNIVERSITY OF FLORIDA IN PARTIAL FULFILLMENT
OF THE REQUIREMENTS FOR THE DEGREE OF
DOCTOR OF PHILOSOPHY

UNIVERSITY OF FLORIDA

2007

To my family, Pingping and Nini

ACKNOWLEDGMENTS

I thank Dr. Weihong Tan for his support and encouragement during my studies at the University of Florida. I also thank the many past and current members of the Tan research for their support and encouragement.

I appreciate Dr. Arup Sen for his insightful discussions and assistance with my intracellular projects especially in regard to molecular beacon synthesis. I thank Dr. Richard Rogers for his expertise in cancer genomics which provided great guidance and assistance to my work and Dr. Nico Omenetto for his interest and fruitful discussions regarding the SERS project. In particular, I thank Joshua Smith for his continuing insight, support, and hard work in making many of our collaborative projects a success. I also thank Tim Drake for his assistance and guidance in learning about molecular beacons and intracellular analysis and Hui Lin for her DNA synthesis mastery.

None of my success would have been possible without the unconditional support and love of my family. Particularly, the love and support of my wife Pingping and my daughter Leilani made my achievements possible. I also sincerely thank my parents Donnell and Dianne Medley, my sisters Colleen and Shauna, Aunt Maria, Grandma Jo and all of our extended family whose lover and prayers made this work possible. I owe a debt to all of them for their support.

TABLE OF CONTENTS

page

ACKNOWLEDGMENTS 4

LIST OF TABLES 9

LIST OF FIGURES 10

ABSTRACT 13

CHAPTER

1 INTRODUCTION 15

Challenges in Cancer Detection 15
Nanomaterials and Nanotechnology 16
Gold Nanoparticles 17
Magnetic Nanoparticles 19
Fluorescent Nanoparticles 22
Semiconductor nanocrystals 24
Encapsulated nanoparticles 26
Molecules for Bio-Recognition 29
Measuring and Analyzing Gene Expression 33
Traditional Methods of Gene Expression Analysis 33
Molecular Beacons 35
Intracellular Applications of Molecular Beacons 37
Intracellular Ion Levels 41

2 DNA AND NANOPARTICLE SYNTHESIS 43

DNA Synthesis 43
Nanoparticle Synthesis 48
Nanoparticle Bioconjugation to DNA 51
Silica Nanoparticles 51
Gold Nanoparticles 53
Conclusion 54

3 TWO-PARTICLE ASSAY FOR THE COLLECTION AND ENRICHMENT OF TARGETED CANCER CELLS 56

Introduction and Scheme 56
Methods and Materials 57
DNA Aptamer Synthesis. 57
Fluorescent Nanoparticle Synthesis 58
Magnetic Nanoparticle Synthesis 60
Cell Culture 61

Two Particle Assay Methodology 61
Fluorescence Imaging 62
Flow Cytometry 62
Plate Reader Measurements 62
Two-Particle Assay Proof of Concept 63
Characterization of the Two Particle Assay 65
Dye and Nanoparticle Fluorescent Intensity Comparison 65
Collection Efficiency 66
Enrichment Validation 67
Limit of Detection 68
Improving LOD with Multiple Aptamers 70
Separations from Complex Samples 71
Mixed Cell Sample Assays 71
Bone Marrow Samples 73
Whole Blood Sample Assays 74
Collection and Detection of Multiple Cancer Cells 75
Instrumental Validation 75
Single Cell Type Extractions 77
Multiple Cell Type Extraction Method 80
Mixed Cell Samples 81
Serum Samples 83
Small Cell Lung Cancer Cell Extractions 85
Conclusion 86

4 COLORIMETRIC ASSAY FOR DIRECT DETECTION OF CANCER CELLS 88

Introduction 88
Experimental Methods 89
DNA Aptamer Synthesis 89
Aptamer Conjugated Gold Nanoparticle Synthesis 90
Cells 90
Assay Protocol 91
Results and Discussion 91
Nanoparticle Size Effect 93
Assay Response 94

5 MOLECULAR BEACON DESIGN, DELIVERY, AND EVALUATION 100

Introduction 100
Methods and Materials 101
Equipment 101
Fluorescence Imaging 102
Plate Reader Experiments 102
Cell Culture 103
Fluorescent Probes 103
Molecular Beacon Design 104
Molecular Beacon Delivery 107

Electroporation 109
Reversible Permeabilization 111
Liposome Delivery 112
Viral Vector Delivery 114
Microinjection 116
Incubation 117
Delivery Method Conclusions 118
Ratiometric Analysis 119
In Vitro Testing of Molecular Beacons 121
Conclusions 122

6 STUDY OF CANCER CELLS THROUGH MULTIPLE GENE MONITORING 124

Introduction 124
Methods and Materials 125
Cell Culture 125
RNA Isolation and Northern Blot Analysis 125
Equipment 126
Fluorescence Imaging 126
Molecular Beacon Design for Multiple Gene Monitoring 127
Multiple Gene Monitoring 128
Monitoring Stimulated Gene Expression 130
Gene Expression Pattern Comparison 134
Conclusions 136

7 STUDY OF CANCER CELLS BY MONITORING MULTIPLE ANALYTES 139

Methods and Materials 139
Fluorescent Probes 139
Cells 140
Protein Isolation and Western Analysis 140
Equipment 141
Fluorescence Imaging 141
Data Analysis 142
Simultaneous Detection of Ca^{2+} and Gene Expression Inside Single Cells 142
Studying the Effects of Trichostatin A on Ca^{2+} Levels and Gene Expression 145

8 INTRACELLULAR APPLICATIONS OF LOCKED NUCLEIC ACID MOLECULAR BEACONS 153

Introduction 153
Methods and Materials 155
Equipment 155
Molecular Beacon Synthesis 156
Hybridization Study 157
DNase I Sensitivity 157

Cell Culture 157
Fluorescence Imaging 157
Results and Discussion 158
LNA MB Optimization 161
Solution Experiments 161
Neuron Imaging 164

LIST OF REFERENCES 167

BIOGRAPHICAL SKETCH 182

LIST OF TABLES

Table page

3-1 Single cell type extraction....79

3-2 Multiple cell type extraction....83

5-1 Molecular beacon sequences....104

LIST OF FIGURES

Figure		Page
1-1	Typical Jablonksi diagram illustrating the fluorescence process.	23
1-2	Cell-based aptamer selection (cell-SELEX)	32
2-1	DNA chemical synthesis three primary steps, Detritylation, Coupling, and Oxidation are repeated until the desired DNA sequence has been synthesized.	44
2-2	The coupling step in DNA synthesis depicting the activiation of the phosphoramidite derivative and the subsequent coupling of the two nucleotides.	46
2-3	Typical chromatograph of a molecular beacon purification using reverse phase HPLC using absorbance for detection.	48
2-4	TEM images of iron oxide nanoparticle and silica coated iron oxide nanoparticles.	51
3-1	Two-particle assay.	57
3-2	Fluorescence images of samples analyzed using the two-particle assay.	64
3-3	Fluorescence images of extracted samples after five minute incubation with different labels	66
3-4	Flow cytometric determination of magnetic nanoparticle collection and separation efficiencies between target and control cells.	67
3-5	Study of the effects of magnetic enrichment.	68
3-6	Limit of detection for the stepwise addition of the MNP and FNP.	69
3-7	Comparison of magnetic nanoparticle with multiple aptamer sequences conjugated to the surface.	71
3-8	Fluorescence images of mixed cell samples extractions.	72
3-9	Fluorescence images of cells extracted from bone marrow samples.	74
3-10	Confocal images of extractions from whole blood.	75
3-11	Plate reader measurements of multiple dyes to test spectral compatibility.	76
3-12	Fluorescence images of pure cell samples in buffer after magnetic extraction and washes.	78
3-13	Multiple extraction procedure of analyzing cell samples.	81

3-14 Fluorescence images of buffer extracted mixed cell samples using the multiple extraction procedure....82

3-15 Fluorescence images of target and control SCLC cells extracted....86

4-1 Plots depicting the absorption spectra obtained for various samples analyzed using ACGNPs. 92

4-2 Spectra of the different sizes of Aptamer Conjugated Gold Nanoparticles with target cells. 93

4-3 Images and spectra of cell samples analyzed with ACGNPS.. 95

4-4 Calibration curve and response of the ACGNPs in complex samples. 96

5-1 Comparison of the enhancements of molecular beacons with FAM/Dabcyl and higher quality fluorophore quencher pairs. 107

5-2 Fluorescence images and data plot of cells after electroporation in a 5μM DNA spiked medium. 110

5-3 Fluorescence images and data plot of cells using reversible permeabilization. 112

5-4 Fluorescence images and data plot of cells using a lipid based transfection reagent. 114

5-5 Fluorescence images and data plot of cells after incubation with FITC-streptavidin linked viral vectors. 115

5-6 Fluorescence images and data plot of cells microinjected with the fluorophore labeled DNA sequence. 117

5-7 Fluorescence images and data plot of cells incubated with the fluorophore labeled DNA. 118

5-8 Average intensities from the cells for each DNA delivery method tested. 119

5-9 Fluorescent intensities and ratiometric values over time for five cells injected with different amounts of fluorophore labeled DNA. 121

5-10 Signal enhancements in buffer solution for each MB utilized in the intracellular experiments. 122

6-1 Time elapsed fluorescent images of each MB inside of a single MDA-MB-231 cell. 129

6-2 Northern analysis of LPS-inducible MnSOD mRNA expression in MDA-MB-231 cells. 131

6-3 Ratiometric analysis of the real time monitoring of gene expression. 132

6-4 Histograms showing distribution of ratiometric responses for control and LPS induced MDA-MB-231 cells. 134

6-5 Plots showing the relationship between the relative β-actin mRNA expression and the relative MnSOD mRNA expression in both the LPS-induced and non-induced cells. 135

7-1 Time resolved fluorescence images and plots of cells with MBs and Fluo-4. 144

7-2 Calcium and MnSOD control experiments....146

7-3 Fluorescence images and plots showing the effect of TSA on cells.....148

7-4 Histograms showing the distribution of intensities from each probe in the basal cell group and the TSA exposed cell group.....149

7-5 Correlation plots comparing the levels of MnSOD to the control and Fluo-4 levels. 150

8-1 Locked Nucleic Acid bases.....155

8-2 Fluorescence image of cells injected with LNA MB.....159

8-3 Comparison of the LNA and DNA MBs with and without target inside of living cells. 159

8-4 Monitoring of the ratiometric values of the probes inside of cells depicting the degradation of the probes.....160

8-5 Hybridization rates of the different molecular beacon compositions.. 162

8-6 The response of the different MB compositions to the addition of DNase I. 164

8-7 Representative images for neurons injected with the negative control sequence and the B-tubulin sequence.....165

8-8 Fluorescence intensity versus time for each neuron injected with the alternating LNA/DNA molecular beacon. 166

Abstract of Dissertation Presented to the Graduate School
of the University of Florida in Partial Fulfillment of the
Requirements for the Degree of Doctor of Philosophy

METHOD AND MATERIAL DEVELOPMENT FOR THE DETECTION AND ANALYSIS OF CANCER CELLS

By

Colin D. Medley

August 2007

Chair: Weihong Tan
Major: Chemistry

One of the most important aspects to cancer treatment is the early and accurate diagnosis of the disease. Early diagnosis enables current treatments to much more effective and leads to greatly improved survival rates. In an effort to realize this, I developed two diagnostic assays based on aptamer conjugated nanoparticles. Aptamers are single stranded oligonucleotide chains that forms a three dimensional structure that can bind with high affinity and specificity to a targeted molecule. We developed a novel cell-based aptamer selection strategy called cell-SELEX to produce a group of aptamers for the specific recognition of individual cells without prior knowledge of the biomarkers on the cells. The cell-SELEX process uses whole cells as targets to select aptamers that can distinguish target from control cells. Once selected, the aptamer can be chemically synthesized and easily functionalized for bioconjugation to different nanomaterials, fluorophores, or therapeutic agents.

The first assay is based on two types of silica nanoparticles, one where a fluorescent dye has been doped inside the particle while the other has a magnetic nanoparticle doped inside the silica. The aptamers allow the nanoparticles to bind to the cell surface. After the application of a magnetic field, the magnetic nanoparticles and anything bound to them are immobilized and the

unbound materials can be washed away. This allows for the selective enrichment and detection of the target cells.

The second assay uses gold nanoparticles instead of silica-based nanoparticles. The gold nanoparticles are in close proximity and their surface plasmons can interact. The interaction results in a red shift of the absorption of the particles and an increase in the extinction coefficient of the particles. Using these properties of the gold nanoparticles with the selectivity and affinity of the aptamers results in colorimetric assay where a solution containing the target cells changes color.

However, detection is only one important criterion for cancer treatment. A better and more complete understanding of the disease at a biomolecular level is critical to developing more effective treatments. By microinjecting multiple molecular beacons with different fluorophores inside of single breast carcinoma cells and monitoring with advanced fluorescent microscopy, the expression of multiple genes can be simultaneously monitored inside of single living cells. The mRNA for B-actin, Manganese Superoxide Dismutase, and a control sequence were detected simultaneously using this method. Using ratiometric analysis as a basis for the measurements allows the different gene expression levels to be compared from cell to cell. Not only does this allow differentiation of individual mRNA expression levels between multiple single cells, but it also allows for mRNA expression trend analysis at the single cell level. This can be further coupled with *in vivo* ion monitoring experiments to allow a more complete understanding of cellular processes.

CHAPTER 1
INTRODUCTION

Challenges in Cancer Detection

Cancer is the second leading cause of death in the United States. Half of all men and one-third of all women in the US will develop cancer during their lifetimes. Today, millions of people are living with cancer or have had cancer. It is well accepted that the sooner a cancer is found, correctly diagnosed, and treated then the better the chances are for survival and remission of the disease. However except for skin cancer all other types of cancer manifest internally making detection and diagnosis difficult. There are currently several methods utilized for the diagnosis of cancer including magnetic resonance imaging, X-rays, genetic analysis,[1] biopsy,[2] and immunophenotyping.[3] Biopsy is typically used as a diagnostic method to histologically identify whether a previously detected tumor, lesion, or other abnormal tissue is cancerous. Magnetic resonance imaging is considered too costly to be effective for cancer screening purposes however it has been shown to be useful for staging cancers and deciding on treatment avenues.

Immunophenotypic analyses of leukemia cells use antibody probes to exploit the variation of specific surface antigens in order to differentiate malignant cells from normal cell lines. The limitation to this method is that antigens used for cell recognition are normally not exclusively expressed on any single cell type, dramatically influencing sensitivity, and resulting in false positive results. Due to of this, immunophenotypic analyses often require multiple antibody probes for accurate cell detection, increasing both the complexity and cost of the method.

Genetic analysis and PCR based methods have proven to be highly sensitive diagnostic techniques for cellular recognition,[1,4,5] but they are indirectly detecting cells by monitoring RNA expression, and require prolonged RNA isolation steps before analysis. In addition, the variable

sensitivity of PCR can limit its effectiveness as a diagnostic technique leading to false-negative results, particularly with occult tumor cells where low-level signals are expected. Immunophenotypic analyses are also time consuming and costly, and therefore, there is still a need to develop new technologies for rapid, economical cell recognition.

The work described herein will explore the use of nanomaterials and molecular probes to aid in the detection and analysis of cancer cells. In particular different types of nanoparticles with different characteristics will be utilized for the sensitive and selective detection of cancer cells. Two major directions will follow this course including the development of a sensitive and selective screening method for cancer from even very complex samples. The other direction will focus on developing a colorimetric method for cancer cell detection for use in point of care diagnostics for circumstances where sending a sample to a laboratory would not be practical or ideal. However detection of the cancerous cells is only one aspect to improving the prognosis for cancer. More attention has to be paid to the underlying biology behind cancer and developing methods that would allow identifying the optimal treatment paths through the study of gene expression and other analytes on a cellular level.

Nanomaterials and Nanotechnology

To realize rapid, sensitive, and cost effective methods for the early detection of cancer many researchers have focused on the use of nanotechnology. Nanoparticles can be comprised of many different materials such as silica,[6] gold,[7] carbon,[8] or silver.[9] Silica nanoparticles in particular offer many advantages since they can be doped with a variety of materials such as fluorophores,[10] semiconductor nanocrystals,[11] or magnetic materials.[12] Each material has it's own characteristics and advantages, yet by combining the materials and exploiting the unique advantages of each material type sensitive, accurate and cost effective methods for the early detection of cancer can be realized.

Gold Nanoparticles

Gold nanoparticles have several advantageous properties that have fueled their increasing use for a wide variety of applications. Gold nanoparticles exhibit many aspects such as their assembly of multiple types involving materials science, the behavior of the individual particles, size-related electronic, magnetic and optical properties, and their applications to catalysis and biology. Their overall utility is mainly related to their different physical properties. In particular, the size dependant optical properties have made gold nanoparticles very attractive for biosensing and labeling schemes. Gold nanoparticles exhibit a strong plasmon absorption band absent in the bulk material due to a collective oscillation of the conduction electrons in response to optical excitation[13] whereas it's condition for optical excitation of its plasmon band is also shifted compared to the bulk material.[14,15] These properties are strongly size dependant and also result in the size dependant color variation exhibited by gold nanoparticles.

The first reported synthesis of gold nanoparticles dates to 1857[16] although colloidal gold has seen use as a pigment[17] and a curative agent[18] for hundreds of years prior to that. While many methods of gold nanoparticle involve the reduction of gold complexes, the most widely used synthetic method is the citrate reduction of HAuCl4 in water that was introduced by Turkevitch in 1951.[19] It leads to gold nanoparticle approximately 20 nm in diameter with good uniformity and a negative surface charge due to the coverage of citrate. Since then many methods have described the synthesis of gold nanoparticles is various shapes and sizes.[20,21] Gold particle diameters can be tuned reliably and routinely from 1 nm to 200 nm,[21] and have been modified with a vast array of protective and functional ligands. As such many different functional groups, ligands, and biomolecules have been incorporated with gold nanoparticles including carboxylic acids,[22,23] phosphines,[22] oligonucleotides,[24-32] amines,[33] proteins,[34-36] enzymes,[34] and small drug molecules.[27,37]

Owing to their long established biostability and ease of bioconjugation gold nanoparticles have been used in a wide array of different applications. One of the most widely used applications is the use of gold nanoparticles to label biological molecules for detection. Gold particles adsorbed to antibodies,[38] proteins,[39] or peptides[40-42] are widely used for the detection of molecular and macromolecular targets especially for localization studies. The most widely used example of this is a popular home pregnancy test kit that when positive develops a pink line. The pink line is actually the congregation of 40nm gold nanoparticles adsorbed to an antibody, antihuman chorionic gonadotropin (hCG).[43] In terms of colorimetric labels, the extinction coefficient of 40nm gold nanoparticles is significantly larger compared to single molecule labels such as fluorescein. This translates into an increase in detection sensitivity of several orders of magnitude if colloidal gold is used as a molecular label rather than other single molecule labels allowing for the easy detection with the naked eye.[44] It is well known that the optical signature of gold nanoparticles is strongly dependent on the particle size and interparticle distance[45,46] because of the interaction of the surface plasmons between individual gold nanoparticles. When the interparticle distance is substantially greater than the average particle diameter, the nanoparticle suspension appears red or pink, but as the interparticle distance decreases to less than approximately the average particle diameter, the color shifts to blue or purple, depending on the size of the particles and the particle concentration. More importantly, the changes in optical properties have been widely used in colorimetric detection schemes for oligonucleotide conjugated gold nanoparticles, as developed by Mirkin.[24,31,47,48] In these studies, the color changes from red to blue–purple accompanying the aggregation of the gold nanoparticles after hybridization of the target DNA. This allows for the colorimetric detection of the DNA with the

naked eye. A similar approach has also been developed for the detection of proteins using oligonucleotide based aptamers that induce aggregation by hybridizing to their target protein.

Magnetic Nanoparticles

Magnetic nanoparticles have been studied for an array of different fields including magnetic fluids,[49] catalysis,[50,51] biotechnology/biomedicine,[52] magnetic resonance imaging,[53,54] data storage,[55] and environmental remediation.[56,57] Magnetic nanoparticles function through exploiting the properties of magnetism for different functions. The electrical basis for the magnetic properties of matter stems down to the atomic level. Electrons have both charge and spin and can therefore be though of as a charge in motion. The charge in motion can produce an atomic level magnetic field. In most atoms, the electrons are paired within energy levels, according to the exclusion principle, so that the electrons in each pair have antiparallel spins thus canceling their atomic magnetic fields. However, in some atoms there are more electrons with spins in one direction resulting in a net magnetic field for the atom as a whole.

All materials however are affected by magnetic fields to varying degrees in one of two ways. Diamagnetic is used to describe materials that line up at right angles to a nonuniform magnetic field and are slightly repelled by that field. Diamagnetism results from magnetic field's interference with the motion of electrons. When diamagnetic matter is placed in a magnetic field, the magnetic field causes the some electrons to speed up some electrons and others to slow down. This interferes with the motion of the magnetic field, so the atoms internally oppose the field causing the material to be slightly repelled by the magnetic field. Paramagnetism generally occurs in materials possessing unpaired electrons. Many elements like iron, palladium, platinum, and the rare earth elements have single electrons that generate a small magnetic field. These elements when placed in a magnetic field, results in the field of the atom aligning with the applied magnetic field and causes the atom to be slightly attracted to that magnetic field.

Superparamagnetism occurs when a naturally magnetic material is composed of nano-scaled particles from 1nm to 10nm. In this case, ambient thermal energy is sufficient to change the direction of electron spin in the entire crystallite. These variations in the direction of electron spin cause the magnetic field of the atom to cancel itself. However when an external magnetic field is applied, the materials act in paramagnetic nature exhibiting a strong attraction to the source of the magnetic field.

Magnetic nanoparticles have been synthesized using a variety of elements and materials including Iron oxides,[58] pure Iron,[59] pure Cobalt,[60] MgFe2O4,[61] MnFe2O4,[61] CoFe2O4,[63] CoPt3,[64] and FePt.[65] Co-precipitation is common synthesis method for Iron oxide nanoparticles from Fe3+/Fe2+ salts through the addition of a base at room or elevated temperatures.[66] The size, shape, and composition of the nanoparticles can then be tuned through the adjustment of the salts used, the Fe2+/Fe3+ ratio, temperature, pH, and the ionic strength of the solution.[67] The addition of different organic molecules have also been shown to stabilize the co-precipitation method and results in a higher monodispersity of the nanoparticles synthesized through this route.[68-70]

Another method of magnetic nanoparticle synthesis is through thermal decomposition following similar procedures to semiconductor nanocrystal synthesis.[71-73] Monodisperse magnetic nanoparticles can be formed through the decomposition of organometallic compounds in boiling organic solvents containing certain stabilizing surfactants. The advantage of this approach is that elements such as Fe, Mn, Co, Ni, and Cr can be incorporated into the nanoparticle through using different organometallic precursors.[74-77] The size and morphology of the nanoparticles are controlled through the ratio of the starting reagents like the organometallic

compounds, solvents, and surfactants. In addition, the temperature, reaction time, and aging time can be varied to precisely control the size and morphology of the nanoparticles.[78-80]

Magnetic nanoparticle can also be synthesized through microemulsion.[81] In water-in-oil microemulsions, the aqueous phase is dispersed as microdroplets surrounded by a monolayer of surfactant molecules. In the microemulsion methodology, two different microemulsions containing the desired reactants are mixed and through the interaction of the different microdroplets the nanoparticles are formed. By adding an appropriate solvent to the mixture, the nanoparticle can be precipitated and then centrifuged or filtered to obtain the nanoparticle. This method has been successful in producing metallic cobalt, cobalt/platinum alloys, and gold-coated cobalt/platinum nanoparticles in reverse micelles of cetyltrimethlyammonium bromide, using 1-butanol as the cosurfactant and octane as the oil phase.[82] MnFe2O4 nanoparticles with controllable sizes from about 4–15 nm are synthesized through the formation of water-in-toluene inverse micelles with sodium dodecylbenzenesulfonate (NaDBS) as surfactant.[83] Although a wide variety of magnetic nanoparticles have been synthesized via microemulsion, the particles have a higher variation in size in comparison to other techniques. In addition, the technique suffers from poor yields owing to the large amounts of solvents required making scale up of the synthesis difficult.

The other common method for magnetic nanoparticle synthesis is hydrothermal synthesis although it is less matured of the four synthetic routes. The system consists of a solid metal linoleate, an ethyllinoleic acid liquid phase, and a water–ethanol solution at different temperatures under hydrothermal conditions.[84] This strategy is based on a general phase transfer and separation mechanism occurring at the interfaces of the liquid, solid, and solution phases present during the synthesis although the precise mechanism of the formation of the particles has

not been fully elucidated. Nonetheless, highly Monodisperse 9nm to 12nm Fe3O4 and CoFe2O4 particles have been synthesized as well ferrite spheres with tunable sizes from 200-800nm.[84,85]

After synthesis of the magnetic nanoparticle, the particle is typically post-coated to increase the stability of the nanoparticle and to also reduce aggregation. Many different materials have been used for this function including polymers, precious metals like gold and silver, carbon, and silica.[86-88] The post-coating step not only protects the nanoparticle, but it also allows the further functionalization of the particle for many different applications. The addition of different functional groups make magnetic nanoparticle ideal scaffold for catalyzing reactions. Magnetically driven separations make the recovery of catalysts in a liquid-phase reaction much easier than by filtration and centrifugation, especially when the catalysts are in the sub-micrometer size range allowing the efficient reuse of expensive catalysts. In addition, they offer a high potential for numerous biomedical applications, such as cell separation,[56] automated DNA extraction,[57] gene targeting,[89] drug delivery,[90] magnetic resonance imaging,[91] and hyperthermia.[92] When coated with, for example, an antibody, they can be applied for highly sensitive immunoassays[93-95] or small substance recoveries.[96] Furthermore, single-stranded DNA or oligonucleotide immobilized on magnetic particles were successfully used for DNA hybridization analyses with the aim of identifying organisms[97,98] and single-nucleotide polymorphism analyses for human blood.[99,100] Thus, a wide array of applications for magnetic nanoparticles have been previous explored with particular emphasis on using their unique properties to facilitate the efficient separation of materials from even complex mixtures and samples.

Fluorescent Nanoparticles

Fluorescence is a highly useful phenomenon in which light used for the excitation of fluorescence in absorbed and converted to light with a different wavelength. This allows for the

sensitive and efficient detection of a fluorescent species. As such fluorescence has been utilized in a tremendous number of applications. Jablonski diagrams are typically used to illustrate the underlying mechanism behind fluorescence. As seen in Figure 1-1, the excitation light is absorbed by a fluorophore and the electrons are induced to an excited singlet state. The excited state typically undergoes certain non-photonic relaxation processes between vibrational levels called internal conversion before returning to the ground state. When the electrons return to the ground state, a photon will typically be emitted. The emitted light is designated fluorescence. The emitted photon from this process is lower in energy, or longer in wavelength, than the absorbed excitation photon. The difference between the excitation and emission wavelengths of light is called the Stokes' shift.

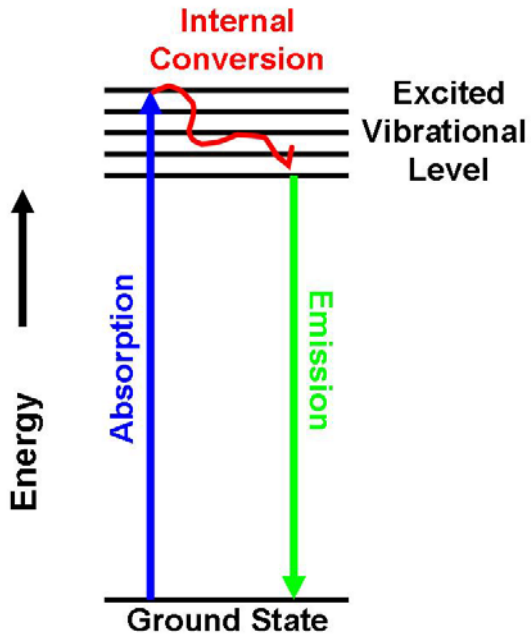

Figure 1-1. Depiction of a typical Jablonksi diagram illustrating the fluorescence processes wherein the photon is absorbed, the internal conversion processes through which some energy is lost non-photonically, and the final photonic transition from the excited state to the ground state.

While labeling with fluorescent molecules is a very sensitive technique it is often advantageous to increase the amount of fluorescence as much as possible. One very effective method for doing this is through the use of fluorescent nanoparticles that can emit thousands of times as much fluorescence as a single fluorescent molecule. Fluorescent nanoparticles are generally either constructed from semiconductor nanocrystals or through the encapsulation of many fluorescent molecules in polymers or silica.

Semiconductor Nanocrystals

Fluorescent semiconductor nanocrystals are currently of wide interest for their potential for biological applications. As such they possess several advantageous properties including their small size, generally less than 10nm, very broad excitation spectra, and emission spectra that are narrower than conventional fluorophores. The spectral properties of quantum dots are based on quantum confinement conditions under which the crystal is on the order or smaller than the material's Exciton Bohr radius. This results in a discrete bandgap between the valence and conduction bands of electrons in the crystals that is not present in the bulk materials. After the electrons are induced to an excited state, they emit a photon when returning to the ground state. The emission bandwidth of the photons is much narrower as it correlates to the discrete and narrow bandgap between the valence and conduction bands.

Both group II-VI quantum dots like CdSe, CdTe, CdS, and ZnSe and group III-V quantum dots like InP and InAs have been synthesized and studied extensively in the past.[101-104] Prior to 1993, quantum dots were mainly prepared in aqueous solution with different stabilizing agents such as thioglycerol or polyphosphate. This process produced low-quality QDs with poor fluorescence efficiencies and large size variations due to imperfect crystal structures. In 1993, Bawendi[105] reported the synthesis of highly luminescent CdSe quantum dots by using a high-temperature organometallic procedure similar to the previous mention thermal decomposition

methodology. The quantum dots possessed nearly perfect crystal structures and narrow size variations, however the quantum yields were still low compared to conventional fluorophores. This limitation was later addressed through the deposition of CdS or ZnS surface capping layers. The ZnS capping was particular successful as the Zn/S chemical bonds are similar in length to the Cd/Se bond lengths allowing the growth of thin ZnS films with the same crystalline orientation around the CdSe core. The ZnS capped CdSe crystals exhibited quantum efficiencies around four times higher than CdSe nanocrystals by themselves. More recently, quantum dots with excellent quantum efficiencies have been produced through the use of nontraditional precursors to realize high quality quantum dots with no need for capping. The size of quantum dots can also be controlled through careful modification of the synthesis temperature, reaction time, and reagents.

One of critical aspects to any fluorescent moiety however is the attachment to biological molecules for labeling or biosensor applications. As such many different molecules have been adapted for use as solubilization or crosslinking agents for quantum dots. These include ligand exchange with simple thiol-containing molecules[105,106] or more sophisticated ones such as oligomeric phosphines,[107] endrons,[108] and peptides,[109]encapsulation by a layer of amphiphilic diblock[110] or triblock copolymers,[111] or in silica shells,[112,113] phospholipid micelles,[114] polymer beads,[115] polymer shells,[116] or amphiphilic polysaccharides.[117] Also, combinations of different layers have also been utilized to instill necessary parameters like solubility, stability, and attachment to molecular recognition elements. The development of so many surface chemistry has also led to the attachment of molecules through many different chemistries including thiol group,[114,118,119] N-hydroxysuccinimyl ester moieties,[109,112] or streptavidin/biotin conjugations.[120]

Due to their excellent spectral properties, quantum dots have been used for a variety of different applications. These including cell surface protein targeting through streptavidin,[120,121] secondary[122] or primary antibodies,[123] receptor ligands such as epidermal growth factor (EGF) [124,125] or serotonin,[126] recognition peptides,[127] and affinity pairs such as biotin-avidin after engineering of the target protein.[128] In addition, their stability and brightness make them possible candidates for in vivo imaging applications. As such they have been demonstrated in imaging blood vessels in live mice,[129] as tissue specific vascular markers in mice,[118] and targeted delivery through antibody conjugated quantum dots.[111,130]

The major issue preventing quantum dots for more widespread use in imaging studies is concerns to possible toxicity. While some studies have shown quantum dots are safe at lower concentrations many other studies have documented the toxicity of quantum dots including on embryo development,[114] cytotoxicity in EL4 lymphoma cells,[131] and DNA damage.[132] It has also been demonstrated that the less protected the quantum dot is, the faster the onset of the adverse cell effects[133] through the release of Cd2+ and Se2- in core/shell and core only nanocrystal structures. Therefore, the work described herein focused on mainly the fluorescent nanoparticles that possess higher biostability and less cytotoxic side effects.

Encapsulated Nanoparticles

In lieu of using nanoparticles with very different spectral properties from conventional fluorophores, another strategy to increase the fluorescence intensity is to simply add as many fluorophores as possible to a particular label or biorecognition element. Therefore, the label has the same spectral properties as a conventional fluorophore but has a much higher intensity. As it is impractical to covalently attach multiple fluorophores to a label, the fluorophores are typically encapsulated inside of a material like silica or a polymer matrix. The matrix imbues the fluorophores with many advantageous properties such as photostability, wider pH stability, and

the use of simple well established conjugation schemes. As such, silica and polymer based fluorescent nanoparticles have been use for a wide array of applications. While polymer nanoparticles possess many of the same advantages as silica nanoparticles, the bioconjugation routes for silica are better established and offer an additional degree of flexibility and versatility and thus will be the focus of the work described.

One of the most important aspects of using nanoparticles is the synthesis of the nanoparticle and method for trapping the dye inside its matrix. While other synthesis methods exist, the two most well established methods for silica nanoparticle synthesis are the Stober method[134] and the microemulsion method.[135] The microemulsion method incorporates the use of water, oil, and surfactant molecules in order to hydrolyze tetraethyl orthosilicate. In this method, the surfactant molecules form micelles around the water droplets containing a polar fluorophore. The size of the droplets can be control through the water to oil ratio. Then, ammonium hydroxide and tetraethyl orthosilicate can be added to the mixture. Both hydrophilic species are brought together in the water droplets and the ammonium hydroxide hydrolyzes the tetraethyl orthosilicate into a solid silica matrix. The hydrolysis of the tetraethyl orthosilicate forms produces Silicic acid which forms the silica matrix through a subsequent condensation reaction. The matrix forms around the fluorophores in the water droplet entrapping them to yield highly fluorescent silica nanoparticles. Typically inorganic dyes are used for this method as they are more water soluble and they are typically positively charged and form stable electrostatic interaction with the silica matrix preventing them from leaking out of the nanoparticle. However, many strategies have been developed to use organic fluorophores such as introducing a hydrophobic silica precursor,[136] using water-soluble dextran-molecule-conjugated dyes, and synthesizing in acidic conditions.[137]

The other commonly used method for silica nanoparticle synthesis is the Stober method. While microemulsion simply entraps the fluorophore in the silica matrix, the Stober method utilizes a covalent attachment to link the fluorophore directly to the silica matrix.[138,139] In the Stober method, a silicate precursor, generally tetraethyl orthosilicate, is hydrolyzed in a mixture of ethanol and ammonium hydroxide. To incorporate a fluorophore, the procedure requires a slight modification. First, the fluorophore, typically an isothiocyanate or succinimidil ester based fluorophore, is reacted with an amine containing silane forming a covalent linkage. Then the fluorophore linked silane is added to the tetraethyl orthosilicate. The mixture is then allowed to hydrolyze in water, ethanol, and ammonium hydroxide and undergo the subsequent condensation reaction to form the nanoparticle from both the tetraethyl orthosilicate and the fluorophore linked silane. This method allows any fluorophore with an amine reactive functional group to be combined into the silica matrix.

One of the more advantageous aspects of employing silica based nanoparticles is the flexibility and versatility of the silica in terms of bioconjugation. The simplest method for conjugation involves the physical adsorption of a biomolecule like avidin followed by a crosslinking step to encase the nanoparticle in an avidin shell. Then any biotinylated ligand can easily be attached. There are also many methods that utilize a covalent attachment if other surface functionalities are wanted or required for the particular application. Ligands requiring a covalent attachment require first that the nanoparticle surface is modified with a particular functional group whether a thiol, amine, or carboxy group. This is achieved during a post coating step using a silane with the proper group and undergoing an additional round of hydrolysis and condensation that leaves the silane as part of the nanoparticle matrix and the functional group exposed on the surface.[140-142] After the functionalization step the nanoparticles

can be conjugated to oligonucleotides,[143] antibodies,[144] peptides,[145] or organic molecules.[146] Owing to their wide versatility, silica based nanoparticles have been used a wide variety of applications. These applications include biosensing,[147] gene delivery,[146] drug delivery,[148] and labeling of biological molecules.[147]

Molecules for Bio-recognition

While nanomaterials offer many benefits in terms of sensitivity, detection, and separation they possess no inherent selectivity. Therefore, any method using nanomaterials is only as good as the species used for molecular recognition. The importance of molecular interactions has become increasingly clear in disease states. As such, many diseases have been shown to have characteristic biomarkers associated with them. The identification of these biomarkers has greatly aided in the diagnosis and subsequent treatment of those diseases. However, the vast majority of diseases currently do not currently have specific biomarkers associated with them, greatly limiting the diagnosis and treatment capabilities in the field of medicine. The problem lies in the great amount of time and effort that is necessary for biomarker discovery. It involves the systematic separation and identification of biological molecules from complex bodily fluids or tissues that requires a large effort with sufficient controls to avoid identifying the wrong molecule as a biomarker. Typically there are two classes of molecules that are used for molecular recognition; antibodies or aptamers.

Antibodies are generally large Y-shaped glycoproteins used to identify and neutralize foreign objects by the immune system. There are two major types of antibodies, polyclonal antibodies and monoclonal antibodies. Polyclonal antibodies are a combination of antibodies active against a particular antigen each recognizing a particular epitope of the antigen. Polyclonal antibodies are normally obtained by injecting the antigen into a small animal, such as a mouse or rabbit and then isolating the antibody from the animal's blood although larger

animals are used in cases were a large amount of the antibody is required. Monoclonal antibodies are instead produced in the laboratory using a specially prepared an antibody producing cell line for a specific antigen.

In research, purified antibodies widely used for the identification and localization of proteins or other biologically relevant molecules. Antibodies are used in flow cytometry to differentiate cell types,[149] in immunoprecipitation to separate proteins in a cell lysate,[150] in a Western blot to identify proteins after electrophoresis,[151] or in immunohistochemistry to examine protein expression in tissues,[152] and to examine the localization of proteins within cells by immunofluorescence.[149] The major problems with antibodies is that since they are typically produced through biological pathways instead of through chemical synthesis they can be difficult to reproduce, difficult to chemically modify, are very sensitive to environmental factors, and have a finite shelf life.

Aptamers are single-stranded DNA (ssDNA), RNA, or modified nucleic acids that have the ability to bind specifically to target molecules ranging in size from small organic molecules to large proteins.[153-155] The dissociation constants of aptamers to targets can range from 10^{-12} M-10^{-8} M making them comparable to antibodies in many instances. Aptamers recognize their targets with high specificity and are capable of discriminating between protein targets that are highly homologous or differ by only a few amino acids.[156,157] The tertiary structures formed by the single-stranded oligonucleotide molecules are the basis for target protein recognition.[158,159] These single-stranded oligonucleotide aptamers are selected by a process called SELEX (Systematic Evolution of Ligands by Exponential enrichment), where the aptamers are selected from libraries of random sequences of synthetic DNA or RNA by repetitive binding of these oligonucleotides to the target molecules.[153,160-162] Through this in vitro selection process, single-

stranded oligonucleotide aptamers with high specificity and affinity to their targets can be obtained. Most of the aptamers reported so far have been selected using pure molecules, such as purified proteins as the targets. However, the aptamer selection against complex targets (such as red blood cells and single protein on live trypanosomes) was also demonstrated and interesting aptamers have been generated.[163-168]

To produce probes for molecular profiling of tumor cells, researchers in our lab have developed a novel method, the cell-based aptamer selection process (cell-SELEX) that has generated the aptamers for the work described herein. Instead of using a single type of molecules as targets, the Cell-SELEX process uses whole cells as targets to select single stranded DNA aptamers that can distinguish target cells from control cells (see Figure1). In addition to low molecular weight, easy and reproducible synthesis, easy modification,[169] fast tissue penetration, low toxicity or immunogenicity,[170,171] easy storage, high binding affinity and specificity,[153,172] the biggest advantage of the Cell-SELEX-based aptamer technology is the unique cell-based selection process illustrated in Figure 1-2. A group of cell-specific aptamers can be selected using a subtraction strategy in a relatively short period without knowing which target molecules are present on the cell surface. There is no easy way to produce a similar panel of monoclonal antibodies in such a short time without purified antigens for any unknown antigens. Compared to 2-D gel electrophoresis and mass spectrometry used for proteomic studies aiming at identifying proteins, the cell-SELEX will produce molecular probes in less time then use the specific probes to identify the target proteins. Thus, not only can the selected aptamers be used as molecular probes for molecular profiling, but also they can be used as tools for identifying new biomarkers expressed by tumor cells or other cells in disease status.

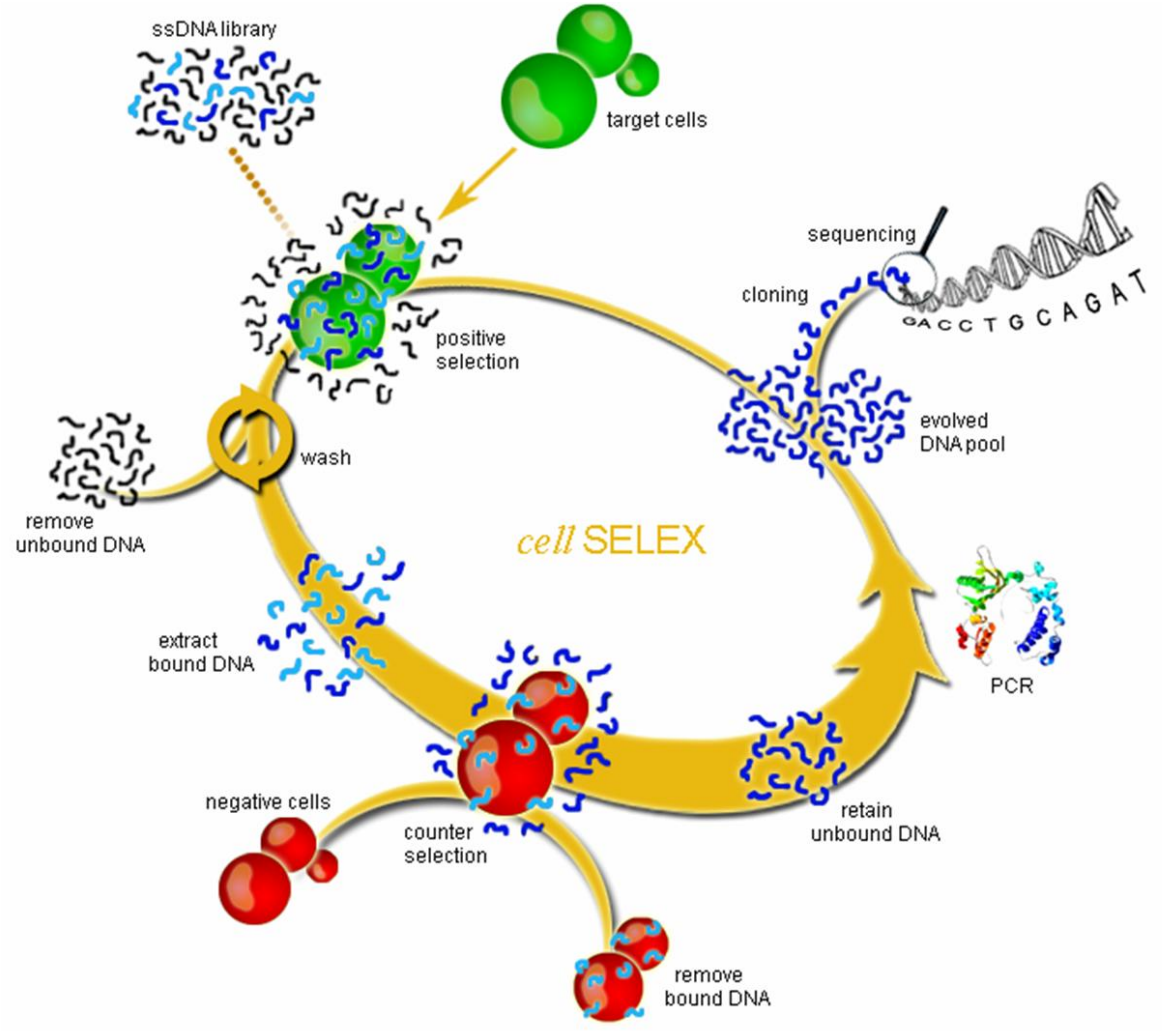

Figure 1-2. Schematic of cell-based aptamer selection (cell-SELEX). Briefly, ssDNA pool is incubated with target cells. After washing, the bound DNAs are eluted by heating in binding buffer. The eluted DNAs are then incubated with control cells (Negative cells) for counter-selection. After centrifugation, the unbounded ssDNAs in supernatant are collected, and then amplified by PCR. The amplified DNAs are used for next round selection. The selection process is monitored using fluorescent imaging by confocal microscope or fluorescent analysis by flow cytometry.

The aptamers can easily be conjugated with fluorophores, radioisotopes, or various other functional groups for in-vivo molecular imaging of cancer cells and tissue, for molecular profiling of cancers in flow cytometry analysis, and for potential biomarker discovery in cancer samples. In the work described herein, aptamers will be used as a molecular recognition element for not only the detection of cancerous cells but also the collection and enrichment of the cells.

Using functional groups attached to the aptamers during the synthesis process, the aptamers can be attached to the various types of nanomaterials that have been previously discussed to enable not only the easy colorimetric detection of cancer cells, but also the collection and enrichment of cancer cells. Once the cancer cells are collected and enriched they can be further studied to shed new light into the underlying disease processes and to help determine effective treatment options by exposing the cells to different cancer fighting agents. Thus the work described in this dissertation pertains not only to the development of new methods for cancer detection but also new methods on the study and characterization of cancer.

Measuring and Analyzing Gene Expression

Traditional Methods of Gene Expression Analysis

The initial techniques used for gene expression analysis were developed to examine expression of individual known genes beginning in 1977 when the northern blot technique was introduced.[173] In Northern Blot analysis, the total cell RNA is first prepared and different size classes are separated electrophoretically. The targeted size is transferred to nitrocellulose film and mixed with radiolabeled DNA probes for a particular mRNA. This is followed by radioautographic detection of DNA-RNA hybrids. This allows for the expression of particular gene expressions to be compared to other gene sequences to gain a qualitative understanding into the relative expression levels in a group of cells. This technique is still widely used and is often performed to validate the results of other types of gene expression studies and newly developed approaches. Introduced in 1977, a method was developed that protects a DNA labeled probe against degradation by single-stranded nuclease S1 by annealing the probe with RNA.[174] This led to RNase protection assays that were developed to detect the expression of specific RNA sequence and to compare the levels of expression through labeled cDNA. The cDNA forms a hybrid with its complementary mRNA and after exposure to a single-strand specific nuclease,

unhybridized strands are degraded leaving only the targeted hybrids that are detected using gel electrophoresis.

Another widely used technique, the serial analysis of gene expression (SAGE) allows for the quantitative measurement of entire transcriptomes. The method is based on averaging the individual cell responses through the use of sequencing tags that are derived from different populations of cells.[175] In 1993, subtractive hybridization techniques became available for constructing subtractive cDNA libraries. This methodology uses cDNA from one pool to hybridize to mRNA from the other allowing cDNA libraries to be constructed from the transcripts that are not hybridized and are used to identify specific mRNAs. A modification of this technique, representational difference analysis (RDA), also uses preferential amplification of non-subtracted fragments. In RDA, simplified versions or representations of the genomes being studied are created using restriction enzyme digestion. While this tehcnique was first developed to study variations between different genomes, it has also proven useful for cloning differentially expressed genes.

One more modern technique for gene expression analysis is fluorescence-based microarrays. Microarrays are simply ordered sets of DNA molecules of known sequences plated in an array format where different sequences are spatially separated. Usually rectangular, they can consist of a simple arrangement of a few sequences to hundreds of thousands of sequences for the massively multiplexed comparison of gene expression levels. Modern microarray technology employs sensitive and high resolution instrumentation to detect differences fluorescence intensities of thousands of different sequences as changes as small as 1.3 to 2-fold are detectable.[176,177] This allows the detection of the upregulated and downregulated expression levels of many genes compared to the basal level. However, the technique does suffer from a

lack of sensitivity when analyzing changes in genes that have very high or very low expression, although there has been effort towards nanoparticle based arrays in order to increase both the sensitivity and the overall limit of detection.[178]

Traditionally, mRNA subcellular localization has been performed using in situ hybridization (ISH) in conjunction with light and fluorescent microscopy.[179] ISH involves using labeled antisense DNA or RNA probes that hybridize to mRNA in pretreated fixed cells in culture or tissue sections. The unhybridized probes are then washed away from the cells and the hybridized probes are then detected using emulsion autoradiography, light microscopy, or fluorescence microscopy depending on the nature of the probe. ISH can provide very precise and sensitive localization information for the mRNAs. Unfortunately, ISH is very difficult to quantitate and is not practical for mRNAs that have a complex secondary and tertiary structure that sterically inhibits hybridization of the probe to the RNA of interest. Due to this phenomena, even highly abundant mRNAs can be undetectable by ISH if the mRNA has a strong secondary structure.[180,181]

Molecular Beacons

Traditional RNA detection and localization methods such as in situ hybridization are generally used with fixed and pretreated cells or tissues.[182] The fixed cells samples are dead cells which prevents monitoring dynamic cellular events such as synthesis and transport. With MBs on the other hand, living cells can be tested and explored allowing for new applications and discoveries into the dynamic processes of the cells. Molecular beacons (MBs) are fluorescent nucleic acid probes that offer excellent specificity and sensitivity for monitoring the expression of mRNA at the single cell level. Molecular beacons are synthetic DNA molecules in a hairpin structure with a fluorophore-quencher pair that undergo a conformational change upon hybridization to a complementary nucleic acid target. As hybridization occurs, the fluorophore-

quencher pair is separated and the fluorescence of the fluorophore is restored. Fluorescence based detection methods can be highly sensitive due to the detection of emission photons that are spectrally separated from the excitation photons. While fluorescence has been previously discussed, an important consideration for molecular beacons is the concept of fluorescence quenching.

The quenching of the fluorescence emission is accomplished primarily through two mechanisms. The first mechanism is referred to as dynamic or collisional quenching. In this case, a quencher molecule makes contact with the fluorophore during the lifetime of its excited state. The diffusion controlled collision between the two molecules results in the fluorophore returning to the ground state without emitting a photon thus resulting in no fluorescence. Neither molecule is chemically altered during this process and many different types of molecules can act as collisional quenchers. However, the collisional quenching is a random process and is not suitable for use in biosensor based applications as it would be very difficult to integrate a random diffusion based phenomena into a signal transduction scheme. The other type of quenching, static quenching, is far more suitable to biosensor applications. It involves the formation of a complex between the fluorophore and quencher moieties. While the fluorophore outside of the complex relaxes from the excited state through a photonic emission, the complex relaxes through thermal and Vibrational modes due to the structure of the quencher portion of the complex. This results in the prevention of the photonic emission and eliminates the fluorescence. While the two process can occur in the same, the molecular beacon is designed to rely on static quenching when the fluorophore and quencher are in close proximity in the stem region of the beacon. Thus upon undergoing the forced conformational change after target hybridization, the quencher is

separated from the fluorophore preventing formation of the complex and allowing the fluorophore to emit fluorescence once again.

Using molecular beacons *in vivo* for mRNA expression detection offers several advantages over traditional means of mRNA analysis. Traditional RNA analysis methods involve fixed pretreated cells or tissues that represent pooled averages from millions of cells, but may not represent individual cellular processes in living systems.[182] Similarly, single cell RT-PCR exhibits variations in the amplification among different RNA sequences.[183] Molecular beacons do not require any pre- or post-treatment of the cells, since, in theory, they will only open upon hybridization with their specific target. Thus, molecular beacon fluorescence occurs only when the complementary target is present, making separation of hybridized from unhybridized molecular beacons unnecessary. The molecular beacon detection of mRNA inside of the cell does not require amplification like RT-PCR so there is no chance of preferential amplification. Molecular beacons inherently possess the specificity through Watson-Crick base pairing and the sensitivity through fluorescence detection that makes them ideal for intracellular mRNA detection. Successful use of MBs for intracellular mRNA detection depends on a valid sequence design, optimal delivery of the probe, and optimized fluorescence imaging conditions that will be explored in further detail in chapter 5.

Intracellular Applications of Molecular Beacons

To date MBs have been used for intracellular detection in a variety of cell systems. In 2001, the real-time hybridization of a MB to mRNA was visualized inside of a single cell.[184] In this study, MBs specific for β-actin and β-1 andrenergic mRNA were used to detect their respective mRNA targets in kangaroo rat kidney (PtK2) cells. The MBs were delivered to the cells using microinjection and then monitored for 18 minutes. In the PtK2 cells, an increase in fluorescence intensity was detected for both the β-actin and β-1 andrenergic MBs. In order to

prove that increase of fluorescence was due to the intended interaction a negative control MB was also used in this experiment. The negative control MB, which has no complement inside of the cells, showed no increase in fluorescence inside of the cell. This indicates that the fluorescence from the targeted MBs was due to hybridization to its target as opposed to a non-specific interaction since any non-specific interaction or degradation would have equally affected the negative control MB. This study demonstrated the real-time detection capabilities of MBs for mRNA detection and showed conclusively that MBs could be very valuable tools for detecting gene expression inside of single living cells.

In 2003, Tyagi et al demonstrated that MBs could be used for the visualization of the distribution and transport of mRNA.[185] In this study an MB for oskar mRNA was investigated in Drosophila melanogastar oocytes. Initially they demonstrated visualizing the distribution of oskar mRNA in the cell. Due to the fluorescence background exhibited from the MBs, they decided to use a binary MB approach that utilized two MBs that targeted adjacent positions on the mRNA. When both MBs were hybridized to the mRNA sequence the donor and acceptor fluorophore were brought within close proximity allowing FRET to occur. This generates a new signal that indicated hybridization of both MBs with the mRNA. In addition to visualizing the mRNA distribution, they were also able to track the migration of the mRNA throughout the cell and even into adjacent cells in the oocyte. This study demonstrated the potential of MBs not only for studying the localization of mRNA inside of single cells but it also demonstrated that MBs could be used for tracking mRNA migration even into different cells. Other studies have built on this line of investigation and imaged MBs on viral mRNA inside of host cells to study the behavior of the mRNA. This study investigated both the localization of the mRNA inside of cell and also utilized photobleaching the fluorophore on the MB in order to study the diffusion of

the MB mRNA hybrid. These studies demonstrate the wealth of information that can be gained through the visualization of MB hybridization inside a single cell.

In addition to localization and distribution, expression levels of mRNA have also been studied inside of living cells using MBs. Using a two MB FRET approach the relative expression levels of K-ras and survivin mRNA were determined in human dermal fibroblasts.[186] In this study, human dermal fibroblasts and pancreatic carcinoma cells were used to study the expression levels and the localization of K-ras and survivin mRNA. In order to accomplish this, a two MB FRET approach was used. This encompassed designing two MBs for adjacent target regions. Once both MBs hybridized to the same mRNA, the fluorophores on the MB were brought within a close distance and FRET was allowed to occur. Using this process they demonstrated the localization of the two mRNA sequences in different cell types and how the different mRNA was localized at different regions inside of the cell. The use of the two MBs allowed for much greater specificity since the signal required two separate hybridization events to be generated.

One of the limitations of MBs for intracellular analysis has been the inherent variability in the fluorescent measurements obtained. However, it is difficult to attribute these variations to any one cause such as instrument or experimental variability, variations in gene expression, or simply different amounts of probe being delivered into the cell. In an effort to eliminate the experimental and instrumental variations in order to study the stochasticity of gene expression a method of ratiometric analysis was developed and applied to cancer cell genomics.[183] In this approach a fluorophore labeled DNA reference probe was injected along with the MBs. The reference probe exhibited a constant level of fluorescence relative to the MB signal that resulted in a ratio value for the MB that was independent of instrumental variations like the amount of

probe delivered to the cell and experimental variations like different cell volumes. This is due to the ratio of the reference probe to the MB being constant, therefore any increase in the ratio was due to the increase of the molecular beacon fluorescence indicating target hybridization.

While MBs have shown a great deal of promise in these applications, there are some limitations that currently exist. One of the most significant limitations is a susceptibility of the MB to endogenous nucleases and single strand binding proteins (SSBs). Both of these can induce a false positive response from the MB and greatly limit the viability of the MB inside of a cell. SSBs can bind to loop region of the MB causing the separation of the fluorophore and quencher while nucleases can cleave apart the MB also separating the fluorophore and quencher. The opening of the MB from specific and non-specific interactions is impossible to distinguish. In the human breast cancer cells studied, MBs regardless of sequence are degraded inside of the cell after approximately 30 minutes. This greatly limits the types of applications and processes that can be studied. There have been many strategies developed to deal with these problems. These include the use of modified DNA backbones to imbue the MB with resistance to nucleases like 2'-O-methyl bases,[187] 2'-fluoro bases,[188] peptide nucleic acids,[189] phosphothiolates,[190] and locked nucleic acid bases.[191] However, the modifications have been shown to affect the hybridization rates of the MBs. Peptide nucleic acid bases have also been used to synthesize MBs however their neutral charge would create solubility issues inside of living cells. phosphothiolates have also been shown to exhibit toxicity to cells.[190] Therefore while different approaches have been tried the issue of intracellular stability still requires additional attention.

Another issue confronting the MBs is the problem of low expression genes. These are genes that while biological are very significant express very low copy numbers of mRNA. To overcome this biological issue, MBs require further refinement in the areas of superior

quenching and brighter fluorescence. The presence of background fluorescence even in the closed state can hinder the limit of detection of the MB inside of the cell. Therefore improved quenching efficiency is an area that has been explored with promising results. Both gold nanoparticles[192,193] and novel superquenching moieties[194] have been utilized to achieve lower fluorescence backgrounds. Additionally, brighter fluorescent moieties have also been explored. These include the use of quantum dots[195] and fluorescent polymers[196/] to make MBs as bright as possible. The continuing improvement of MB design and synthesis further extends its potential as an intracellular probe however many of these improvements have yet to make the transition from buffer solutions to the complex realm of the cell.

Intracellular Ion Levels

Beyond mRNA expression, there are other types of molecules that are critically important to understanding the underlying biological function inside of the cell. These are the proteins and the ions inside of the cell. The proteins are the functional structures that carry out the biological processes in the cells. While some methods for studying proteins expression inside of the cell exist, they involve altering the genome of cells through the use of fluorescent proteins, in particular they involve altering the gene sequence of the very proteins to be studied. Other methods involve the use of fluorophore labeled antibodies, however with no inherent signal transduction method it is difficult to differentiate the bound antibodies from the unbound antibodies. Ions on the other hand also perform many of the critical functions inside the cell as signaling molecules, stabilizing proteins structures, and enabling many protein functions. Unlike proteins however, there many molecules that exist that can chelate ions with a good degree of specificity. The careful manipulation of there structure has produced molecules that will chelate selectively to certain ions to produce a fluorescent species. This allows for the fluorescent

detection of the ions even inside of cells. Therefore if one can study gene and ion levels inside of single cells more in depth studies of the fundamental biological processes can be achieved.

Therefore the work described herein not only focuses on the early detection of cancer cells in samples ranging simple to complex but also on developing methods to analyze the cells. This way once a type of cancer is detected, the actual cancer cells themselves can be collected, cultured, and further studied to reveal a specific molecular diagnosis and what treatment options will be the most effective. This would allow a more personalized treatment of the illness leading to ultimately not only a more effective treatment but one with fewer side effects. Also, when the cancer is detected at an early stage it responds much more favorable to treatment and leads to ultimately a much more favorable prognosis for the patient.

CHAPTER 2
DNA AND NANOPARTICLE SYNTHESIS

DNA Synthesis

Before using the various materials and probes that have been mentioned, the first step encompasses actually making and characterizing the various constituents. After their synthesis, the different parts can be combined together to create nanomaterials and probes that will allow the detection and study of cancer cells. Therefore, this chapter will focus on the synthesis of the DNA portions of the materials and the synthesis and characterization of the nanomaterials. Once both types of materials have been synthesized they can either be used individually or conjugated together and used for various applications.

One of the primary advantages of the aptamer is that it is based on DNA and therefore cannot only be chemically synthesized, it can be chemically synthesized with different functional groups or other molecules integrated into its structure. This makes aptamers ideally suited for coupling to different nanoparticles using well established conjugation strategies. Similarly, molecular beacons also benefit from the chemical synthesis of DNA as the whole molecular beacon structure from the quencher to the fluorophore can be synthesized on column. However, it is often advantageous to use off column coupling of the fluorophores. While resulting in an overall lower yield due to reaction efficiencies and increased purification steps, the fluorophores are not subjected to the harsh deprotection schemes and higher quality fluorophores not available as a phosphoramidite can be used. The higher quality fluorophores, such as the Alexa Fluor line available from Invitrogen, have better environmental stabilities, resistance to photobleaching, higher quantum efficiencies, and higher molar absorptivities yielding a more stable and sensitive molecular beacon. Therefore, probes based on DNA offer many advantages due to its the versatile and well established chemical synthesis process.

Several different methods for the chemical synthesis of DNA have been reported including the use of phosphodiesters,[197] phosphoramidites,[198] and the H - phosphonate method.[199] Among these, the phosphoramidite method remains the most commonly used as it is useful in the production of long oligonucleotide strands with artificial modifications in high yields and purity which is much more difficult with other synthetic routes.[200] Synthesizing oligonucleotides using phosphoramidite chemistry was first developed by Caruthers and later improved by Kosters and others. It involves the use of a series of cycled controlled reactions utilizing either a liquid or solid phase. For each repetition of the phosphoramidite cycle, one base is added on the sequence until the desired DNA sequence has been completed. The aptamers and molecular

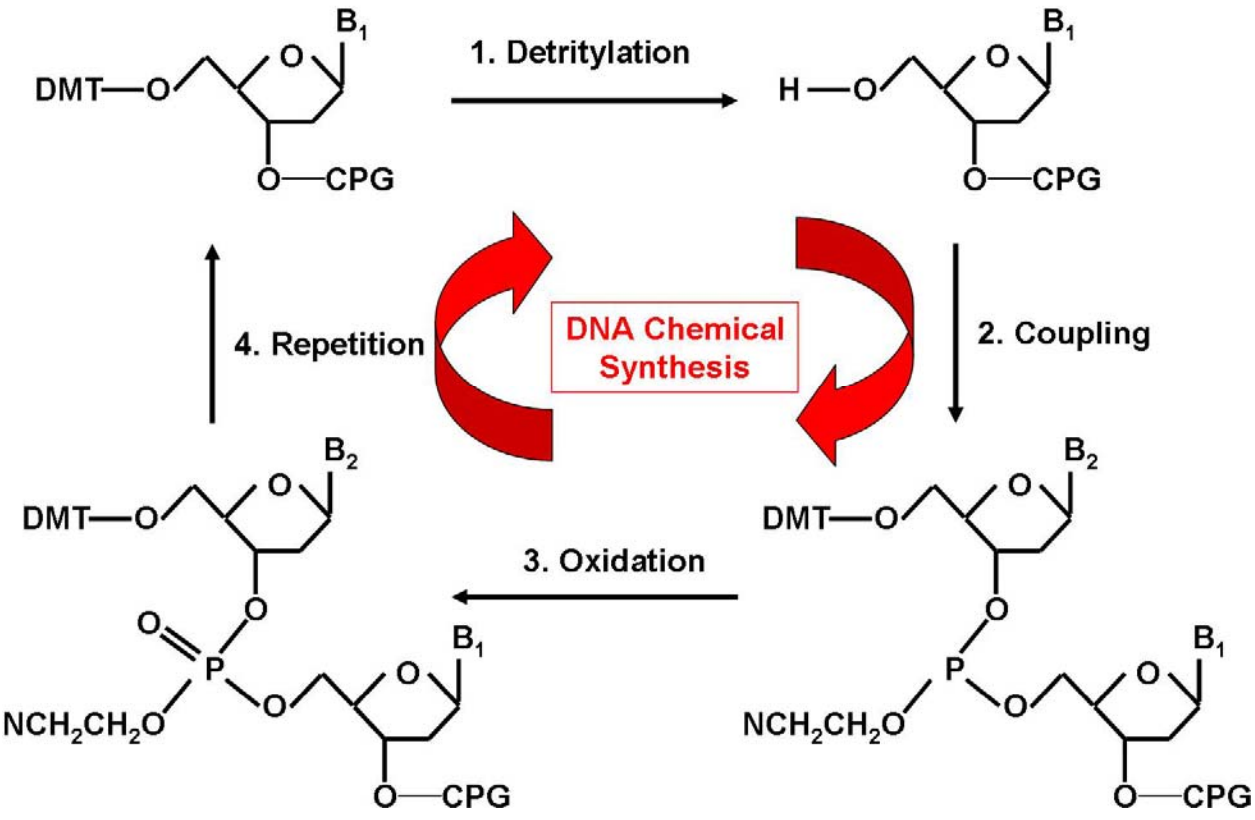

Figure 2-1. In automated DNA chemical synthesis three primary steps, Detritylation, Coupling, and Oxidation are repeated until the desired DNA sequence has been synthesized.

beacons covered herein were synthesized on an ABI 3400 DNA/RNA synthesizer using standard phosphoramidite chemistry. As the solid phase synthesis using phosphoramidite chemistry was used in the production of the aptamers and molecular beacons, it will be covered in more detail. The reaction cycle of the solid phase synthesis can be broken down into three critical steps referred to as Detritylation, Coupling, and Oxidation as shown in Figure 2-1.

For the solid phase synthesis, the starting molecule whether the DNA base, biotin, or other molecule is immobilized on a controlled porous glass support (CPG) at the 3' position. Thus, the synthesis proceeds from the 3' end to 5' end of the DNA sequence. The Detritylation step involves removing the dimethoxytrityl (DMT) protecting group from the nucleoside, leaving a hydroxyl group that forms the foundation for the next reaction in the cycle. The DMT group is removed by adding a dilute acid solution of either dichloroacetic acid or trichloroacetic acid in dichloromethane. The DMT group leaves the nucleoside and the column is washed to remove any extra reagents or byproducts yielding the hydroxyl group. Next is the Coupling step in the reaction in which the next base is added onto the chain. This involves the addition of the next nucleotide as a phosphoramidite derivative and tetrazole to the reaction mixture. As depicted in Figure 2-2, the tetrazole activates the phosphoramidite cleaving off protecting group leaving the phosphoramidite vulnerable to the nucleophilic attack of the hydroxyl group. This forms an unstable phosphate linage and the excess reactants and byproducts and washed away.

After the coupling step, the uproduct is then stabilized in the Oxidation step. The product is stabilized via the oxidation of the phosphite linkage to a phosphate linkage through the addition of dilute iodine, pyridine, and tetrahydrofuran. The product is now about to repeat this series of steps until the full sequence of the strand is synthesized.

In addition to these steps, another critical process referred to as capping occurs after the coupling step to ensure any failed sequences are prevented from further reaction. Failed sequences occur because the coupling step yield is not always 100%. This would leave some reactive hydroxyl groups that could react in subsequent cycles resulting in deletions in the sequence. The deletion of a base could drastically alter the properties of the probe being synthesized whether it is a molecular beacon or an aptamer. In addition, the deletion would be difficult to separate using standard purification techniques. Therefore, to remove the unreacted hydroxyl groups a Capping step is performed after the coupling step. The Capping step involves adding acetic anhydride and N-methylimidazole resulting in the acetylation of any unreacted hydroxyl groups. The acetylation prevents the chain from ongoing further coupling reactions resulting in a much shorter fragment. The shorter fragments are easily purified from the complete sequence resulting in a much purer final product.

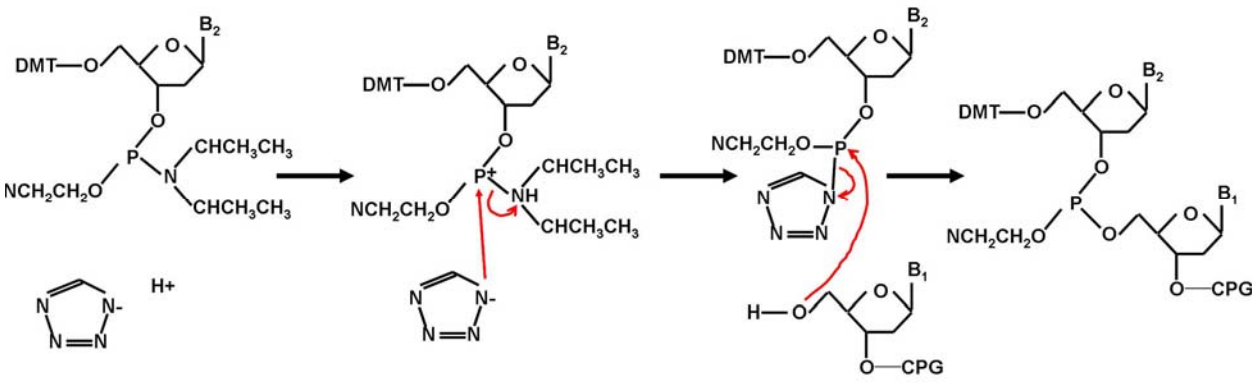

Figure 2-2. The Coupling step in DNA synthesis depicting the activiation of the phosphoramidite derivative and the subsequent coupling of the two nucleotides.

After the synthesis is finished, the oligonucleotide must be deprotected and removed from the solid support. This is accomplished by incubating the DNA/CPG complex in ammonium hydroxide for 2 hours at 65°C followed by centrifugation to remove the CPG. The DNA is then put in the SpeedVac to evaporate the ammonium hydroxide. This is followed by resuspension in

0.1M TEAA. The sequence is then purified using reverse phase HPLC on a C18 column running a gradient of acetonitrile to 0.1M TEAA in HPLC-grade water. This protocol does require some optimization depending on the different constituents of the DNA sequence.

The HPLC separates the full sequence from those sequences that failed during the synthesis procedures. This is an important step as any sequence that has not been properly synthesized can greatly affect future experimental results. For example, if a molecular beacon sequence has been synthesized and some of the sequences have been synthesized without a quencher, that probe will have a much higher background fluorescence. This will limit the sensitivity and signal enhancement of the beacon. Conversely, if a beacon sequence or an aptamer sequence has been synthesized without a fluorophore, its hybridization will not only be undetectable but it will block fluorophore labeled sequences creating a lower response to the target molecule. To illustrate this phenomenon, Figure 2-3 depicts a typical molecular beacon purification. The PDA detector of the HPLC can measure the absorbance spectra on column which allows for the detection of the individual constituents. The DNA portions absorb in the 250nm to 300nm range while the quenchers and fluorophores absorb in their characteristic range. Figure 2-3 shows that there are three major complexes that can be separated, a fluorophore labeled sequence, an unlabeled sequence, and the full probe sequence labeled with a fluorophore and quencher thus highlighting the need for proper purification.

Once the sequence has been properly prepared, it can then be used in experiments or undergo further modification through the conjugation to different nanomaterials, the next section details the preparation and characterization of the nanomaterials used in the work described herein followed by the conjugation schemes used to attach the DNA based probes to the nanomaterials.

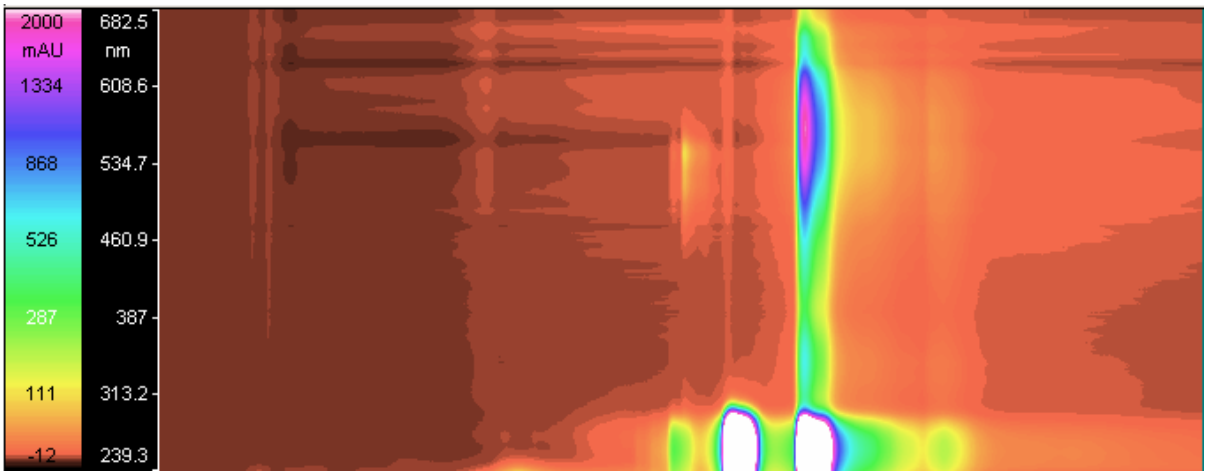

Figure 2-3. Typical chromatograph of a molecular beacon purification using reverse phase HPLC using absorbance for detection.

Nanoparticle Synthesis

In order to separate the target species from complex biological samples, it is often necessary to perform a separation procedure. However, when separating targets as large as cells there are few techniques that can be applied to keep them intact. Centrifugation and magnetic separations are the two most common procedures to cell separations. While centrifugation is a simple and effective method, it does not allow for the selective separation of cells. However, when selective biorecognition elements like aptamers or antibodies are conjugated to magnetic particles, cells can be separated from other cells with good selectivity. Therefore, magnetic nanoparticles were synthesized to enable the selective extraction of the target cells from complex samples. The iron oxide core magnetic nanoparticles were prepared by coprecipitation of iron oxide salts. Solutions of ammonium hydroxide (2.5%) and iron chlorides were added together under nitrogen, and continuously stirred at 350 RPM using a mechanical stirrer for 10 minutes with a final volume of around 255mL. The iron chloride solution was made from ferric chloride hexahydrate (0.5 M), ferrous chloride tetrahydrate (0.25 M), and HCl (0.33 M) at a final volume of approximately 100 mL. The ammonium hydroxide solution was diluted in a 500 mL beaker at

a volume of about 155 mL. The bulk solution of the formed iron oxide nanoparticles was stored as is at room temperature until needed for further experiments.

The problem with iron oxide however is that it is very difficult to conjugate biomolecules to as it lacks any usable functional group and there are difficult to attach to iron oxide. To compensate for this, the iron oxide nanoparticles were coated with silica following the Stober sol gel protocol. To begin, a 6 mL aliquot of the magnetic particle solution was magnetically extracted and washed three times with water and once with ethanol, and the washed samples were suspended in an ethanol solution containing ~1.2 % ammonium hydroxide. The final concentration of the washed particles was around ~7.5 mg/mL, which contained 60 mg of iron oxide in 6 mL of solvent. To this sample, 210μL of tetraethoxyorthosilicate (TEOS) was added and then sonicated for 90 minutes to complete the hydrolysis process to form the silica coating. A postcoating layer of pure silica was created by adding an additional 10μL aliquot of TEOS, and the sample was sonicated for an additional 90 minutes. The resulting silica nanoparticles were magnetically extracted and washed three times with a 6mL aliquot of ethanol to remove excess reactants. The silica coating allows for a large variety of conjugation schemes to be used to prepare the aptamer conjugated nanoparticles.

Next, the fluorophore doped nanoparticles were synthesized. The inorganic fluorophore based nanoparticles like the RuBpy nanoparticles were prepared by the reverse microemulsion method. First, 1.77mL Triton x-100, 7.5mL cyclohexane, 1. mL n-hexanol were added to a 20 mL glass vial with constant magnetic stirring. Then, 400 μL of H_2O and 80 μL of 0.1M tris(2,2' –bipyridyl) dichlororuthenium (II) hexahydrate (Rubpy) dye (MW=748.63) were added, followed by the addition of 100 μL Tetraethyl Orthosilicate (TEOS). After thirty minutes of stirring, 60μL NH_4OH was added to initiate silica polymerization.

Tetramethylrhodamine (TMR SE) and Cy5 doped NPs were synthesized according to the following method: TMR SE and Cy5-NHS were each dissolved in DMSO at a concentration of 5 mg/mL, and (3-aminopropyl)triethoxysilane (APTS) was added at a molar ratio of 1.2:1 APTS:dye. The APTS was allowed to conjugate to the amine reactive dye for 24 h in the dark with shaking prior to synthesis of the particles. Glass reaction vessels and Teflon-coated magnetic stir rods were washed with 1 M NaOH solution for 30 min, rinsed with DI water and ethanol, and allowed to dry. This wash step was performed to clean the glass vessel and stir rods and smooth the inside surface of the glass vessel, which prevents unwanted seeding and NP formation. After conjugation, 4.19 mL of ethanol was mixed with 239 μL of ammonium hydroxide solution in the reaction vessel. A 36 μL volume of TMR-APTS conjugate or 54 μL of Cy5-APTS conjugate was added to the reaction vessels, yielding 3.44×10^{-7} mol of dye/reaction (ratio of 2300 mol of silica/mole of dye). A 177 μL volume of TEOS was added rapidly to the reaction mixture, and the vessels were sealed. The reaction was allowed to proceed for 48 h in the dark before the particles were recovered by centrifugation at 14 000 rpm. The particles were washed three times with phosphate buffer to remove any dye molecules that are weakly bound.

Nanoparticle Characterization. Following the synthesis of the nanoparticle, they still needed characterization to ensure the proper synthesis of the iron oxide nanoparticles and the successful coating with silica. A Hitachi H-7000 transmission electron microscope (TEM) was used to obtain the size and shape of the formed nanoparticles from dried samples. The uncoated magnetite particle were found to be roughly 10 ± 2 nm in diameter, however these particles had poor uniformity in shape. Based on the TEM images, the silica coated nanoparticles had an average diameter of 65 nm and were uniformly spherical in shape. However, the size of silica

coated iron oxide particles was more variable ranging from 30nm to 90nm in diameter. Representative images for each are shown in Figure 2-4.

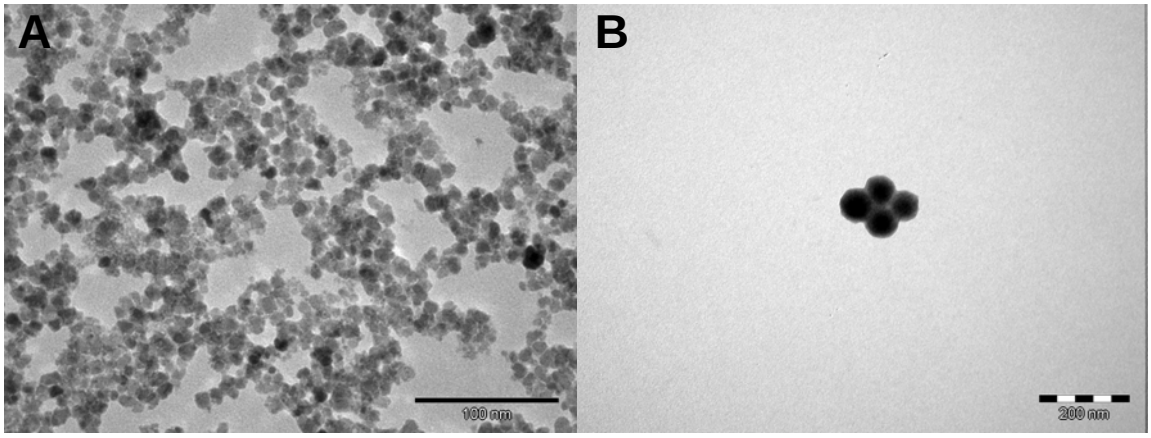

Figure 2-4. TEM images of iron oxide nanoparticle (A) and silica coated iron oxide nanoparticles (B).

Given the difficulty in analyzing samples on the TEM instrument, characterization of the particles was also performed using light scattering for routine characterizations. Light scattering and zeta potential measurements were performed on 1270 Brookhaven Zeta Plus instrument. The light scattering can effectively measure the size of the nanoparticles while the zeta potential is useful for probing the surface charge of the particles and was mainly used for verifying the surface modifications. After synthesis and characterization of the nanoparticles, the nanoparticles need to be functionalized for conjugation to the biomolecules used for recognition. Fluorescent nanoparticles were characterized in a similar fashion although their fluorescence spectra were also analyzed to ensure that the fluorophore was properly encapsulated inside tzhe silica matrix.

Nanoparticle Bioconjugation to DNA

Silica Nanoparticles

Since both types of particles both magnetic and fluorescent were comprised of silica, the same conjugation schemes can be utilized for either type of particle. Two different strategies

were utilized for attaching the biomolecules to the silica nanoparticles. The first involved the use of a biotin/avidin conjugation. For avidin coating, a 0.1 mg/mL Fe_3O_4-SiO_2 (silica coated magnetic nanoparticles) solution and a 5 mg/mL avidin solution were mixed and then sonicated for 5-10 minutes. The mixture was incubated at 4° C for 12-14 hours. The particles were then washed three times with 10 mM phosphate buffered saline (PBS) pH 7.4 and dispersed at 1.2 mg/mL in 10 mM PBS, and the avidin coating was stabilized by cross-linking the coated nanoparticles with 1% glutaraldehyde (1 hour at 25° C). After another separation, the particles were washed three times with 1M Tris-HCl buffer. Then, the particles were dispersed and incubated in the 1M Tris-HCl buffer (3 hours at 4° C), followed by three washes in 20 mM Tris-HCl, 5 mM $MgCl_2$, pH 8.0. In order to verify that the avidin had been coated on the surface, the Zeta potential before and after coating was measured. Prior to the coating step, the silica surface of the nanoparticle had a Zeta potential of -19.59 while after coating the Zeta potential was -4.37. This change in surface charge can be explained by the addition of the positively charged avidin to the surface thus neutralizing the negative charge of the silica surface.

Now that the avidin is on the surface of the nanoparticle, biotinylated DNA sequences can be attached. First the particles are dispersed in 0.2 mg/mL in 20 mM Tris-HCl, 5 mM $MgCl_2$, pH 8.0. Biotin labeled DNA was added to the solution at a concentration of 30 μM. The reaction was incubated at 4° C for 12 hours, and three final washes of the particles were performed using 20 mM Tris-HCl, 5 mM $MgCl_2$ at pH 8.0. With the DNA now attached to the nanoparticle the surface of the nanoparticle is now more negatively charged due to the negative charge of the oligonucleotides. This is reflected in the new Zeta potential for the particle that is now measured at -14.56. Now the DNA conjugated nanoparticle can be used for a variety of different applications.

The other methodology used to conjugate the DNA to the silica nanoparticles involves the functionalized silica nanoparticles and exploiting those functional groups for the attachment of DNA also functionalized with different groups. Typically carboxy groups are added to the nanoparticle surface and amine modified DNA is used to conjugate the DNA to the nanoparticle. However, this basic methodology also works for amine modified nanoparticles with a carboxy or thiol functionalized oligonucleotide or thiolated nanoparticles with thiol or amine modified DNA. To obtain carboxy modified nanoparticles, a post coating step is required.

After the silica polymerization steps, the post coating process begins with adding 50 µL TEOS, 40 µL carboxylethylsilanetriol sodium salt, and 10 µL 3-(Trihydroxyl)propyl methyl phosphonate. At this point, polymerization proceeds for 18 hours, and particles were centrifuged, sonicated, and vortexed four times with 95% ethanol, followed by one wash with H_2O. The silica nanoparticles can then be modified with DNA by adding 1.2 mg EDC, 3.5 mg Sulfo-NHS, and 0.5 nmoles DNA with 2 mg of particles dispersed in 1.5 mL of 10 mM MES buffer (pH= 5.5). The solution is then mixed for three hours. The nanoparticles are then washed by centrifugation at 14000 rpm three times with 0.1 M Phosphate Buffered Saline (PBS) (pH=7.2). The post coating and amine attachment can be verified for either method by again measuring the Zeta potential. After the addition of the carboxy groups on the surface of the nanoparticle, the Zeta potential drops to -43.27 due to the negatively charged carboxy groups. After the amine modification, the Zeta potential increases to -33.31 representing the neutralization of the carboxy groups through the reaction with the positively charged amines. After this process the DNA conjugated silica nanoparticles are ready for use.

Gold Nanoparticles

While the avidin and functionalized silica coatings are quite useful for silica based nanoparticles, a different strategy is required for gold nanoparticles. While either method in

theory could be used, the silica and avidin coating would insulate the gold nanoparticle and prevent its surface plasmons from interacting with other gold nanoparticles. This would prevent the change in spectral properties that makes the gold nanoparticles so useful for detection. Therefore to attach oligonucleotides to gold nanoparticles, the well established gold/thiol based chemistry is utilized to attach the aptamer directly to the nanoparticle surface. In a 2mL microcentrifuge tube, 1mL of the 20nm gold colloid nanoparticles (GNPs), containing $7.0x10^{11}$ particles/mL, taken directly from the manufacturer (Ted Pella, Inc. Redding, CA) was centrifuged for 15 minutes at 14,000 RPM. The GNPs were washed three times with 1mL aliquots of 5mM phosphate buffer (PB) pH 7.5 by decanting the supernatant, adding fresh PB, dispersing by sonication, and centrifuging for 15 minutes at 14,000 RPM. From decantation to dispersion, the wash step was performed within 3-5 minutes. After the final wash step, the GNPs were dispersed in 1 mL of the PB. To each washed GNP sample, 150μL of a 1μM thiol labeled DNA sequence was incubated for 3-5 days at 4ºC. The samples were sonicated to disperse the GNPs every 12 hours. When the incubations were completed, the samples were centrifuged at 14,000 RPM for 5 minutes and the samples washed as described previously with the PB. After the final wash, each GNP sample was dispersed in 0.25mL PB with approximately $6.0x10^{11}$ particles, and the samples stored at 4ºC until used.

Conclusion

By following these various synthetic protocols, biofunctionalized nanoparticles can be constructed for a wide array of applications. Nanomaterials for magnetic separations, fluorescent detection, or colorimetric detection can then applied to the collection and detection of a variety of biomolecules such as proteins, peptides, DNA, RNA, or even entire cells. The next two chapters will focus on using the nanomaterials for the detection of cancer cells through both fluorescent and colorimetric detection. Chapter 3 will focus on the use of two different types of

nanoparticles to accomplish both the collection of the cells and their detection. This approach uses the magnetic nanoparticles to magnetically separate the cells of interest while fluorescent nanoparticles enable their sensitive detection. Then, Chapter 4 will demonstrate the use of gold nanoparticles for a colorimetric assay for cancer cell detection. After detection of the cells, further analysis of cancer cells will be demonstrated using other DNA based probes thus illustrating the investigatory power of nanomaterials combined with DNA based probes.

CHAPTER 3
TWO PARTICLE ASSAY FOR THE COLLECTION AND ENRICHMENT OF TARGETED CANCER CELLS

Introduction and Scheme

In the previous chapter, the synthesis and bioconjugation schemes were detailed for the preparation of aptamer conjugated nanoparticles for the detection of cancer cells. The majority of cancers including lung cancer arise from epithelial surfaces. Often as the tumors develop, they exfoliate cells spontaneously into bodily fluids like blood and sputum. These cancerous cells often contain genetic or molecular abnormalities, but most of these abnormalities are not clearly defined and there are essentially no biomarkers that can distinguish them from normal cells. The exfoliated cells are generally far outnumbered by normal cells in bodily fluids especially during the early development of the disease when it is most treatable. Therefore a technology that is able to collect, enrich, and preserve abnormal cells from bodily fluids could greatly assist cancer diagnosis and the discovery of biomarkers while allowing earlier detection of the disease.

To accomplish the collection and detection of cancer cells from bodily fluids, we have used a group of aptamers for specific cancer cells and then conjugated the aptamers to nanoparticles to allow not only the collection, enrichment, and preservation of the cancer cells, but also the rapid detection of the cancer cells directly from bodily fluids. The method involves the use of two separate aptamer-conjugated nanoparticles, one magnetic nanoparticle and one fluorescent nanoparticle. The magnetic nanoparticle allows for the collection and enrichment of the cancer cells while the fluorescent nanoparticle clearly marks the cell for fluorescence detection. The overall strategy is schematically shown below. While many magnetic extraction techniques also collect non-target cells through non-specific interactions, the use of the second fluorescent nanoparticle offers a second level of discrimination. This is because only the target cells will have high fluorescence intensity from being covered with the aptamer-conjugated

fluorescent nanoparticles and the unbound fluorescent nanoparticles will be washed away during the magnetic extraction. Thus, the use of the two different types of nanoparticles gives the assay the ability for the efficient collection characteristic of the magnetic nanoparticles while the fluorescent nanoparticles enable the sensitive detection of the cells.

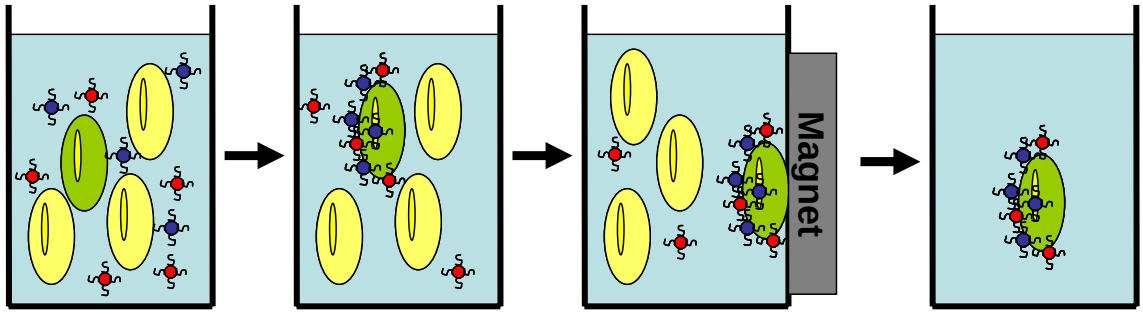

Figure 3-1. Schematic representation of the two particle assay. In the assay, the magnetic (blue) and fluorescent (red) nanoparticles bind to the target cell. After a magnetic field is applied the magnetic nanoparticles immobilize the target cells and any bound fluorescent nanoparticles while the unbound cells and fluorescent nanoparticles are washed away.

Methods and Materials

All materials were purchased from Sigma-Aldrich (St. Louis, MO) unless other noted. Whole blood samples were obtained from Research Blood Components, LLC (Brighton, MA). Fluo-4 was purchased from Molecular Probes (Eugene, OR), and carboxylethylsilanetriol sodium salt was purchased from Gelect, Inc. (Morrisville, PA). N-hydroxysulfosuccinimide (Sulfo-NHS) and 1-Ethyl-3-[3-dimethylaminopropyl] carbodiimide Hydrochloride (EDC) were purchased from Pierce Biotechnology, Inc.(Rockford, IL). Hydrochloric acid and Ammonium Hydroxide were obtained from Fisher Scientific.

DNA Aptamer Synthesis.

The following aptamers have been selected for the CCRF-CEM, Ramos, and Toledo cells respectively: 5'-TTT AAA ATA CCA GCT TAT TCA ATT AGT CAC ACT TAG AGT TCT

AGC TGC TGC GCC GCC GGG AAA ATA CTG TAC GGA TAG ATA GTA AGT GCA ATC T-3'; 5'-AAC ACC GGG AGG ATA GTT CGG TGG CTG TTC AGG GTC TCC TCC CGG TG-3'; 5'-ATA CCA GCT TAT TCA ATT ATC GTG GGT CAC AGC AGC GGT TGT GAG GAA GAA AGG CGG ATA ACA GAT AAT AAG ATA GTA AGT GCA ATC T-3'. Both the amine and biotinylated versions of the aptamer sequencers were synthesized in-house. An ABI3400 DNA/RNA synthesizer (Applied Biosystems, Foster City, CA) was used for the synthesis of all DNA sequences. A ProStar HPLC (Varian, Walnut Creek, CA) with a C18 column (Econosil, 5u, 250 × 4.6 mm) from Alltech (Deerfield, IL) was used to purify all fabricated DNA. A Cary Bio-300 UV spectrometer (Varian, Walnut Creek, CA) was used to measure absorbencies to quantify the manufactured sequences. All oligonucleotides were synthesized by solid-state phosphoramidite chemistry at a 1 μmol scale. The completed sequences were then deprotected in concentrated ammonia hydroxide at 65 °C overnight and further purified twice with reverse phase high-pressure liquid chromatography (HPLC) on a C-18 column.

Fluorescent Nanoparticle Synthesis

Dye doped nanoparticles were synthesized by the reverse microemulsion method.[21] First, 1.77 mL Triton x-100, 7.5 mL cyclohexane, 1.6 mL n-hexanol were added to a 20 mL glass vial with constant magnetic stirring. Then, 400 μL of H_2O and 80 μL of 0.1M tris(2,2' –bipyridyl) dichlororuthenium (II) hexahydrate (RuBpy) dye (MW=748.63) were added, followed by the addition of 100 μL Tetraethyl Orthosilicate (TEOS). After thirty minutes of stirring, 60μL NH_4OH was added to initiate silica polymerization. After 18 hours, the carboxyl modified silica post-coating was initiated by adding 50 μL TEOS, 40 μL carboxylethylsilanetriol sodium salt, and 10 μL 3-(Trihydroxyl)propyl methyl phosphonate. Polymerization proceeded for 18 hours, and particles were centrifuged, sonicated, and vortexed four times with 95% ethanol, followed by

one wash with H_2O. Carboxyl functionalized RuBpy nanoparticles were modified with DNA by adding 1.2 mg EDC, 3.5 mg Sulfo-NHS, and 0.5 nmoles DNA with 2 mg of particles dispersed in 1.5 mL of 10 mM MES buffer (pH= 5.5). The solution was then mixed for three hours. Particles were then washed by centrifugation at 14000 rpm three times with 0.1 M Phosphate Buffered Saline (PBS) (pH=7.2). RuBpy nanoparticles were stored at room temperature and were dispersed in cell media buffer at a final concentration of ~10 mg/mL.

Tetramethylrhodamine (TMR SE) and Cy5 doped NPs were synthesized according to the following method: TMR SE and Cy5-NHS were each dissolved in DMSO at a concentration of 5 mg/mL, and (3-aminopropyl)triethoxysilane (APTS) was added at a molar ratio of 1.2:1 APTS:dye. The APTS was allowed to conjugate to the amine reactive dye for 24 h in the dark with shaking prior to synthesis of the particles. Glass reaction vessels and Teflon-coated magnetic stir rods were washed with 1 M NaOH solution for 30 min, rinsed with DI water and ethanol, and allowed to dry. This wash step was performed to clean the glass vessel and stir rods and smooth the inside surface of the glass vessel, which prevents unwanted seeding and NP formation. After conjugation, 4.19 mL of ethanol was mixed with 239 μL of ammonium hydroxide solution in the reaction vessel. A 36 μL volume of TMR-APTS conjugate or 54 μL of Cy5-APTS conjugate was added to the reaction vessels, yielding 3.44×10^{-7} mol of dye/reaction (ratio of 2300 mol of silica/mole of dye). A 177 μL volume of TEOS was added rapidly to the reaction mixture, and the vessels were sealed. The reaction was allowed to proceed for 48 h in the dark before the particles were recovered by centrifugation at 14 000 rpm. The particles were washed three times with phosphate buffer to remove any dye molecules that are weakly bound. The synthesis method was found to reproducibly produce a number average particle size of 50

nm ± 5 nm with a monomodal distribution when measured with a Honeywell UPA 150 dynamic light scattering instrument.

Magnetic Nanoparticle Synthesis

The iron oxide core magnetic nanoparticles[32] were prepared by means of precipitating iron oxide by mixing ammonia hydroxide (2.5%) and iron chloride at 350 RPM using a mechanical stirrer (10 minutes). The iron chloride solution contains ferric chloride hexahydrate (0.5 M), ferrous chloride tetrahydrate (0.25 M), and HCl (0.33 M). After three washes with water and once with ethanol, an ethanol solution containing ~1.2 % ammonium hydroxide was added to the iron oxide nanoparticles, yielding a final concentration of ~7.5 mg/mL.

To create the silica coating for the magnetite core particles, tetraethoxyorthosilicate (200 μL) was added, and the mixture was sonicated for 90 minutes to complete the hydrolysis process. For post coating, an additional aliquot of TEOS (10 μL) was added and additional sonication was performed for 90 minutes. The resulting nanoparticles were washed three times with ethanol to remove excess reactants.

For avidin coating, a 0.1 mg/mL Fe_3O_4-SiO_2 (silica coated magnetic nanoparticles) solution and a 5 mg/mL avidin solution were mixed and then sonicated for 5-10 minutes. The mixture was incubated at 4° C for 12-14 hours. The particles were then washed three times with 10 mM phosphate buffered saline (PBS) pH 7.4 and dispersed at 1.2 mg/mL in 10 mM PBS, and the avidin coating was stabilized by cross-linking the coated nanoparticles with 1% glutaraldehyde (1 hour at 25° C). After another separation, the particles were washed three times with 1M Tris-HCl buffer. Then, the particles were dispersed and incubated in the 1M Tris-HCl buffer (3 hours at 4° C), followed by three washes in 20 mM Tris-HCl, 5 mM $MgCl_2$, pH 8.0.

DNA was attached to the particles by dispersing the particles at 0.2 mg/mL in a buffer of 20 mM Tris-HCl and 5 mM $MgCl_2$ at a pH 8.0. Biotin labeled DNA was added to the solution at a concentration of 31 μM. The reaction was incubated at 4° C for 12 hours, and three final washes of the particles were performed using 20 mM Tris-HCl, 5 mM $MgCl_2$ at pH 8.0. Magnetic nanoparticles were used at a final concentration of ~0.2 mg/mL and stored at 4° C before use.

Cell Culture

CCRF-CEM cells (CCL-119 T-cell, human acute lymphoblastic leukemia), Toledo cells (CRL-2631, non-Hodgkin's B cell lymphoma) and Ramos cells (CRL-1596, B-cell, human Burkitt's lymphoma) were obtained from ATCC (American Type Culture Association). The cells were cultured in RPMI medium supplemented with 10% fetal bovine serum (FBS) and 100 IU/mL penicillin-Streptomycin. The cell density was determined using a hemocytometer prior to any experiments. After which, approximately one million cells dispersed in RPMI cell media buffer were centrifuged at 920 rpm for five minutes and redispersed in dye free cell media three times, and were then redispersed in 5 mL dye free cell media. During all experiments, the cells were kept in an ice bath at 4^oC.

Two Particle Assay Methodology

Approximately 105 of the cells were obtained in individual test tubes. To each cell sample, 5 μL of the MNP solution was added, and the mixture was incubated for 15 min. After incubation, the cells were washed by magnetic extraction with 200 μL of fresh cell media three times and resuspended in 200 μL of the media buffer. The wash was performed by removal of the supernatant and addition of fresh buffer, and the sample was resuspended in the fresh buffer typically within 3-5 min. To complete the stepwise process, 2 μL of FNPs was added and incubated for 5 min. The concentration of MNPs to FNPs in the samples was 2:1. Again, the

sample was washed three times with 200 μL of cell media as described previously and then dispersed in 20 μL of media for imaging and microplate reader analysis.

Fluorescence Imaging.

All cellular fluorescent images were collected using the confocal microscope setup. The confocal consists of an Olympus IX-81 automated fluorescence microscope with a Fluoview 500 confocal scanning unit. There are three lasers providing laser excitation at 458nm, 488nm, 514nm, 543nm, and 633nm. The TMR nanoparticles were excited at 543nm and collected at 570nm. Cy5 nanoparticles were excited at 633nm and collected at 660nm. RuBpy nanoparticles were excited at 488nm and the emission was collected at 610nm. Images were taken after a five to ten second period during which the instrument was focused to yield the highest intensity from the fluorescence channels. The images were assigned color representations for clarity and are not indicative of the actual emission wavelengths.

Flow Cytometry

Fluorescence measurements were also made using a FACScan cytometer (Becton Dickinson Immunocytometry Systems, San Jose, CA). To support imaging data, RuBpy fluorescence of pure samples initially containing 10^5 cells were measured by counting 30000 events. Cell experiments were performed exactly as stated for imaging experiments, except all solutions were diluted to a final volume of 200 μL. Cell sorting allowed for accurate quantitative analysis of cell samples, as well as a platform for collection efficiency determination.

Plate Reader Measurements

Fluorescence measurements were taken using a Tecan Safire Microplate Reader in a 384 well small volume plate. 20μL aliquots from each sample were deposited in the well and sample fluorescence intensity at defined wavelengths were measured at a constant gain at 5nm slit widths. TMR based nanoparticles were excited with 550nm light and its emission was measured

at 575nm. RuBpy nanoparticles were excited at 458nm and its emission was measured at 610nm. Cy5 was excited at 640nm and its emission was detected at 670nm.

Two Particle Assay Proof of Concept

The first in evaluating the assay was simply trying to extract the target cells and ensure that both the magnetic and fluorescent nanoparticles were binding to the target cells. Additionally, it was similarly important that the particles not bind to the control cells. If the assay was going to function well enough for any future clinical analysis it needed above all to be as selective as possible as the targeted cells in a clinical sample would be overwhelmed by non-target cells and other species. Sensitivity is also a secondary concern however with the magnetic extraction larger initial sample volumes could always to be used to detect a clinically relevant level of cells. To demonstrate the concept of our two particle based magnetic collection and detection methodology, individual CEM and Ramos cell samples were analyzed according to our two particle protocols, followed by fluorescent imaging and analysis using flow cytometry. Before nanoparticle incubation, cells were dispersed in 500 μL cell media buffer and centrifuged three times at 920 rpm for five minutes, and were then redispersed in 200 μL media buffer. Fluorescent and magnetic nanoparticle solutions were then added to the cell samples using excess of the fluorescent nanoparticles. After a five minute incubation with the nanoparticles, the cells were magnetically extracted and washed with 500 μL of buffer three times, and redispersed in 20 μL buffer for imaging and 200 μL buffer for flow cytometric analyses respectively. All pure sample experiments started with 1.0×10^5 - 5.0×10^5 cells before nanoparticle incubation. Each pure cell extraction was repeated 10 times. Figure 3-2A shows representative confocal images of 2 μL aliquots of target cells after five minute incubation and three magnetic extractions and Figure 3-2B shows the results for the control cells after the same treatment.

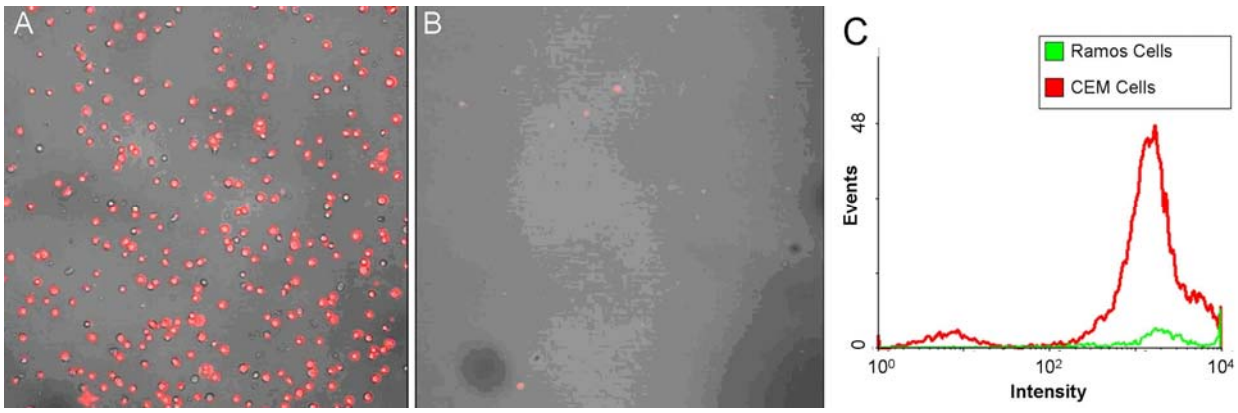

Figure 3-2. Images of extracted samples from (A) target cells and (b) control cells, and (C) flow cytometric comparison of target and control signal after 5 minute incubation with magnetic and fluorescent nanoparticles, followed by three washes by magnetic separation.

There is a noticeable change in both the amount of cells present and fluorescent signal between the extracted cell solutions. Magnetic collection pulled out few control cells, while a significant number of target cells were extracted using the same procedures. In addition, the few control cells inadvertently collected by magnetic extractions were labeled with few RuBpy nanoparticles and had no significant fluorescent signal. Conversely, the target CEM cells that were subjected to the assay had very intense fluorescent signals that made them easily distinguishable from the control cells. The flow cytometric analysis of the pure sample assay, Figure 3C confirms that fewer control cells were collected than target cells, and the control cells showed less fluorescent emissions than the extracted target cells. Thus, the selectivity of the assay appears to be very good and if the assay can perform similarly on more complex samples the assay could prove quite useful for clinical samples. With the initial proof of concept demonstrated, the next series of experiments will focus primarily on validation and characterization of the assay.

Characterization of the Two Particle Assay

Dye and Nanoparticle Fluorescent Intensity Comparison

The rationale for using the fluorescent nanoparticles was to increase the amount of fluorescence signal thus making the assay more sensitive than using simply fluorophore labeled aptamers. Since the fluorescent nanoparticles incorporate thousands of individual fluorophores it should have a significantly higher intensity than a single fluorophore. However since fluorophores are known to self quench and the larger nanoparticles may block some of the binding sites for other nanoparticles it was unclear the actual level of enhancement that would be obtained by using the nanoparticles. To demonstrate the fluorescence enhancement capabilities of RuBpy doped nanoparticles, individual RuBpy probes were linked with our DNA aptamer and directly compared to RuBpy Nanoparticle-aptamer conjugates after immobilization on our target cells. Equal concentrations of magnetic and RuBpy nanoparticles (0.5 nM) were incubated with CEM cells, then washed by magnetic extraction with 500 μL media buffer three times, and redispersed in 20 μL buffer for imaging and 200 μL buffer for flow cytometric analysis. Figure 3-3A and 3-3B compare cell extractions labeled with fluorescent nanoparticles to extractions labeled with RuBpy dye. There is a significant difference in the amount of fluorescent signal seen in the two images. Flow cytometry was used to verify that the RuBpy nanoparticles provide enhanced fluorescence signal, and Figure 3-3C confirms over a 100-fold enhancement of RuBpy nanoparticle labeled cells to RuBpy dye labeled cells. This figure also shows the nanoparticle labeled cells in an apparent bimodal distribution. While the exact cause of this pattern is unknown possible explanations include the formation of nanoparticle aggregates, the formation of cell/nanoparticle aggregates, different levels of receptors on cells, or simply an artifact of the experimental method used. Nonetheless the experiment illustrates the significant advantage that the fluorescent nanoparticles possess over single fluorophores.

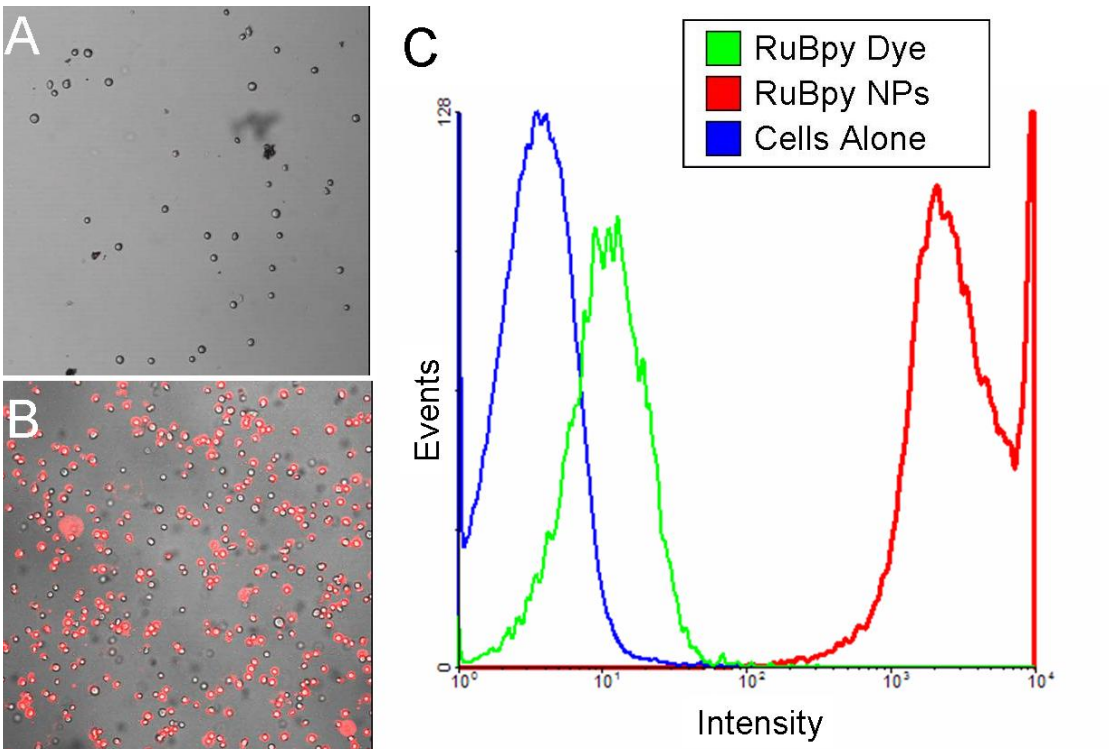

Figure 3-3. Fluorescence images of extracted samples after five minute incubation with (A) 40 µM RuBpy Dye-aptamer conjugates, and (B) 0.5 nM RuBpy nanoparticle-aptamer conjugates, followed by three magnetic washes. (C) Comparison of dye labeled cells to nanoparticle labeled cells by flow cytometric analysis.

Collection Efficiency

While magnetic nanoparticles have been successful in our lab in extracting DNA and proteins, no one had yet attempted using magnetic nanoparticle for detecting something as large as a cell. Therefore we wanted to verify that the nanoparticles could effectively extract the target cells from the samples. Values for the collection efficiency were obtained by incubating increasing amounts of magnetic nanoparticles with the target CEM cells and Ramos control cells. The number of cells collected was determined by flow cytometry by the counting of signal events. In addition, the cell counting was performed on a control sample of both cell types that did not undergo the magnetic extraction and was taken as the total amount of the cells. The

collection efficiency was calculated by dividing the number of events for each sample by the total cell number.

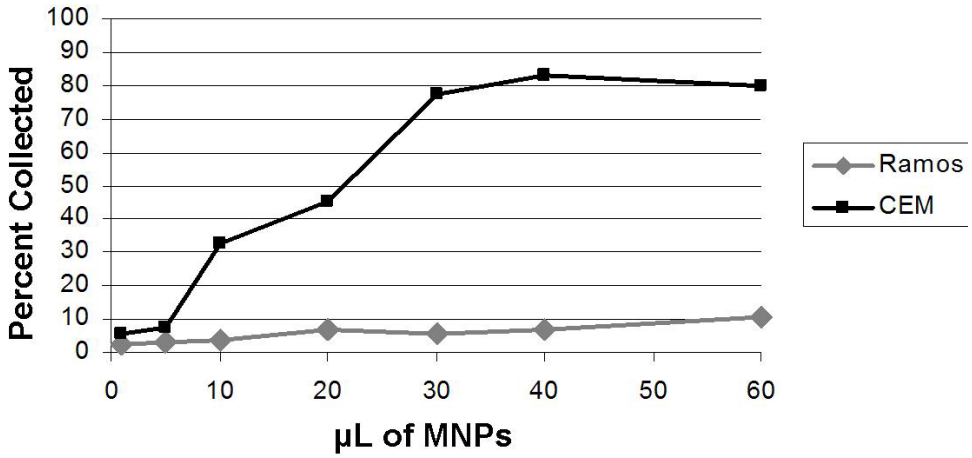

Figure 3-4. Flow cytometric determination of magnetic nanoparticle collection and separation efficiencies between target and control cells.

As seen in figure 3-4, the collection efficiency of target cells from ranges from 30-80%, however the collection efficiency seems to plateau at around 80%. In addition, the Ramos control cells had collection efficiencies ranging from 0.5-5% for the same magnetic nanoparticle concentrations. This indicates that the target cells can be preferentially extracted from a sample, while few of the Ramos cells are extracted using the same method. Since the use of 10µL of magnetic nanoparticles had the highest separation efficiency, this amount was used for sample assay experiments.

Enrichment Validation

In order to verify that the samples were indeed being enriched, several samples were extracted and then resuspended in varying amounts of buffer. Samples were extracted using the previously mentioned protocols with only the final volume changing. After resuspension the samples were analyzed on the plate reader to compare their fluorescence intensities. Figure 3-5 shows the results of these experiments normalized to the highest intensity. The results indicate

that the volumetric based enrichment succeeded in enriching the samples. When the cells were resuspended in the original volume of the sample, the cells had the lowest overall fluorescence while suspended in 50 times less buffer resulted in 48.7 fold increase in fluorescence intensity. Other suspension volumes had a similar linear enrichment compared to the original sample volume. Thus the results clearly show the cell samples can be enriched through the magnetic separation and resuspension process.

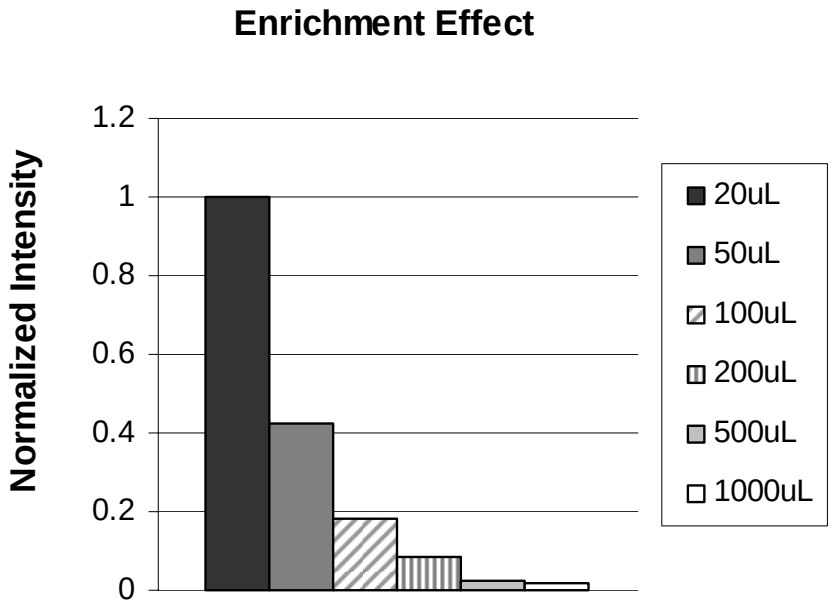

Figure 3-5. In order to validate the enrichment effect of the magnetic extraction, samples were resuspended in different volumes and their fluorescence intensities were measured.

Limit of Detection

An important consideration for the assay is the limit of detection (LOD). While larger volumes of any clinical samples could be used to increase the total amount of cells, it is still necessary to determine the absolute amount of cells that can be reliably detected so that the volume needed for clinical samples can be known. The LOD was determined using pure cell samples and the extractions were performed as described previously. The limit of detection threshold was taken to be three standard deviations above the blank, and because of this any

residual fluorescence in the blank was accounted for. The LOD was performed using CEM target cells. Each of the samples was then analyzed with NPs using the previously mentioned protocols with the fluorescence intensity being determined on the microplate reader following completion of the ACNP technique.

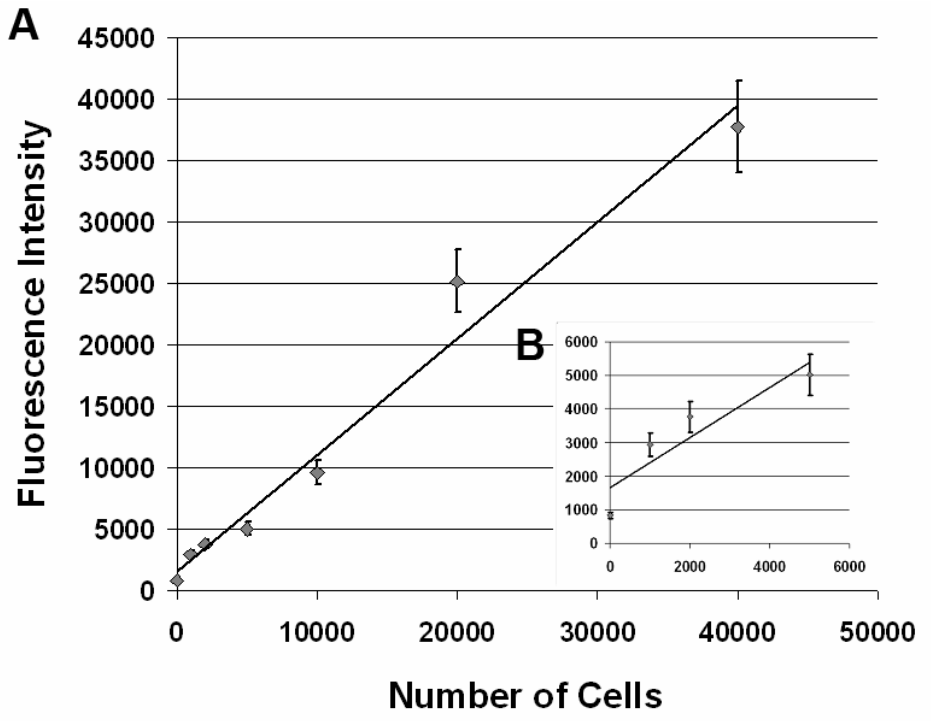

Figure 3-6. Limit of detection for the stepwise addition of the MNP and FNP using the microplate reader for detection **A)** the full calibration curve and **B)** an enlarged depiction of the lower concentration regime.

The detection limit was computed by plotting the fluorescence intensity versus the cell number present in the sample. Consequently, the plotted data produced a linear response as seen in Figure 3-6A and Figure 3-6B displays the data focused in on the lower sample concentrations. From this plot the detection limit was determined to be approximately 250 cells with a dynamic range covering more than two orders of magnitude. This indicates that the ACNP system has the ability to sensitively detect low amounts of intact targets cells from a given sample, and that a wide range of cell concentrations can be analyzed by this method with little to no sample

preparation depending on the amount of ACNPs used. Estimates of exfoliated cancer cells in bodily fluids such as blood put the number of cancer cells at around 20 cells per mL indicating that clinical samples of 15-20 mL would be required for analysis. That is roughly the amount of blood collected in a single vial for normal diagnostic testing.

Improving LOD with Multiple Aptamers

One of major advantages of the Cell-SELEX methodology is that once the selection is complete there is generally a panel of different aptamer sequences that are specific for the cells of interest. Since the cells are a living biological system unto themselves, it is very possible that some of the aptamer targets on the surface will have a higher or lower expression depending on different circumstances like their cell cycle, overall health, or genetic stochasticity. Thus, in some cells the target for a single aptamer may be downregulated resulting in a worse limit of detection. In addition, since the fluorescent and magnetic nanoparticles have the same aptamer, they must compete for binding sites which can also reduce the sensitivity of the assay. In order to address this possibility, magnetic nanoparticles were prepared with different aptamer sequences. In all four different magnetic nanoparticles were compared corresponding to one, two, three, and four different aptamer sequences conjugated to the nanoparticle. Figure 3-7A shows the intensity of the same amount of target cells with each type of magnetic nanoparticle. The results indicate that increases the number of different sequences on the nanoparticle, increases the fluorescent signal from the sample. This increase in signal likely results from two different phenomena, more cells being collected and more fluorescent nanoparticles being bound to the cells since there is less competition for the binding sites. To determine whether the increase in intensity results in an increase in the limit of detection the one and four aptamer nanoparticles were directly compared. Using varying amounts of target cells, calibration curves were prepared for the one and four aptamer nanoparticles. Based on the calibration curves the

four aptamer magnetic nanoparticles had a limit of detection of 85 cells while the one aptamer nanoparticles had a limit of detection of 250 cells. While the increases in the intensity and limit of detection were not overwhelming, it is important to consider that the samples used cultured cells. The cultured cells would likely have less variation than the cells from different patients. Therefore, the multiple aptamer nanoparticles would likely be far more effective using actual patient samples than the results here indicate.

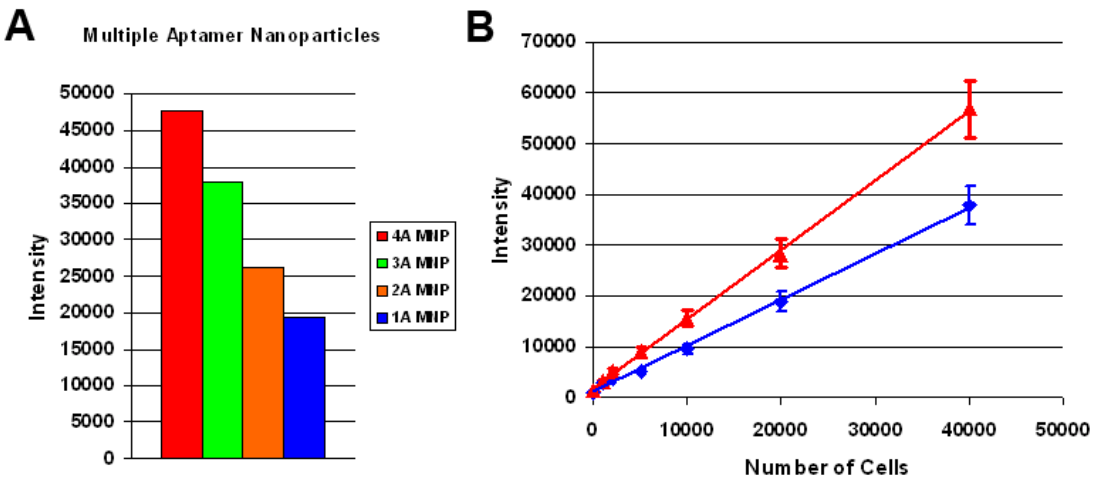

Figure 3-7. Comparison of magnetic nanoparticle with multiple aptamer sequences conjugated to the surface. A) The fluorescent intensities of 30,000 cells with the different magnetic nanoparticles. B) Calibration curves of the one and four aptamer magnetic nanoparticles.

Separations from Complex Samples

Mixed Cell Sample Assays

In order to evaluate the potential of the assay, complex samples needed to be tested to determine extraction and detection capabilities in complex matrices. Rather than start out with very complex biological samples, first samples were prepared by simply mixing different cultured cell lines together. In Figure 3-8, we show the results from our artificial complex sample where equal amounts of CEM and Ramos cells were mixed and our two particle assay was

applied. To differentiate CEM from Ramos cells, Fluo-4, a fluorescent calcium ion indicator, was used to label Ramos cells prior to nanoparticle incubation.

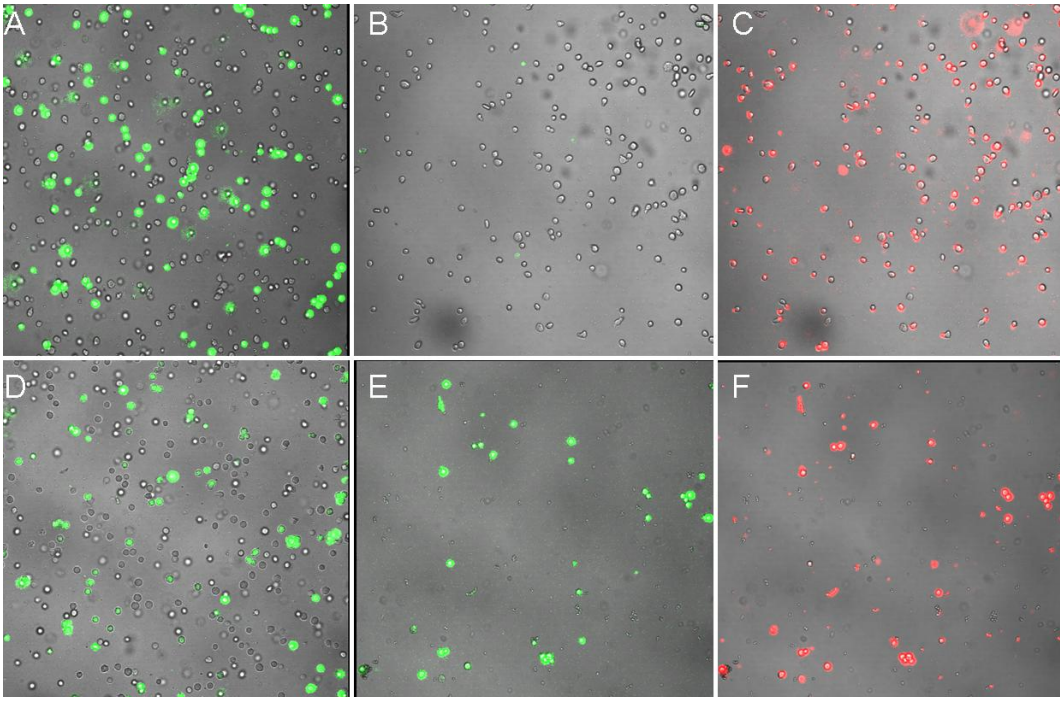

Figure 3-8. Fluorescence Images of A) 1:1 ratio of target cells mixed with Fluo-4 stained control cells. B) Fluo-4 signal, and C) RuBpy signal after 5 minute, two particle incubation and three magnetic washes of the mixture in 3A. D) 1:1 ratio of Fluo-4 stained target cells mixed with control cells. E) Fluo-4 signal, and F) RuBpy signal after 5 minute, two particle incubation and three magnetic washes of the mixture in 3D.

Fluo-4 labeled control cells were mixed in a one to one ratio with unlabeled CEM cells shown in Figure 3-8A. Magnetic and fluorescent nanoparticles were simultaneously added and incubated at 4ºC for five minutes with occasional gentle stirring. After incubation, a magnetic field was applied to remove cells which were not attached to the aptamer labeled iron oxide particles. A 2 µL aliquot of the extracted sample was then illuminated to monitor Fluo-4 and RuBpy fluorescence as shown in Figure 3-8B and 3-8C, respectively. Based on the images, the assay was able to collect the CEM cells in the sample and bright fluorescence from the RuBpy nanoparticles made them easily distinguishable. The experiment was also performed by labeling CEM cells with Fluo-4 and mixing them with unlabeled control cells as in Figure 3-8D. The

cells shown in Figure 3-8E were separated by the two particle assay, and all exhibit a Fluo-4 signal. In Figure 3-8F, the same cells are shown with the RuBpy emission overlaid. The presence of the Fluo-4 fluorescence proves that only the CEM cells were collected and imaged. The lack of Fluo-4 signal in Figure 3-8B, along with the presence of the Fluo-4 signal in Figure 3-8E prove that only target cells are being collected using this method for extractions from 1:1 cell mixtures. These samples were repeated 5 times with similar results achieved for each experiment.

Bone Marrow Samples

Since leukemia cell samples were predominantly used for the verification of this methodology, we also sought to test the performance of the assay in bone marrow samples from actual patients. In these experiments bone marrow aspirates were obtained from the Pathology department of Shands Hospital. The bone marrow samples were from healthy patients and the target cells were then spiked in the bone marrow sample and analyzed followed the established procedures. The results were then analyzed using fluorescence microscopy and the plate reader with the results from the experiment shown in Figure 3-9. The imaging results clearly show that the target cells were extracted from the complex sample. In the unspiked sample, few cells were extracted although some cellular debris was pulled out. In the plate reader results that measured the fluorescence intensity of the entire sample, there is a clear difference between the spiked and unspiked samples. This indicates that the two particle assay is indeed capable of being used even in bone marrow aspirates.

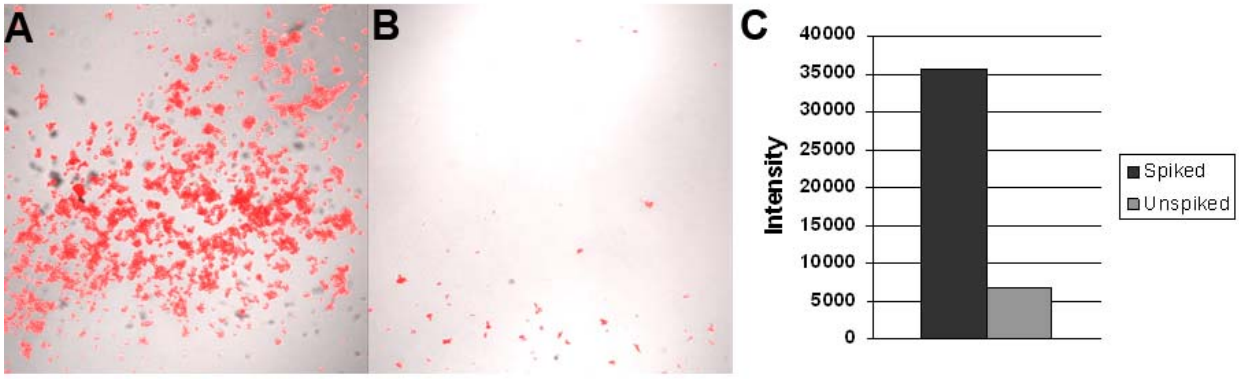

Figure 3-9. A) Extraction of target cells from a spiked bone marrow sample. B) Extraction performed on an unspiked bone marrow sample. C) Fluorescence measurements from the spiked and unspiked bone marrow samples.

Whole Blood Sample Assays

Blood samples were also used to determine detection capabilities from complex biological solutions. Control experiments indicated that the aptamer sequence used was stable in serum samples for up to 2 hours. Target cells were spiked into whole blood samples (500 µL) and compared to unspiked samples after magnetic extraction to make certain that target cells could be detected in complex biological samples. As shown in Figure 3-10, nonspecific interactions caused the unwanted collection of some red blood cells, but the lack of RuBpy fluorescent signal on the unwanted cells allows for target cells to still be accurately distinguished. For magnetic extractions from whole blood samples, 40% of the spiked target cells were routinely recovered after three magnetic washes and after accounting for dilution. This is consistent with current extraction efficiency values reported by immunomagnetic separation.[201,202] These experiments were repeated for total of five times with similar results being obtained in each sample. This experiment was meant to mimic a real clinical sample which normally would contain thousands of different species. By successfully extracting our target cell line from whole blood, we have shown that this method is applicable for biomolecular and cellular detection in real clinical applications. Our assay selectively removes our target cells from

this complex mixture with collection efficiencies rivaling or surpassing current methods for cellular detection from clinical samples.

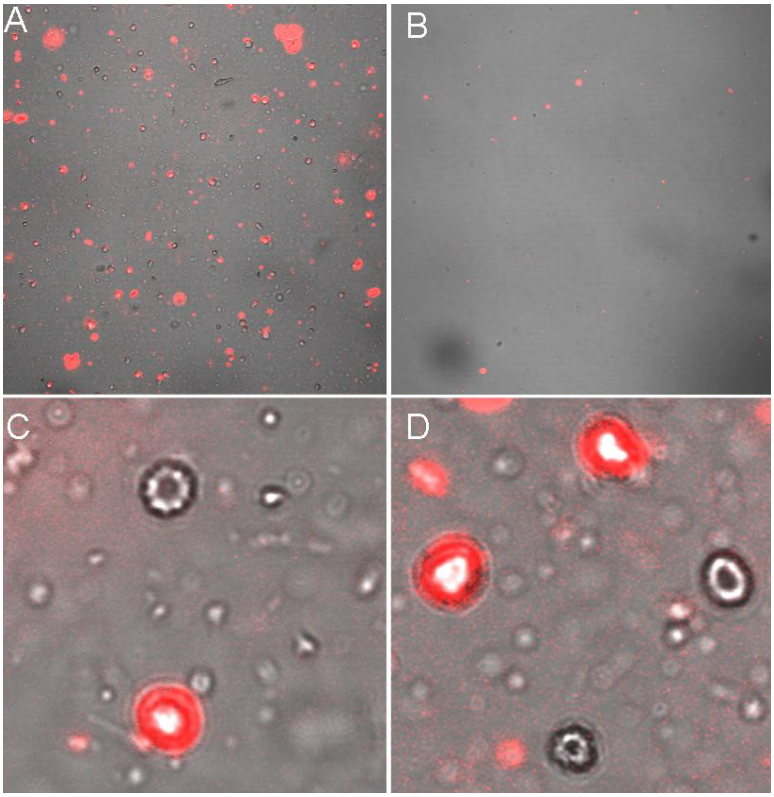

Figure 3-10. Confocal images of extractions from whole blood. (A) Extracted sample from target cell spiked whole blood. (B) Extraction from unspiked whole blood. (C) and (D) show magnified images of extracted cells from 4(A).

Collection and Detection of Multiple Cancer Cells

Instrumental Validation

The first step detecting multiple cell types was first optimizing the confocal microscope and plate reader settings to ensure that the different cell samples could be detected reliably and without any crosstalk between channels. In order to accomplish this, 1μM samples of different fluorophores were analyzed on both instruments in order to determine which fluorophores could be best detected. The samples were first analyzed on the plate reader as it was decided that demonstrating this more complex methodology on a simple instrument would illustrate the wide

applicability of the technique. Figure 3-11 shows the plate reader results for six different fluorophores. Each fluorophore was measured at its excitation and emission maximum in addition, each fluorophore was measured at the excitation and emission maximum of the five other fluorophores. This would determine the amount of crosstalk that existed.

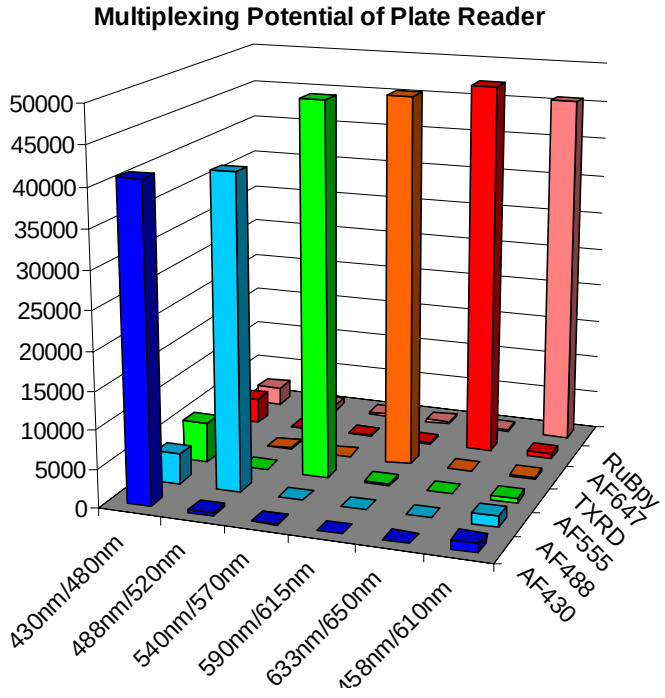

Figure 3-11. Plate reader measurements of multiple dyes to test spectral compatibility. The excitation and emission wavelengths used in each channel are listed on the x-axis while the fluorophore measured is listed on the y-axis.

The results indicate that five of the fluorophores are still candidates for further consideration with only the Alexa Fluor 430 showing an unacceptable amount of crosstalk. Next the fluorophores were evaluated on the confocal microscope in a similar format with 2µL aliquots of each fluorophore solution being placed onto a microscope slide. The fluorescence intensity of each drop was measured with five different optical channels optimized for each individual fluorophore. In these tests, only the Texas Red fluorophore was eliminated due to the difficulty in its detection. The microscope could not efficiently excite the fluorophore so it was removed from further consideration. Since only three fluorophores were needed for the three

available aptamer sequences, RuBpy, Cy5, and TMR were selected for use. FAM based nanoparticles had proved rather difficult to synthesize so the experiments went forward with the best fluorescent nanoparticles for the most sensitive detection.

Single Cell Type Extractions

As it is unlikely that a single aptamer would be able to recognize every patient's cancer cells it is likely that multiple aptamer sequences will be require to obtain a reliable diagnosis using the two particle assay. In addition, obtaining the profiling information may prove advantageous in the future for making a more specific diagnosis and staging the progression of the disease. To expand the concept of the two particle-based magnetic collection and detection technique three different cancer cell lines were analyzed using three different aptamer sequences. Each aptamer was selective for a different cell type. CEM, Ramos, and Toledo cell samples were extracted using ACNPs followed by fluorescent imaging and analysis by the microplate reader. Each pure cell sample extraction was repeated 10 times. As was mentioned in the methods section, the control cells used for the CEM experiments were the Ramos and Toledo cell types, for Ramos were the CEM and Toledo, and for the Toledo were the CEM and Ramos. Figure 3-12 shows representative confocal images of 2 μL aliquots of the CEM target cells (top) and Ramos nontarget cells (bottom) using CEM ACNPs (red) (A), Toledo target cells (top) and CEM nontarget cells (bottom) using Toledo ACNPs (green) (B), and Ramos target cells (top) and CEM nontarget cells (bottom) using Ramos ACNPs (blue) (C) after NP incubations and magnetic washes. Ramos, CEM, and CEM cells were used as the respective controls for those experiments. The other control cell types were also performed and resulted in similar responses as the one presented in the representative images. In addition, some fluorescence spots were observed in the images. However when the samples were analyzed with the microplate reader

and compared to sample blanks treated with the MNPs and FNPs, the levels of fluorescence signal were the same (images not shown). Based on the fluorescence images a significant difference is evident in both the amount of cells extracted and fluorescent signal present between the target and control cells in all samples. However, some control cells that were inadvertently collected and even labeled with some FNPs, but no significant signal was indicated by the microplate reader data for those samples producing signals in the same realm as sample blanks (images not shown).

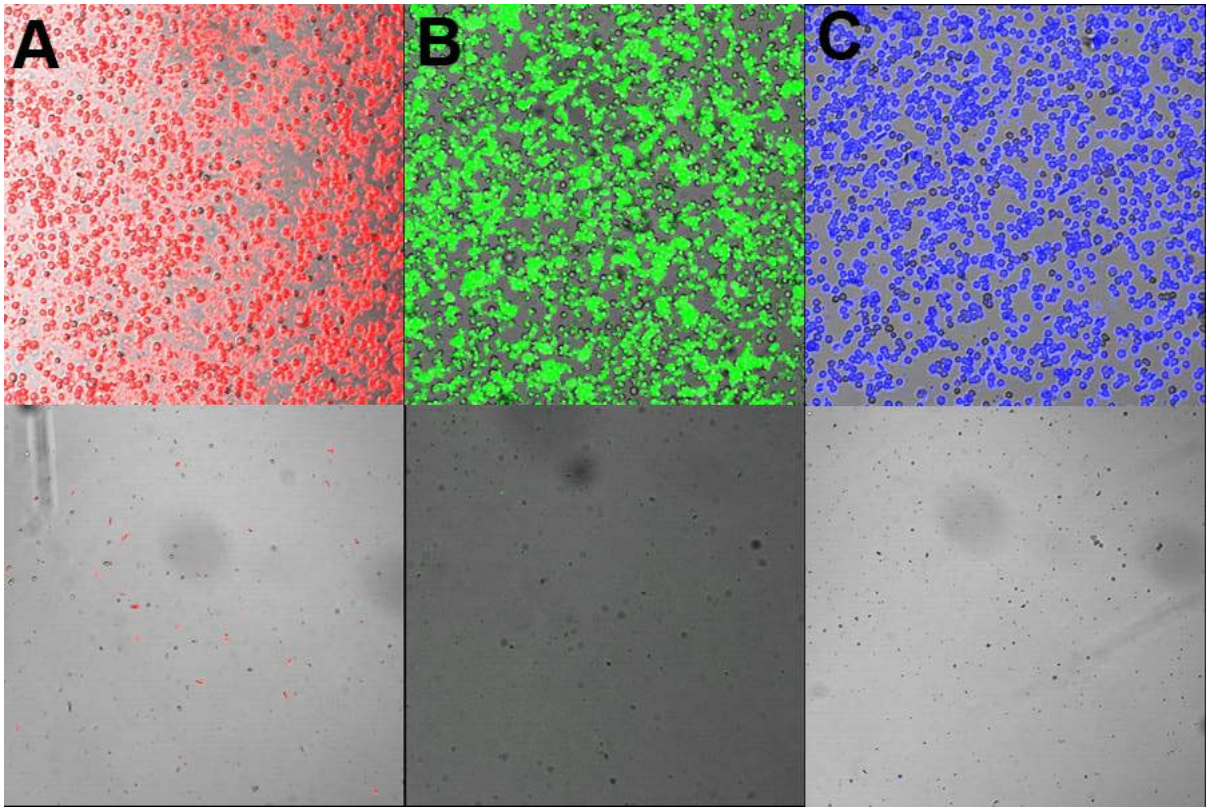

Figure 3-12. Fluorescence images of pure cell samples in buffer after magnetic extraction and washes A) Image of CEM target cells (top) and Ramos nontarget cells (bottom) using CEM ACNPs B) Image of Toledo target cells (top) and CEM nontarget cells (bottom) using Toledo ACNPs C) Image of Ramos target cells (top) and CEM nontarget cells (bottom) using Ramos ACNPs.

Table 1 provides the fluorescence data obtained from the microplate reader. The first column represents the cell sample that was analyzed, the second column represents the signal

produced by the CEM NPs, the third column represents the signal produced by the Toledo NPs, and the fourth column represents the signal produced by the Ramos NPs. The rows in the table display the cell samples that were investigated using the ACNPs.

Table 3-1: Single cell type extraction

Sample cells	CEM NP signal	Toledo NP signal	Ramos NP signal
Ramos	945	965	7,574
CEM	48,967	1,056	314
Toledo	1,075	36,728	438

On the contrary, the target cells subjected to this procedure had very intense fluorescent signals that made them easily discernible from the control cells. A closer look at the characterization of expanding the ACNP technique to multiple cell types the microplate reader data (table 1) demonstrated that when using 100,000 cells in each of the pure cell samples at a collection efficiency of 85% (determined in a previous publication[7]), all target cell samples produced signals in upwards of 24 fold enhancements above the background and as high as 50 fold. The target samples indicated in Table 1 for this experiment were the CEM cells (row 2) for the CEM NPs (column 1), the Toledo cells (row 3) for the Toledo NPs (column 2), and the Ramos cells (column 3) for the Ramos NPs (column 3). The control samples for these experiments were represented in the remainder of the table for each of the NPs and cell types. The signals for the control samples at the conditions mentioned above and the collection efficiency for the MNP amounts used in these experiments for the control cells determined to be no greater than 5% (determined in a previous publication[7]), resulted in fluorescence signals at the same level as a buffer blank sample treated with the ACNPs. This data indicates that the MNPs were both selective for the target cells by discriminating against the control cells and reproducible in all sample types investigated.

Multiple Cell Type Extraction Method

With the aptamers having demonstrated sufficient selectivity to allow the extract each cell type effectively without extract the control cells, the extraction of multiple cell types could then be attempted. Determining the multiple extraction and detection capability of the ACNP was performed by creating artificial complex samples of CEM, Ramos, and Toledo cells. Figure 3-13 displays the schematic diagram of the multiple cell extraction procedure that was employed. A stepwise extraction protocol was used as it proved to be the most effective for the blood samples and initial experiments using a simultaneous extraction of multiple cell types proved unsuccessful. The samples with one, two, and three cell types were analyzed using previously established ACNP protocols. The samples were prepared by obtaining approximately 10^5 cells of each type for the respective sample type. The stepwise extraction protocol was performed by adding the specified amounts of MNPs for Ramos cells, followed by CEM aptamer-conjugated MNPs, and finally with Toledo specific MNPs. Each set of MNPs were incubated with the cell samples separately for 15 minutes. After the Ramos MNPs were incubated with the cell samples, magnetic extraction was performed, and the supernatant kept to be treated with the CEM specific MNPs. The remainder of the magnetic extractions was carried out as described in the magnetic extraction section. The sample was redispersed in 200 μL cell media, followed by addition of the Ramos aptamer-conjugated FNPs with 5 minute incubation, and magnetic extraction procedure performed. Similarly, the respective CEM and Toledo aptamer-conjugated FNPs were subsequently introduced to their samples. After the final wash, the cell sample was dispersed in 20 μL media buffer. The samples were analyzed using fluorescence imaging with the 2 μL aliquots and with the plate reader spectrometer with 20 μL aliquots.

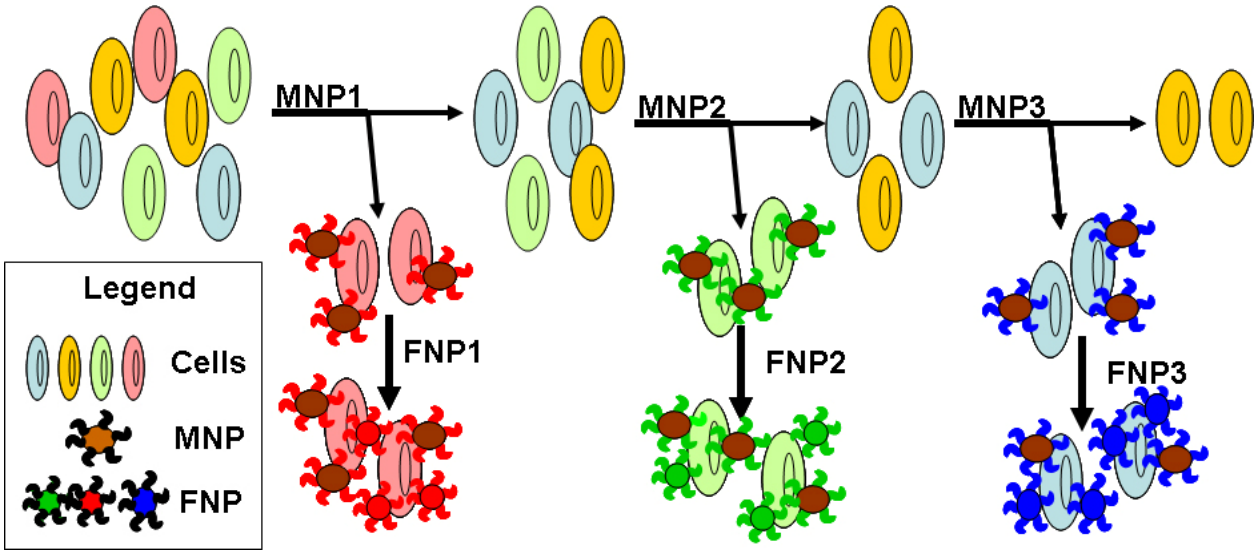

Figure 3-13. Schematic representation of the multiple extraction procedure with the MNPs being added and extracted stepwise and the corresponding FNPs being added post magnetic extraction of cell samples.

Mixed Cell Samples

The power of the multiple extraction procedure needed to be evaluated using complex sample mixtures. Figure 3-14 A, B, and C demonstrates the results from artificial complex samples by mixing equal amounts of the appropriate cell types for the three different multiple extraction samples diluted in cell media buffer, where CEM, Ramos, and Toledo cells were mixed and the ACNP process applied as described above. A total of 100,000 cells in all samples were used, cell and buffer volumes were adjusted accordingly. To exhibit that the MNPs indeed have the ability to selectively differentiate the cells from one another in a multiple cell mixture format, single, double, and triple cell mixed samples were evaluated. Figure 3-14A illustrates the selective nature of the technique by performing the ACNP steps with a single cell sample, Ramos cells. The single cell sample was first treated with CEM ACNPs followed by Toledo ACNPs, and finally Ramos ACNPs. The samples were incubated at 4 ^{o}C with the MNPs and FNPs as expressed in the previous section.

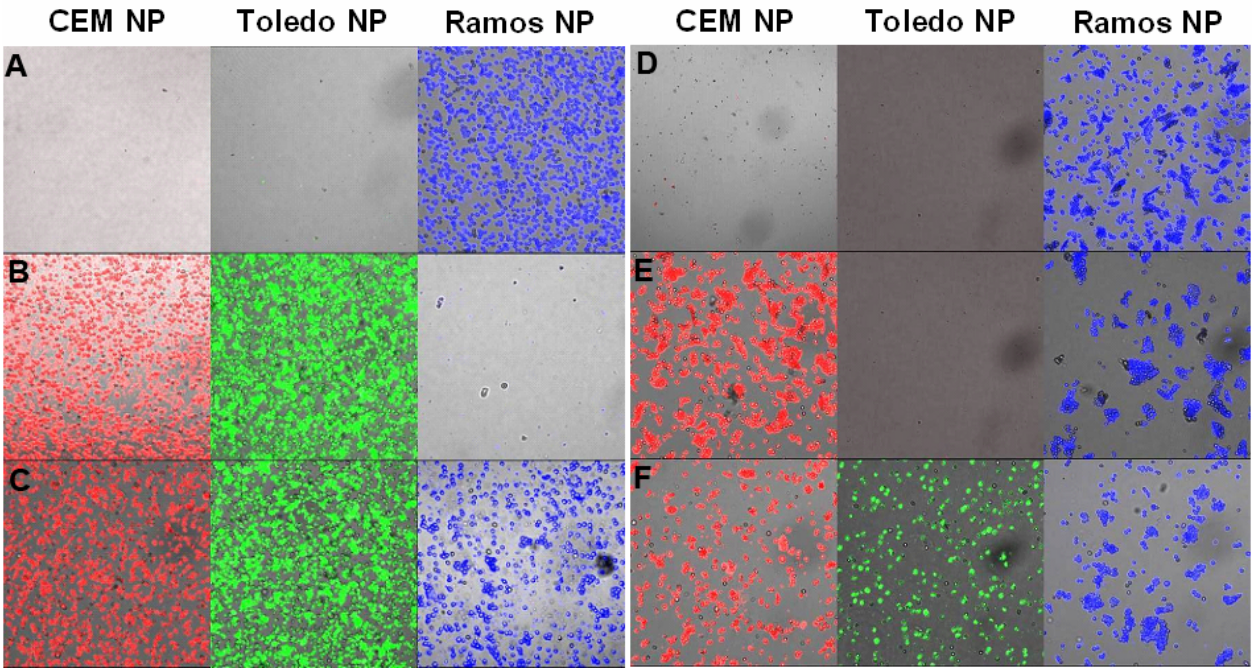

Figure 3-14. Fluorescence images of buffer extracted mixed cell samples using the multiple extraction procedure A) contains only Ramos cells B) contains CEM and Toledo cells C) contains all three CEM, Toledo, and Ramos cells. Fluorescence images D, E, and F displays the mixed cell samples extracted from FBS using the multiple extraction procedure, where D) contains only Ramos cells E) contains CEM and Ramos cells and F) contains all three CEM, Toledo, and Ramos cells.

Based on the fluorescence images, this method was able to selectively collect the Ramos cells (blue) only when the Ramos ACNP were introduced to the cell sample Figure 3-14A. The Toledo and Ramos cells were used in single cell sample extractions as well (image not shown). This method was further tested by performing the ACNP steps with a mixture of two different cell types, CEM and Toledo. Figure 3-14B displays the selective nature of this technique for the cells indicated. The fluorescence images again demonstrate selective isolation of the CEM (red) and Toledo (green) cells. Other CEM, Toledo, and Ramos two cell type mixed samples were performed as well (image not shown). The final test was to perform this technique with a mixture of all three cell types in the same sample using the CEM, Toledo, and Ramos cells at the same time. Figure 3-14C reveals the selective nature of the method for each of the cells

indicated. Fluorescence images again depict the selective isolation of the CEM, Toledo, and Ramos cells, Figure 3-14C left (red), middle (green), and right (blue) images respectively.

Table 3-2: Multiple cell type extraction

Sample cells	CEM NP signal	Toledo NP signal	Ramos NP signal
Ramos	1,281	1,040	7,862
CEM	44,972	920	375
Toledo	1,025	34,972	320
CEM, Ramos	46,874	1,505	7,385
CEM, Toledo	43,890	37,896	414
CEM, Toledo, Ramos	42,145	32,945	7,524

Microplate reader data was in complete agreement with the confocal image data and presented in Table 2. The first column represents the cell samples that were analyzed, the second column represents the signal produced by the CEM NPs, the third column represents the signal produced by the Toledo NPs, and the fourth column represents the signal produced by the Ramos NPs. The rows in the table display the cell samples that were investigated using the ACNPs. With 100,000 total cells present in all samples, samples containing target cells produced signals in upwards of 24 fold enhancements above the background and as high as 47 fold. The signals for the control samples at the conditions mentioned above resulted in fluorescence signals at the same level as a buffer blank sample treated with the ACNPs with the exception of the Toledo nontarget sample in sample 4. Standard deviations determined for all these samples were determined to be 8-12%. This data indicates that the MNPs were both selective for the target cells by discriminating against the control cells and reproducible in all sample types investigated.

Serum Samples

To show applicability of the stepwise process in real biological samples, fetal bovine serum (FBS) was used. FBS was spiked with each of the respective cell types for the corresponding one cell, two cell, and three cell extraction experiments (500 μL). The process

was performed as described above in the buffer solution experiments. Confocal imaging and fluorescence microplate reader were used to characterize cell extractions. Figure 3-14 D, E, and F illustrate the results of the FBS spiked complex samples by mixing equal amounts of the indicated cells at a total cell concentration of approximately 100,000 cells. Figure 3-14D, 3-14E, and 3-14F present the selective nature of the technique for the single, double, and triple mixed cell type samples. The samples were treated with CEM ACNPs followed by Toledo ACNPs, and finally Ramos ACNPs. For the single cell sample experiment, the sample was first treated with CEM ACNPs followed by Toledo ACNPs, and finally Ramos ACNPs. The samples were incubated at 4 ^{o}C with the MNPs and FNPs as expressed previously. Figure 3-14D fluorescence image shows the sample contains Ramos cells extracted and labeled only after being treated with Ramos ACNP (blue). Extractions with the CEM and Toledo cell types were completed as well (images not shown). Figure 3-14E left image (red) and right image (blue) show the CEM cells and Ramos cells extracted when treated with CEM and Ramos ACNP for the two cell type extraction experiment. Other two cell type extractions with the CEM, Toledo, and Ramos cell types were performed as well (images not shown). Figure 3-14F left (red), middle (green), and right (blue) images show the extraction of all three cells treated with all the ACNP.

The fluorescence imaging data was confirmed by collecting fluorescence data using the microplate reader, Table 3. The table layout was the same as in the previous table: first column was cell samples, second column was the CEM NP signals, third column was Toledo NP signals, and fourth column was the Ramos NP signal. The rows in the table display the cells mixed to make the samples that were analyzed. The standard deviations determined to be 8-12% for all samples measured in the FBS. With 100,000 total cells present in each sample dispersed in FBS, the signal enhancements determined above the background ranged from 10 to about 24. In all

cases, the signals for all target samples were lower than those for the cell media buffer, and the background signals were all higher. The Toledo samples produced the lowest enhancement of all the extracted samples, which produced the highest background signal of the three ACNPs pairs. The Toledo aptamer is less selective then the other aptamers that were used, which would explain the higher background produced in this particular sample. The fluorescence images and microplate reader data demonstrated that the MNPs were both selective for the target cells by discriminating against the control cells and reproducible even in spiked FBS samples.

Table 3-3: Multiple cell type extraction in serum

Sample cells	CEM NP signal	Toledo NP signal	Ramos NP signal
Ramos	1,845	3,241	6,776
CEM, Ramos	43,835	3,554	6,980
CEM, Toledo	40,767	31,240	452
CEM, Toledo, Ramos	42,973	33,112	7,078

Small Cell Lung Cancer Cell Extractions

In order to demonstrate the effectiveness of this methodology on an exfoliated cancer cell type, the assay was used to detect small cell lung cancer cells (SCLC). SCLC is a disease that can spread rapidly throughout the body even early in its development making it a very lethal disease and difficult to detect at an early stage. SCLC can even metastasize before being detectable using conventional means. Therefore, developing an effective screening method for it could lead to earlier detection and diagnosis thereby improving the prognosis for the disease which currently has 5 year survival rate of only 15%. Therefore, an aptamer selected for SCLC using Cell-SELEX was conjugated to magnetic and fluorescent nanoparticles. The cells were then extracted using the previously mentioned protocols with the results shown in Figure 3-15. The results indicate that the two particle assay works well with the SCLC cells as the image shows many target cells being extracted with far fewer of the non-target lung cancer cells being

extracted. The plate reader measurements confirm these results as the target samples had a much higher fluorescence intensity compared to the nontarget sample. While these preliminary results are encouraging further optimization needs to be completed and more complex samples still need to be analyzed before any conclusions as to the effectiveness of the methodology can be made.

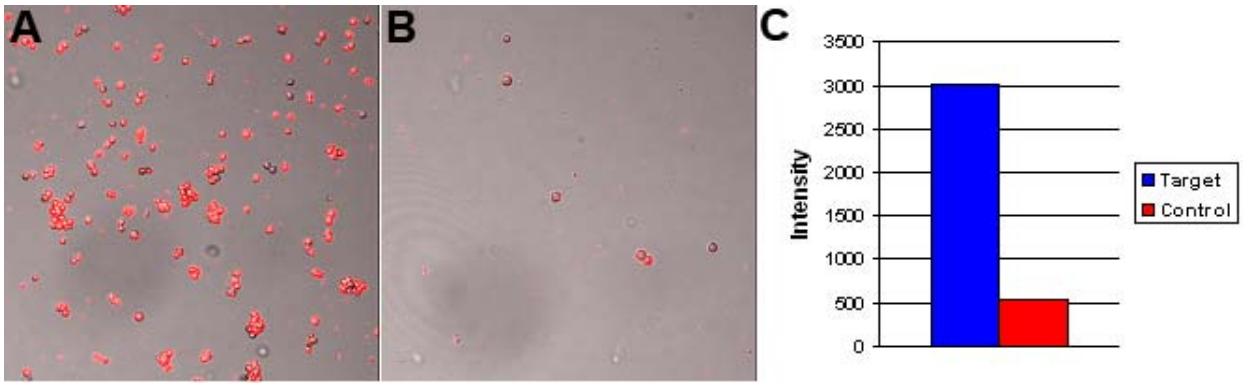

Figure 3-15. A) Fluorescence image of target SCLC cells extracted. B) Fluorescence image of non-target lung cancer cells extracted. C) Plate reader results for each sample.

Conclusion

In this chapter, the two particle assay for the collection and detection of cancer cells has been demonstrated. The assay has been shown to work well even in complex samples owing to the selectivity of the aptamers and unique properties of the nanomaterials used. Future directions for this project are mainly concerned with studying clinical samples and applying the assay to other cancer types such as SCLC. In particular the application of the method to SCLC remains a priority as it can solve a great problem in the medical field, an effective screening method for SCLC. In particular, SCLC is a good candidate for effective screening method as 99% of cases present in people who smoke or who have smoked. Thus, the most susceptible population of people at risk for the disease has already been identified. In addition, over 100,000 people die every year from lung cancer thus confirming the need for more effective means of detection and

diagnosis. These factors combine to form an effective rationale for applying the two particle assay for a screening method for SCLC.

CHAPTER 4
A COLORIMETRIC ASSAY FOR THE DIRECT DETECTION OF CANCER CELLS

Introduction

The key to the effective and ultimately successful treatment of diseases such as cancer is an early and accurate diagnosis. An early diagnosis is only possible with a sensitive method for the detection of the disease. Current methods are time consuming, expensive, and require advanced instrumentation. A more cost effective method requiring simple or no instrumentation yet still providing great sensitivity and accuracy would be ideal for point of care diagnosis. To accomplish this, we have developed the first colorimetric assay for the direct detection of cancer cells using aptamer conjugated gold nanoparticles (ACGNPs). A colorimetric assay would enable diagnosis based on a simple color change enabling diagnostic assays for diseases where sophisticated instruments are unavailable. Due to the Cell-SELEX aptamers, colorimetric assays could be implemented for any disease that results in the expression of different proteins on the cell surface including cancerous cells or cells exposed to viral infections.

To make the assay colorimetric in nature, gold nanoparticles were utilized for their biofunctionalization, biostability, and spectral properties. Due to the plasmon resonance of gold nanoparticles, they possess strong distance dependant optical properties. Once the gold nanoparticles come into close proximity with one another their absorption spectra shift and their scattering profile changes resulting in a change in color and in the resulting absorption spectra of the sample.[203,204] As a result of these properties, many techniques have been developed based on the aggregation of gold nanoparticles to detect genes and proteins.[205,206] However, instead of simple aggregation of the gold nanoparticles using genes or proteins, the ACGNPs are targeted to assemble on the surface of a specific type of cancer cell creating a virtual gold shell on the surface of the cell. The assembly of the gold nanoparticles around the cell surface causes a shift

in the absorption spectra of the particles along with a significant increase in the extinction coefficient. This results in not only a change in the color of the solution but a large increase in the intensity of the measured absorbance of the sample. This allows for the visualization of the target cells with the naked eye or with a microplate reader for increased sensitivity and the potential for automated high throughput analysis. The assembly of gold NPs on cell membrane surface due to cell receptor recognition by aptamers presents a novel approach for direct colorimetric detection of cancer cells.

Experimental Methods

DNA Aptamer Synthesis

The following aptamers have been selected for the CCRF-CEM and Ramos cells respectively: 5'-TTT AAA ATA CCA GCT TAT TCA ATT AGT CAC ACT TAG AGT TCT AGC TGC TGC GCC GCC GGG AAA ATA CTG TAC GGA TAG ATA GTA AGT GCA ATC T-3'; 5'-AAC ACC GGG AGG ATA GTT CGG TGG CTG TTC AGG GTC TCC TCC CGG TG-3';. Both the thiol versions of the aptamer sequencers were synthesized in-house. An ABI3400 DNA/RNA synthesizer (Applied Biosystems, Foster City, CA) was used for the synthesis of all DNA sequences. A ProStar HPLC (Varian, Walnut Creek, CA) with a C18 column (Econosil, 5u, 250 × 4.6 mm) from Alltech (Deerfield, IL) was used to purify all synthesized DNA. A Cary Bio-300 UV spectrometer (Varian, Walnut Creek, CA) was used to measure absorbances to quantify the manufactured sequences. All oligonucleotides were synthesized by solid-state phosphoramidite chemistry at a 1 μmol scale. The completed sequences were then deprotected in concentrated ammonia hydroxide at 65 °C overnight and further purified twice with reverse phase high-pressure liquid chromatography (HPLC) on a C-18 column.

Aptamer Conjugated Gold Nanoparticle Synthesis

In a 2mL microcentrifuge tube, 1mL of the 20nm gold colloid nanoparticles (GNPs), containing $7.0x10^{11}$ particles/mL, taken directly from the manufacturer (Ted Pella, Inc. Redding, CA) was centrifuged for 15 minutes at 14,000 RPM. The GNPs were washed three times with 1mL aliquots of 5mM phosphate buffer (PB) pH 7.5 by decanting the supernatant, adding fresh PB, dispersing by sonication, and centrifuging for 15 minutes at 14,000 RPM. From decantation to dispersion, the wash step was performed within 3-5 minutes. After the final wash step, the GNPs were dispersed in 1 mL of the PB. To each washed GNP sample, 150μL of a 1μM thiol labeled DNA sequence was incubated for 3-5 days at 4ºC. The samples were sonicated to disperse the GNPs every 12 hours. When the incubations were completed, the samples were centrifuged at 14,000 RPM for 5 minutes and the samples washed as described previously with the PB. After the final wash, each GNP sample was dispersed in 0.25mL PB with approximately $6.0x10^{11}$ particles, and the samples stored at 4ºC until used.

Cells

CCRF-CEM cells (CCL-119 T-cell, human acute lymphoblastic leukemia) and Ramos cells (CRL-1596, B-cell, human Burkitt's lymphoma) were obtained from ATCC (American Type Culture Association). The cells were cultured in RPMI medium supplemented with 10% fetal bovine serum (FBS) and 100 IU/mL penicillin-Streptomycin. The cell density was determined using a hemocytometer prior to any experiments. After which, approximately one million cells dispersed in RPMI cell media buffer were centrifuged at 920 rpm for five minutes and redispersed in dye free cell media three times, and were then redispersed in 5 mL dye free cell media. During all experiments, the cells were kept in an ice bath at 4^{o}C.

Assay Protocol

For each assay, $1.0x10^{10}$ ACGNPs were utilized in a total volume of 300μL. The assay were incubated for 30 minutes at $4^{o}C$ in a 500μL microcentrifuge tube and then transferred to a BD Falcon 96-well transparent microplate (Fisher Scientific, Pittsburgh, PA). After incubation, the assays in the microplates were imaged with an Epson Stylus CX3200 flatbed scanner while the absorbance spectra from 400nm to 900nm were measured in a Tecan Safire Microplate reader (Mannedorf, Switzerland) for each sample. All data analysis was performed using Microsoft Excel.

Results and Discussion

To demonstrate the principle behind the assay, it was first determined whether the ACGNPs could differentiate between target cells and control cells. For these experiments, CCRF-CEM acute leukemia cells were used as target cells while Ramos, a Burkitt's lymphoma cell line, were used as control cells. An aptamer sequence with high selectivity and affinity to the CCRF-CEM cells was conjugated to 20nm gold nanoparticles through a thiol functional group on the aptamer sequence. The five samples are: $1.0x10^{10}$ ACGNPs, $1.0x10^{10}$ ACGNPs with 10,000 target cells, the ACGNPs with 10,000 control cells, 10,000 target cells with no ACGNPs, and $1.0x10^{12}$ ACGNPs in cell media. The absorption spectrum for each sample is shown in Figure 4-1. The results establish that the absorbance of the ACGNPs with 10,000 target cells is significantly higher than the same amount of ACGNPs with 10,000 control cells, the same amount of target cells without ACGNPs, or with only the ACGNPs. These results indicate that the ACGNPs are binding selectively to the target cells and that the assembly of the ACGNPs around the target cells causes an increase in the extinction coefficient of the solution. The increase of the extinction coefficient, predominantly in the scatter coefficient, was also observed

colorimetrically as the target cell sample was deep purple in coloration compared to the other samples that were mainly clear and colorless.

However, the signals from the non-binding samples were too low to determine whether there was a shift in the spectra accompanying the binding of the ACGNPs to the target cells. To determine whether a shift occurred, a spectrum from a larger amount of ACGNPs was also measured and plotted in Figure 4-1. This spectrum indicates that a significant shift in the absorption occurs when the ACGNPs bind to the target cells. These results are consistent with the spectral shifts observed by others using the aggregation of gold nanoparticles for detection.[203-206]

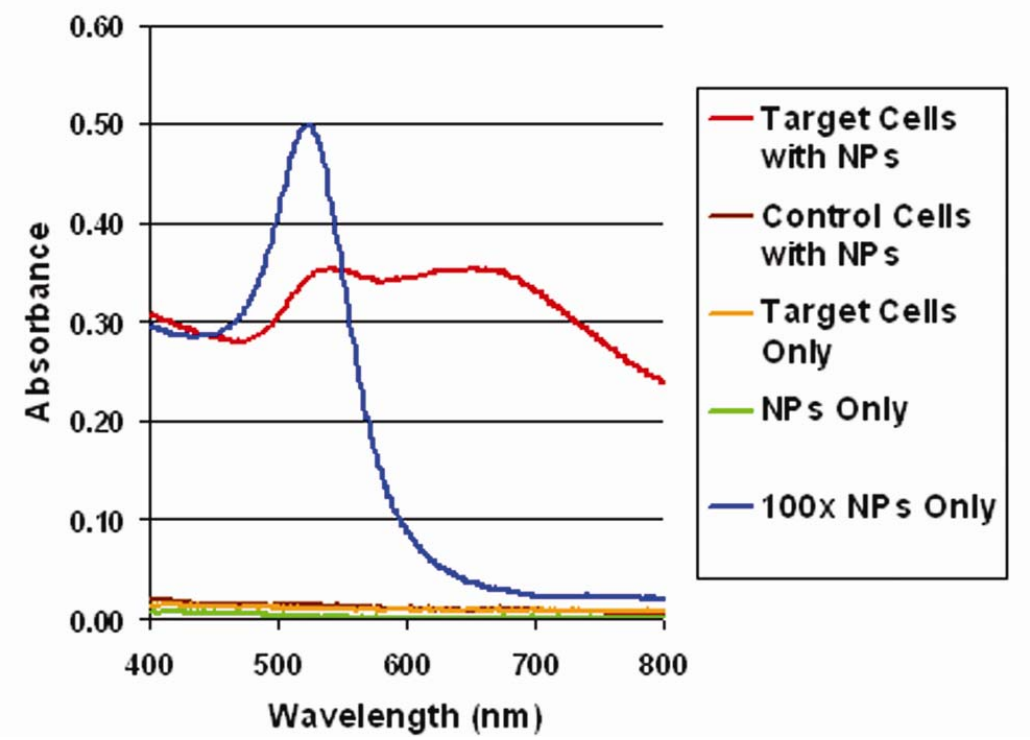

Figure 4-1. Plots depicting the absorption spectra obtained for various samples analyzed using ACGNPs. The spectra illustrate the differences in spectral characteristics observed after the ACGNPs bind to the target cells.

Nanoparticle Size Effect

The next step in the development of the assay was to determine the best gold nanoparticle size to use. Four batches of aptamer conjugated nanoparticles were synthesized with four different gold nanoparticle sizes. The sizes used were 5nm, 20nm, 50nm, and 100nm. Based on published results,[207] the larger nanoparticles should have the longest red shift which would make detection easiest but would also have a higher background. Therefore, the nanoparticles would be evaluated on the basis of its red shift and the difference between target and control cell samples. Figure 4-2 depicts the plots of each nanoparticle type spectra with its target cells. Based on these results, the 20nm and 50nm nanoparticles had the most significant red shift upon target hybridization each having absorbance spectra reaching past 700nm. The 5nm nanoparticles exhibited very little change in spectra with the target cells perhaps indicating the

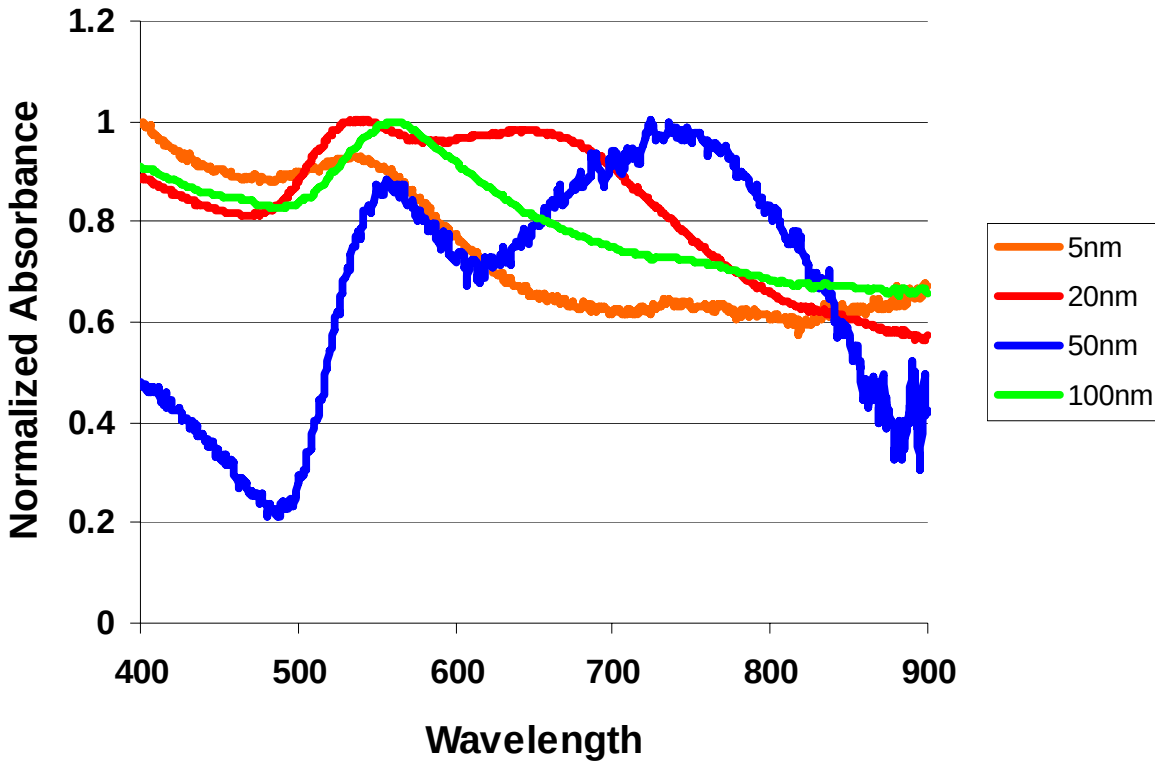

Figure 4-2. Spectra of the different sizes of Aptamer Conjugated Gold Nanoparticles with target cells.

nanoparticles were too far apart to effectively interact or that an unknown problem occurred during the conjugation step. While the 100nm exhibited an effective enhancement upon target cell addition, they did not exhibit as significant of a red shift as the 20nm or 50nm nanoparticles. Based on the spectra the 20nm and 50nm nanoparticles performed the best in terms of red shift while the 20nm particles had the greatest enhancement of the target cells relative to the control cells. Based on the results obtained from these limited tests, the 20nm gold nanoparticles were used in subsequent experiments due to their performance. However, in the future the nanoparticle sizes will be evaluated more rigorously to obtain the optimized performance for each size.

Assay Response

With the best size of nanoparticles identified, the next step was to verify that the assay is indeed colorimetric and that the change in color was proportional to the amount of cells present. In order to accomplish this, $1.0x10^{10}$ ACGNPs were incubated with increasing amounts of target cells. This was repeated with the same amounts of control cells for comparison. The image of both cell types is shown in Figure 4-3A. The results clearly show that the samples with more target cells have a darker color while with the control cells, the samples remain almost colorless and there is no significant difference between the samples regardless of the amount of cells present. Thus the assay allows for the detection of target cells with the naked eye.

In order for a more sensitive detection than allowed by the human eye, the samples were also analyzed using a microplate reader. The spectra for the different amounts of control and target cells are shown in Figures 4-3B and 4-3C, respectively. The absorption spectra correlate well with the colorimetric results in that the samples with an increasing amount of target cells absorb light more intensely. There is little change in the ACGNP absorption spectra of the

control cell samples regardless of the amount of cells present. This is most likely a consequence of the selectivity of the aptamer itself and also the nature of the gold nanoparticles. Realistically, absolute selectivity is difficult to achieve regardless of the molecular recognition element employed and it is highly likely that a few of the ACGNPs bind non-selectively to the control cells. However, in order to generate a signal from ACGNPs there needs to be many gold nanoparticles in close proximity, therefore even if there is a limited amount of non-selective binding it is very unlikely it will be to the extent to cause a positive response to the assay further increasing the apparent selectivity of the assay to the target cells.

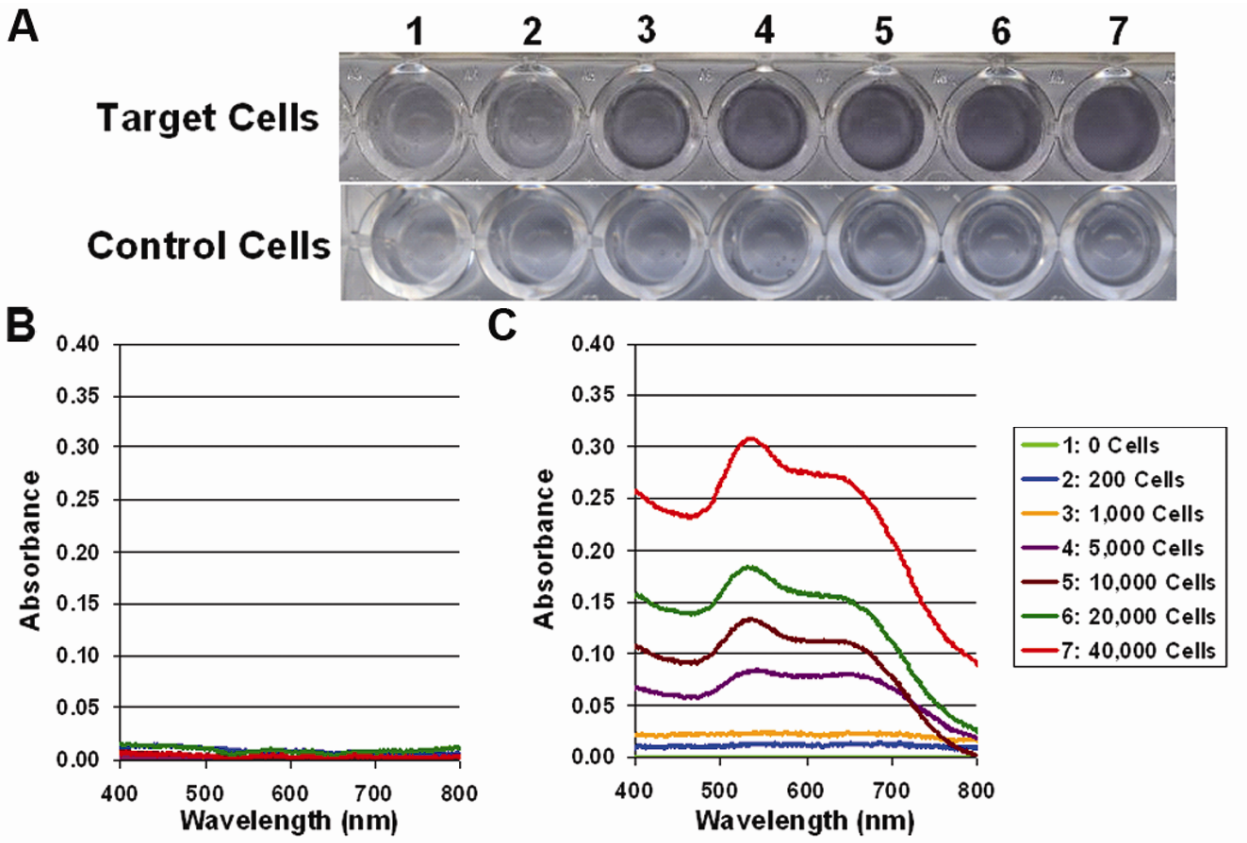

Figure 4-3. A) Images of ACGNPS with increasing amounts of target (top) and control cells (bottom). The amount of cells used in each sample is given in the legend on the bottom right. B) Absorption spectra of the control cell samples with ACGNPs in Figure 2A. C) Absorption spectra of the target samples with ACGNPs in Figure 2A.

In order to determine the limit of detection for the assay, the previous experiment was repeated four more times. The absorbance at 650 nm was then recorded for each amount of cells and plotted in Figure 4-4A. The assay showed an excellent dynamic range with standard deviations ranging from 6-10%. Based on three times the standard deviation of the blank measurement, the limit of detection of the target cells was calculated to be 90 cells. In addition, this experiment was repeated with control cells to measure their response to the assay. The ACGNPs had no response to the control cells at the lower cell concentrations as these samples

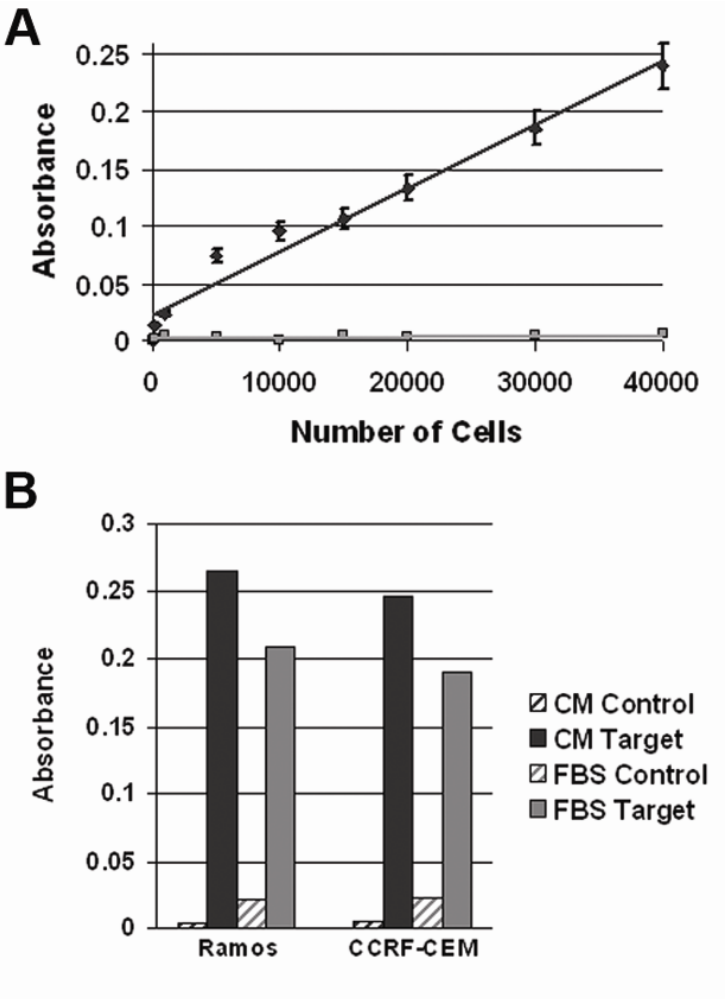

Figure 4-4. A) Calibration curve illustrating the relationship between the amount of cells and the absorbance intensity at 650nm for both target cells (black) and control cells (gray). The assay shows a very good dynamic range in addition to excellent sensitivity. B) Bar graph showing the change in intensity between the target cells and control cells at 650nm in both cell media (CM) and fetal bovine serum (FBS) for both cell types.

had signals comparable to the blank. At the higher cell concentrations, the ACGNPs had a small response to the control cells although it was still significantly lower than even the smallest concentration of target cells that were evaluated. Based on these results, the assay for direct cell detection has demonstrated excellent sensitivity and selectivity.

In order to truly evaluate the assay, more complicated samples also needed to be analyzed to determine whether the assay could be useful for actual samples. In order to accomplish this, the assay was also used on several samples of fetal bovine serum (FBS). In these samples, the 50,000 cells were spiked into FBS and then the $1.0x10^{10}$ ACGNPs were added. Target and control cells were spiked into different samples and then after incubation with the ACGNPS their spectra were measured using the microplate reader. The absorbance at 650 nm from the three samples was averaged and plotted in Figure 4-4B, for comparison, the signals of the same amount of cells in cell media were also measured. The target cells in FBS clearly show a significantly higher signal than the control cells in the FBS, indicating that the assay functions as expected in even complex environments. Colorimetric determination, however, proved difficult due to the color of the FBS. In future experiments with more complex samples, further sample preparation to remove any colored species may be necessary for any colorimetric detection. Regardless, spectroscopic detection of the target cells in FBS was achieved without any further sample preparation steps. In an effort to show the assay is applicable to other cell types, this experiment was repeated along with the same experiment in cell media using an aptamer that is selective for the Ramos cell line while using the CCRF-CEM cells as a negative control. Again, the ACGNPs showed excellent sensitivity and selectivity to the target cells regardless of the line of cells targeted in both the cell media and in the FBS.

In conclusion, ACGNPs have been demonstrated for the sensitive and selective detection of cancer cells through utilizing the unique spectral properties of gold nanoparticles and the excellent selectivity of aptamers. The assay is the first colorimetric assay for the direct detection of cancer cells using molecular aptamers directly selected from whole cells. In addition, spectroscopic detection using ACGNPs proved successful for even complex samples like FBS and demonstrated excellent sensitivity and selectivity. Little non-selective binding was observed, most likely due to the characteristics of the gold nanoparticles in that any binding of a few nanoparticles to the control cells would not have been enough to drastically alter the spectral properties of the particles. We have proven that gold NPs can be assembled on cell membrane surface for spectral change, providing a direct visualization of cancer cells. Future work will include the further development of the assay including optimizing the particle size, incubation times, and sample preparation methods for complex samples. After optimization, the assay will be tested on more complex samples including blood samples using both colorimetric and spectroscopic detection. This assay has the potential to provide a rapid, high throughput, sensitive, and cost effective approach for the early and accurate detection of cancer through the utilization of aptamers and nanotechnology.

Once the assay has been sufficiently optimized, it may prove more useful for other diseases than cancer. Given its rapid, colorimetric based detection, the assay may prove more suitable for the rapid screening of multiple samples in a point of care or triage situation of a viral or bacterial infection outbreak. Infected cells often have different or variable cellular surface marker expression, thus if an aptamer could be selected using Cell-SELEX to exploit the differences between the normal and infected cells, the aptamer could easily be adapted to the assay allowing the colorimetric detection of the infection. This would enable the rapid screening of patients in

hospitals if a particular infection strikes a hospital such as Legionnaire's disease or after a bioterrorism incident.

CHAPTER 5
MOLECULAR BEACON DESIGN, DELIVERY, AND EVALUATION

Introduction

Since their development in 1996,[208] molecular beacons (MBs) have seen ever growing use in a wide variety of fields from chemistry to biology to medical sciences.[209-211] One emerging application of MBs has been their use for intracellular studies of gene expression and localization. Cellular analysis using MBs offer many advantages to traditional forms of gene expression analysis. One distinct advantage is that MBs allow the probing of gene expression without destroying the cell unlike Northern Blot analysis and RT-PCR based methods. To understand why MBs are ideal for intracellular analysis one has to first understand a MB.

MBs are oligonucleotide based probes that use fluorescence for detection. MBs are composed of two discrete oligonucleotide regions; the loop region and the stem region. Due to their unique hairpin structure, MBs undergo a conformational change upon hybridizing to their targets. The conformational change causes the stem portion of the MB to melt and separate. The melting of the stem causes the fluorophore and quencher on each end of the stem to become spatially separated. When unhybridized the fluorophore and quencher are in close proximity, the fluorescent signal is suppressed. After the fluorophore and quencher pair is separated after hybridization, the fluorescence signal is restored. This method of signal transduction gives the MB allows the bound and unbound MBs to be easily distinguished allowing for the detection of bound MBs without separating out the unbound MBs. This feature of MBs is very significant for detection of mRNA inside of living cells since previous methods of mRNA detection inside of cells required fixed or pretreated cells so that the unbound probes could be removed.[212] Such techniques do not allow analysis on living cells thus the MB seems to possess the ideal characteristics for analysis on living cells. In addition, MBs inherently possess excellent

specificity through Watson-Crick base pairing, thus specific gene sequences can be probed inside of cell. The sensitivity of fluorescence detection also makes them ideal for intracellular mRNA detection. The ability to monitor mRNA expression inside of cells selectively and in real time gives MBs the potential to improve the understanding of many biological processes. It can shed light on many fundamental processes like mechanisms and kinetics of mRNA production, transportation and localization of mRNA inside of a living cell, and single cell responses to external stimuli.

In addition, MBs have other important characteristics for intracellular experiments. Since MBs are comprised of DNA, they are readily adapted for intracellular experiments since DNA is non-toxic to cells. Another very important characteristic of MBs is that they can be designed for virtually any mRNA sequence, in principle it is possible to design a MB for any known gene sequence. Combined with their inherent signal transduction method that allows for detection without separation, and the ability to design a MB for any gene, MBs have a wide applicability for various intracellular studies of biochemical, biological, and medical significance. However when designing and using molecular beacons for intracellular experiments there are several important criteria that cannot be overlooked that will be explored in more detail in this chapter. In addition, some critical experimental parameters such as probe delivery and in vitro testing of probes will also be covered.

Methods and Materials

Equipment

Fluorescence imaging was conducted with a confocal microscope setup consisting of an Olympus IX-81 inverted microscope with an Olympus Fluoview 500 confocal scanning system and three lasers, a tunable Argon Ion laser (458nm, 488nm, 514nm), a green HeNe laser (543nm), and a red HeNe laser (633nm) with three separate photomultiplier tubes (PMT) for

detection. The cellular images were taken with a 40x 1.4 NA oil immersion objective. A Leiden microincubator with a TC-202A temperature controller (Harvard Apparatus, Holliston, MA) was used to keep the cells at 37^{o}C during injection and monitoring. An EXFO Burleigh PCS-6000-150 micromanipulator was used for positioning the injector tip. An Eppendorf Femtojet microinjector with 0.5μm Femtotips was used to inject the molecular beacons and reference probe into the cells. All analysis was conducted on the Fluoview 500 software, followed by processing of the data using Microsoft Excel.

Fluorescence Imaging

All cellular fluorescent images were collected using the confocal microscope setup. The confocal consists of an Olympus IX-81 automated fluorescence microscope with a Fluoview 500 confocal scanning unit using either a 20X air objective or a 40X oil objective based on experiment. There are three lasers providing laser excitation at 458nm, 488nm, 514nm, 543nm, and 633nm. The Alexa Fluor 488 were excited at 488nm and collected at 520nm. The Alexa Fluor 555 and TMR based MBs were excited at 543nm and collected at 560nm. The Alexa Fluor 647 and Cy5 based MBs were excited at 633nm and collected at 660nm. RuBpy was excited at 488nm and the emission was collected at 610nm. Images were taken after a five to ten second period during which the instrument was focused to yield the highest intensity from the fluorescence channels. The images were assigned color representations for clarity and are not indicative of the actual emission wavelengths.

Plate Reader Experiments

Fluorescence measurements were taken using a Tecan Safire Microplate Reader in a 384 well small volume plate. 20μL aliquots from each sample were deposited in the well and sample fluorescence intensity at defined wavelengths were measured at a constant gain at 5nm slit widths. Cy3 and Alexa Fluor 555 were excited at 550nm and their emission was detected at

575nm. Alexa Fluor 488 and FAM were excited at 488nm and their emission was measured at 520nm. Alexa Fluor 647 and Cy5 were excited at 640nm while their emission was detected at 670nm. The data for the experiments utilizing the plate reader was analyzed using Microsoft Excel.

Cell Culture

MDA-MB-231 breast carcinoma cells (American Type Culture Collection, Manassas, VA) were maintained in Dulbecco's Modification of Eagle's Medium (DMEM, Fisher Scientific) with 10% fetal bovine serum (Invitrogen, Carlesbad, CA) and 0.5 mg/ml Gentamycin (Sigma, St. Louis, MO) at 37^{o}C in 5% CO_2/air. Cells were plated in 35mm glass bottom culture dishes and grown to 80% confluency (MatTek Corp., Ashland, MA) for 48 hours prior to use.

Fluorescent Probes

All MBs were designed in-house based on published mRNA sequences. The Alexa Fluor based MBs were synthesized by Genomechanix (Gainesville, FL) while the rest of the MBs were synthesized in-house. An ABI3400 DNA/RNA synthesizer (Applied Biosystems, Foster City, CA) was used for the synthesis of all in-house MB sequences. A ProStar HPLC (Varian, Walnut Creek, CA) with a C18 column (Econosil, 5u, 250 × 4.6 mm) from Alltech (Deerfield, IL) was used to purify all fabricated DNA. A Cary Bio-300 UV spectrometer (Varian, Walnut Creek, CA) was used to measure absorbances to quantify the manufactured sequences. All oligonucleotides were synthesized by solid-state phosphoramidite chemistry at a 1 μmol scale. The completed sequences were then deprotected in concentrated ammonia hydroxide at 65 °C overnight and further purified twice with reverse phase high-pressure liquid chromatography (HPLC) on a C-18 column. The fluorophores Alexa Fluor 555 (AF555), Alexa Fluor 488 (AF488) and Alexa Fluor 647 (AF647) were purchased from Invitrogen (Carlsbad, California). All other reagents were purchased from Glen Research (Sterling, VA). The quenchers used for

the MBs were Dabcyl, Blackhole Quencher 2 (BHQ2), and Blackhole Quencher 3 (BHQ3). The sample solutions used in the experiments contained 1μM of each MB and in 20 mM Tris, 50mM NaCl and 5mM Mg_2Cl_2 buffer. Sequences and fluorophore quencher combinations are given in Table 5-1.

Table 5-1: Molecular beacon sequences

MB name	Sequence with fluorophore/quencher pair
Control MB1	5′-Cy5-CCT AGC TCT AAA TCG CTA TGG TCG CGC TAG G-BHQ3-3′
Control MB2	5′-AF555-CCT AGC TCT AAA TCG CTA TGG TCG CGC TAG G-BHQ2-3′
B-actin MB1	5'-TMR-CCG TCG AGG AAG GAA GGC TGG AAG AGC GAC GG-BHQ2-3′
B-actin MB2	5'-AF488-CCG TCG AGG AAG GAA GGC TGG AAG AGC GAC GG-BHQ1-3′
Cyclin D1 MB1	5′-Cy3-ACG ACG GCC ACC ACG CTC CCC GCT GCC ACC GTC GT-BHQ2-3′
Cyclin D1 MB2	5′-Cy3-GCA GCA TCC AGG TGG CGA CGA TCT TGC TGC-BHQ2-3′
MnSOD MB	5′-AF647-CCG AGC CAG TTA CAT TCT CCC AGT TGA TTG CTC GG-BHQ3-3′

Molecular Beacon Design

The use of MBs for intracellular RNA detection and localization requires the design of the MB for mRNA inside of a cell. Designing a MB involves three major areas; the loop, the stem, and the fluorophore/quencher pair. The primary concern in designing MBs for intracellular use is designing the loop region. The first step of which is selecting an appropriate target region on the mRNA sequence for the MB. This is critical due to the complex secondary structure exhibited by the large mRNA sequences. The MB must be able to reach to its complementary sequence through the secondary structure or the MB will not hybridize and produce the fluorescent signal for detection. Unfortunately current mRNA folding programs do

not give a completely reliable secondary structure, thus a series of MBs is generally selected for each mRNA sequence. Once possible target sequences are identified through the RNA folding programs, MBs are designed for them. The stems are created after the loop region is devised. This is to make certain that the stem region is not complementary to any region in the loop. Once the DNA portion of the MB is designed the fluorophore and quencher pair can be decided. This is generally based on the instrumentation available for the experiment to ensure efficient excitation and detection of the fluorophore in the open state and high quenching efficiency in the closed state. A series of probes is then synthesized and tested in vitro to make sure that the MB is functional. Further testing is then done *in vivo* until a probe is found that can hybridize with mRNA inside of a cell.

Another more practical concern when designing and synthesizing molecular beacons for any application is the final nucleotide base positioned before the fluorophore. Several investigators have observed that nucleotides can quench the fluorescence emission of fluorophores.[213-215] While the quenching efficiency of the bases is smaller than those of commonly used quenchers, it can still significantly effect the performance of the molecular beacon. Guanine (G) is the best quencher among the bases, followed closely by adenine (A), while cytosine (C) and thymine (T) exhibit a much lower quenching efficiency. The quenching properties of guanosine are centered on its electron donating ability that allows the energy transfer between the base and the fluorophore.[45] As a result, molecular beacons designed with a C connecting the fluorophore and a G linking to the quencher moiety display better signal enhancements than other arrangements.

When designing MBs for any application, an important factor to consider is the fluorophore and quencher pair. Recently, a systematic study of various static quenching

efficiencies for different fluorophore and quencher pairs has been documented.[213] Properly matching the fluorophore with an effective quencher molecule can lead to substantial improvements in detection capabilities. This is achieved by reducing the background fluorescence from the molecular beacon in the absence of target DNA. Similarly, using quenching moieties that are better able to absorb or transfer energy from the fluorophore can also lead to better fluorescence enhancements. It has also been shown that spectral overlap is less important for effective quenching as the primary mechanism of quenching is static quenching.[213] One observation that further supports the static quenching mechanism of molecular beacons is the alteration that is observed in the spectral properties of the fluorophore and quencher.[216] The hairpin-loop structure brings the fluorophore and quencher into such close proximity that it disturbs their electronic structure.

As such, while many probes are initially tested with FAM/Dabcyl fluorophore/quencher pairs these are often replaced for the actual applications to achieve better sensitivities. Figure 5-1 shows the fluorescence enhancements of several molecular beacons using FAM/Dabcyl pairs and then the higher quality pairs used in subsequent applications. In these experiments only the fluorophore quencher pair was changed, each molecular beacon was at a concentration of 1μM with a target concentration of 10μM. The optimal fluorophore/quencher pairs are Alexa Fluor 647 and Blackhole Quencher 3 for the MnSOD molecular beacon, Alexa Fluor 555 and Blackhole Quencher 2 for the control molecular beacon, Alexa Fluor 488 and Blackhole Quencher 1 for the B-actin molecular beacon, and Cy3 and Blackhole Quencher 2 for both of the Cyclin D1 molecular beacons. The complete sequences and fluorophore quencher pairs are listed in Table 5-1.

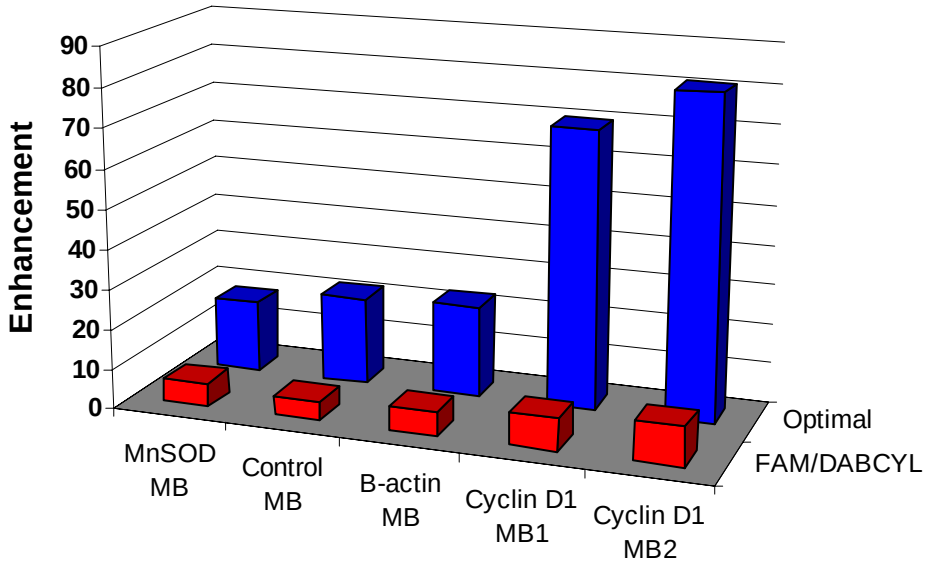

Figure 5-1. Comparison of the enhancements of molecular beacons with FAM/Dabcyl and higher quality fluorophore quencher pairs.

Molecular Beacon Delivery

One of the more important decisions to be made concerning intracellular analysis with MBs is how to get the MBs delivered into the cells. Delivery of the MBs inside of the cell has been an area where a lot of effort has been applied and it has resulted in many very effective options for intracellular delivery. The most common delivery methods include microinjection[6], electroporation[7], peptide assisted delivery[8], and reversible permeabilization[9]. Although any method that has been used to deliver oligonucleotides inside of a cell has the potential to be an effective delivery mechanism of MBs inside of a cell. As each method has its own strengths and weaknesses, the proper means of delivery generally depends on the application.

Microinjection involves the use of special equipment in order to physically pierce the cell and deliver the MBs. This is accomplished through the use of a micromanipulator that allows for the precise positioning of an injector tip. The tips are generally pulled fused silica capillary or

commercially purchased tips. The MB solution is loaded into the tips and connected to a microinjector. Once the tip is positioned inside of the cell, the microinjector sends a pulse of pressure through the tip that forces the MB solution into the cell. The amount of solution delivered can be finely tuned by changing the pressure and duration of the pulse. Microinjection has several advantages, most importantly, it allows for the immediate monitoring of the cell for the response of the probe. Secondly, it delivers relatively reproducible amount of probe to the cell of choice of the experimenter. The disadvantages of using microinjection are related to the technique itself in that it requires additional instruments and expertise while being a very low throughput technique.

Electroporation and reversible permeabilization are analogous techniques that deliver MBs through passive diffusion through pores created in the cell membrane. The two techniques differ through the process in which they create the pores. Electroporation can create pores in the cell membrane through the application of an electrical pulse to the cells. The pulse causes the cell membrane to develop pores which allows any probes surrounding the cells to pass through the cell membrane. Reverse Permeabilization also delivers the MBs through pores created in the cell membrane. This involves the use of the chemical, Streptolysin O to create pores in the cell membrane. Activated Streptolysin O binds to cholesterol molecules in the cell membrane to form channels approximately 30nm in diameter in serum free media. The channels allow the passive diffusion of materials into the cell. However the pores in both methods can also allow the loss of materials from inside of the cell and there are variations in the amount of probes delivered into each cell. In addition, electroporation also requires additional equipment to accomplish the delivery. Reverse Permeabilization also requires time to form the pores and then additional time to allow the pores to reseal.

Peptide-assisted delivery and liposome based transfection methods allow the probes to pass through the cell membrane without disturbing the cell. It allows any materials conjugated to the peptide or inside the liposome to be endocytotically passed through the cell membrane and into the cell. This allows delivery of the MB into the cell without forming artificial pores or physical injection. However peptide assisted delivery requires the peptide to be conjugated to the probe which can increase the cost and complexity of the probe synthesis. Both methods also require time for the probe to be delivered inside of the cell.

The one encompassing theme is that one must select the proper delivery mechanism based on the application and also on the properties of the molecular probes to be delivered. Probes based on non-standard bases can survive longer inside the cell allowing for longer incubation times to be used. In order to evaluate which method would work best for the study of cancer cells using MBs, several different delivery methodologies were tested based on normal DNA molecular beacons.

Electroporation

Electroporation is common method for gene transfection and can refer to either single cell electroporation or the mass delivery of materials to a whole population of cells. The major advantage of electroporation is that it can achieve a mass delivery of the probes with a very short (less than one minute) incubation time, thus allowing real time monitoring of the probe like in microinjection without the limitations of microinjection. For this experiment, the focus is on electroporation as a mass delivery method as single cell electroporation only differs slightly from microinjection. Electroporation was performed using a BTX ECM 830 pulse generator (Harvard Apparatus) with a PP35-2P Petri Pulser electrode. The electrode is designed to fit a 35mm cell culture dish and be able to deliver a sufficient electrical pulse to deliver the DNA into the cell.

The initial settings were based on a protocol for MDA-MB-231 cells provided by BTX using a pulse of 300V for 50μs with a 1μM concentration of fluorophore labeled DNA.

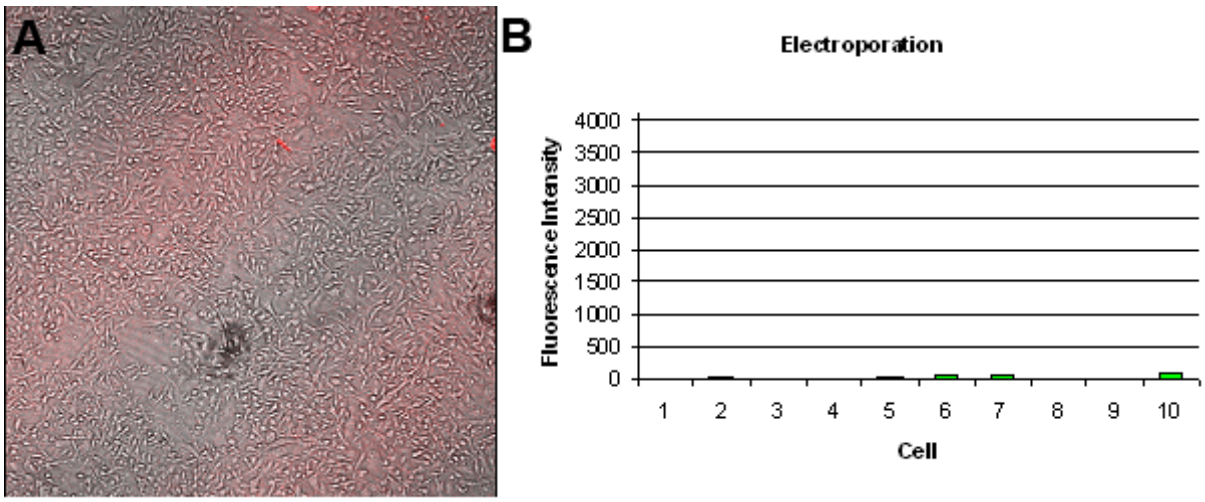

Figure 5-2. A) Fluorescence images of cells after electroporation in a 5μM DNA spiked medium. B) Average cell intensities of ten cells after electroporation.

This protocol produced no noticeable change in the fluorescence of the cells. The voltage, pulse length, concentration of DNA and number of pulses were then increased until reaching the instrument maximums. The results of a representative experiment performed with five 50μs 1,000V pulses in Figure 5-2 with the fluorescence image (A) and the average cell intensities (B) indicating little to no uptake of the DNA transpired. These experiments were repeated using trypsinized cells in BTX electroporation cuvettes and the cell were imaged after replating in a 35mm culture dish however no fluorescence signal reached levels suitable for use as a MB delivery method. These results indicate that while electroporation functions well for gene transfection were only low copy numbers of the genes need to be delivered, the method does not translate well for DNA probe delivery. This is due to the need for a large amount of the probes to be delivered to the cells in order for the gene expression to be reliably detected. The failure of the electroporation delivery method means that obtaining high throughput delivery of the probes for real time measurements may not be feasible at this juncture as other methods for mass

cellular delivery require incubation times of at least 30 minutes and there is no practical method for the high throughput use of microinjection.

Reversible Permeabilization

In order to evaluate the use of reversible permeabilization as a delivery method for molecular beacons, two primary criteria were established. The first and most important was the efficiency of the delivery of the probe material. If an insufficient amount of probe is delivered to the cell, then the overall sensitivity of the measurement is affected. Also, the amount delivered to the cell needs to be relatively reproducible, there will likely be some cell to cell variations in delivery however many variations can be compensated for by using ratiometric analysis which will be discussed at a later point in the chapter. The second criterion is the incubation time required for the probe to be delivered in effective quantities. Since unmodified DNA based molecular beacons will be used for subsequent experiments, the incubation time for the delivery must take less than 30 minutes. This is due to the degradation of the molecular beacon inside the cell that occurs after 30 minutes. The MB degradation also causes the restoration of fluorescence thereby making it indistinguishable from target hybridization. Therefore, in measurements taken after 30 minutes it will be difficult to prove what signal it due to target hybridization and what signal is due to probe degradation.

Fluorophore labeled were delivered into living cells using a previously published reversible permeabilization protocol.[211] The protocol utilizes streptolysin O (SLO), which was shown to be a rapid, efficient, less damaging and more versatile compared with many conventional transfection methods.[212] Specifically, SLO was first activated by adding 5 mM of TCEP to 2 U/ml of SLO for 30 min at 37°C. Cells grown in 35mm dishes were incubated for 10 min in 200 ml of serum free medium containing 0.2 U/ml of activated SLO (0.5 U SLO per 10^6 cells) and 1μM of the AF488 labeled DNA. The cells were then incubated for different

incubation periods of 15 minutes, 30 minutes, 45 minutes, and 60 minutes. The cells showed uptake of the DNA after 15 minutes however the uptake did not plateau until 45 minutes (data not shown). Figure 5-3A shows a representative fluorescence image, Figure 5-3B shows the average fluorescence intensity of ten random cells. After 45 minutes, the cells showed a relatively reproducible fluorescence intensity that was quite suitable for imaging or other applications. While the incubation time was too long for conventional DNA MBs reversible permeabilization will likely be an effective delivery method for probe enhanced with nuclease or protein resistance.

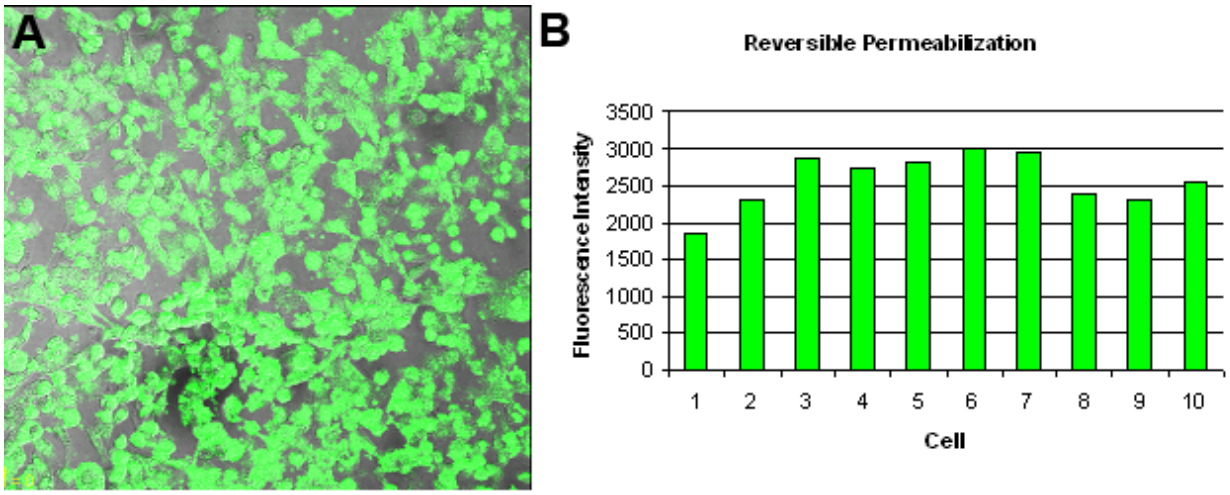

Figure 5-3. A) Fluorescence image of fluorophore labeled DNA delivered through reversible permeabilization. B) Average intensities of ten random cells after delivery of probe using reversible permeabilization.

Liposome Delivery

Another common used method for the delivery of DNA into the cells is the use of lipid based transfection reagents. These reagents form a bilayer similar to the cell membrane when placed in aqueous environments. Any material stable in the aqueous environment is then trapped inside the membrane. When mixed with the cells, the liposome can deliver their contents inside of the cell either through incorporation of the lipid bilayer into the cell membrane or the breakdown of the bilayer by lysosome inside of the cell both of which cause the release of the

materials into the cell. In order to determine whether the lipid based transfection would be suitable for probe delivery a commercially available transfection reagent Lipofectamine 2000 (Invitrogen) was used to deliver the AF488 labeled DNA. Prior to any experiments, the cells were incubated in antibiotic free media to prevent any uptake of the antibiotic into the cell. The uptake of the antibiotic into the cell through the liposome complexes is highly toxic to the cells. The stock DNA was then diluted to 1μM concentration while 10μL of Lipofectamine was diluted in a separate 50μL solution of cell media. Then the diluted Lipofectamine was gently mixed with 50μL of the DNA solution and incubated for 30 minutes. The cell media in the cell culture dish was then replaced with the transfection mixture and incubated for one hour. After the incubation period, the transfection reagents were removed and the cells were washed three times with cell media. The cells were then imaged with the fluorescence image of the cells shown in Figure 5-4A. The average intensities of ten random cells are plotted in Figure 5-4B. Incubation times of less than 1 hour were found to have significantly lower fluorescence intensities. The liposome based transfection results however indicate that this methodology can deliver sufficient amounts of material inside of the cell for analysis using MBs. However the incubations times required are unsuitable for DNA based MBs. As an interesting side note, the liposomes appear to have an affinity for the culture dish surface as well the cell membrane of the cultured cells. In each experiment conducted with the liposomes the bare cell culture dish surface generally had several highly fluorescent spots on the surface even after several washing steps. While this affinity did not appear to effect the overall results, the presence of the spots on the dish can impair the determination of the fluorescence background and lead to some uncertainty in those determinations. In addition, the liposome based methods had the greatest variability in the delivery and further use would likely require some form of normalization.

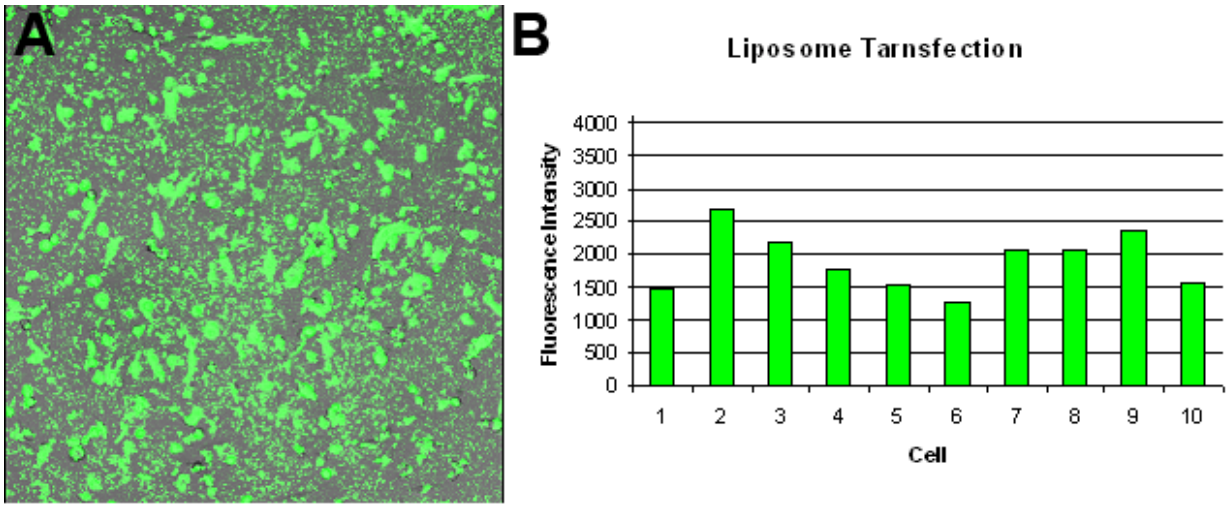

Figure 5-4. A) Fluorescence image of cells after delivery of fluorophore labeled DNA using a lipid based transfection reagent. B) Average fluorescence intensities of ten random cells after delivery of fluorophore labeled DNA.

Viral Vector Delivery

Following the establishment of the first infectious clone of AAV serotype 2 (AAV2) in 1982,[223] viral vectors have rapidly gained popularity in gene therapy applications, due to their lack of pathogenicity, wide range of infectivity, and ability to establish long-term transgene expression.[224] Recombinant AAV2 vectors have been tested in preclinical studies for a variety of diseases such as hemophilia, α1 anti-trypsin deficiency, cystic fibrosis, Duchenne muscular dystrophy, and rheumatoid arthritis. At least 20 clinical trials have been completed or initiated with 15 different AAV2-based vectors being administered in several hundred patients thus far.[224] Also, AAV vectors have been used for gene delivery in a variety of cell types including liver,[225-227] muscle,[226] brain,[228] retina,[229] and cancer cells.[230] Therefore, we have sought to determine whether they have the potential as a delivery vehicle for DNA based molecular probes. AAV viral vectors that were modified to express several biotin molecules on their surface were obtained from the labs of Kenneth Warrington. Prior to incubation with the cells, the virus vectors were incubated with excess FITC-labeled streptavidin for 12 hours. In theory, the

streptavidin would then be used to attach several biotinylated sequences onto the surface of the vector, however for this proof of concept the labeled streptavidin alone was used for the quantification of the amount delivered. After incubation with the streptavidin, the viral vectors were incubated with the cells for 1 hour that was based on published reports at a concentration of 1,000 viral particles per cell.

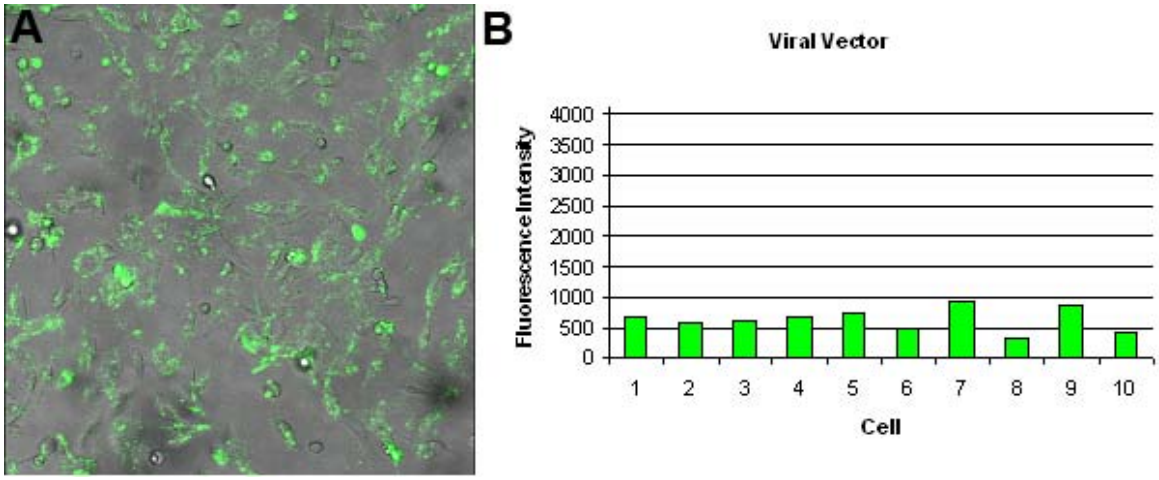

Figure 5-5. A) Fluorescence image of cells after incubation with a FITC-Streptavidin conjugated viral vector. B)The average intensity of ten random cells after incubation with FITC-streptavidin linked viral vectors.

Figure 5-5A depicts a representative fluorescence image of the cells while Figure 5-4B shows the average intensities of 10 random cells. Overall the viral vectors delivered a fair amount of material into the cell although it was less than many of the other methods tested. It should be noted however, that once any biotinylated probe was added to the vector, 2-3 times as much probe material could be delivered due to the multiple biotin binding sites situated on the streptavidin. While further optimization of the delivery protocol would have proved beneficial, there was insufficient virus for subsequent experiments. This indicates that another limitation of the viral vector based delivery is the lack of commercially available vector suitable for use with synthetic DNA probes.

Microinjection

Microinjection is a well established technique for the delivery of materials into the cell. The primary criteria for the delivery of the AF488 labeled DNA using microinjection was the amount of DNA delivered. Since no incubation time is necessary for microinjection, it allows the real time monitoring of hybridization events inside of the cell. However, the low throughput nature and high technical expertise required make systematic studies using microinjection much more difficult and time consuming. A Leiden microincubator with a TC-202A temperature controller (Harvard Apparatus, Holliston, MA) was used to keep the cells at 37^{o}C during injection and monitoring. An EXFO Burleigh PCS-6000-150 micromanipulator was used for positioning the injector tip. An Eppendorf Femtojet microinjector with 0.5μm Femtotips was used to inject the 1μM AF488 labeled DNA sequence into the cell. The cells were injected utilizing a 40x 1.35 NA oil immersion objective. The cells were injected with the DNA at 8psi for a duration of 10μs.

The cells to be injected were selected based on morphology in an effort to inject healthy cells. Cells displaying a small round morphology or a large blob-like morphology were not injected. Figure 5-6A shows a representative injected cell while Figure 5-6B shows the average intensity from 10 different injected cells. Overall the injected cells had the highest signal intensity of the delivery methods tested and showed good reproducibility. The use of microinjection produces several advantages in that the lack of an incubation time allows real time monitoring, an effective amount of probe can be delivered, and the approach is valid for most adherent cell types. That being said the previously mentioned disadvantages cannot be overcome as they are inherent to the microinjection based delivery.

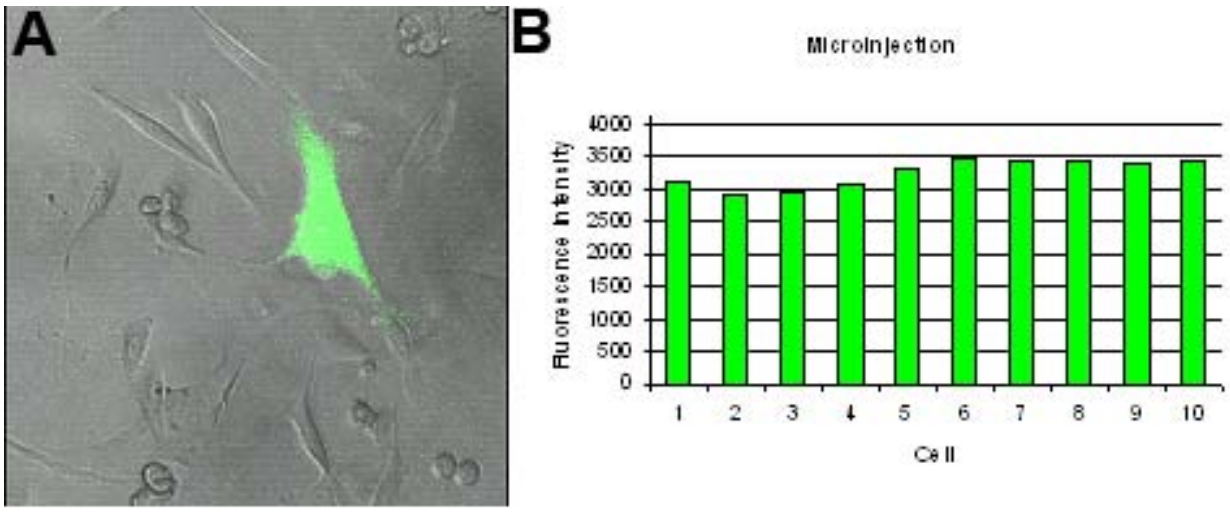

Figure 5-6. A) A representative image of a cell injected with the fluorophore labeled DNA. B) the average cell intensities of ten different cells inject with the fluorophore labeled DNA sequence.

Incubation

The delivery efficiency of a simple incubation of the AF488 labeled DNA sequence was also performed. This experiment was conducted more as a control for the previous techniques that required an incubation time than as a true delivery method. For these experiments, a 1μM solution of AF488 labeled DNA was prepared using cell media. The cells were incubated for 1 hour in the DNA spiked cell media after which the DNA spiked media was replaced with normal cell media. The fluorescence images and analysis were performed at that time. Figure 5-7A shows the cells after the incubation while Figure 5-7B illustrates the average cell intensities of the live cells obtained after incubation. While many of the dead cells (based on morphology) exhibited a high fluorescence intensity indicating an uptake of the probe, living cells showed little to no uptake of the fluorophore labeled DNA. This indicates that incubation alone is insufficient as a delivery method and that the results from the previous experiments where uptake of the DNA occurred were not due to simple incubation of the probe.

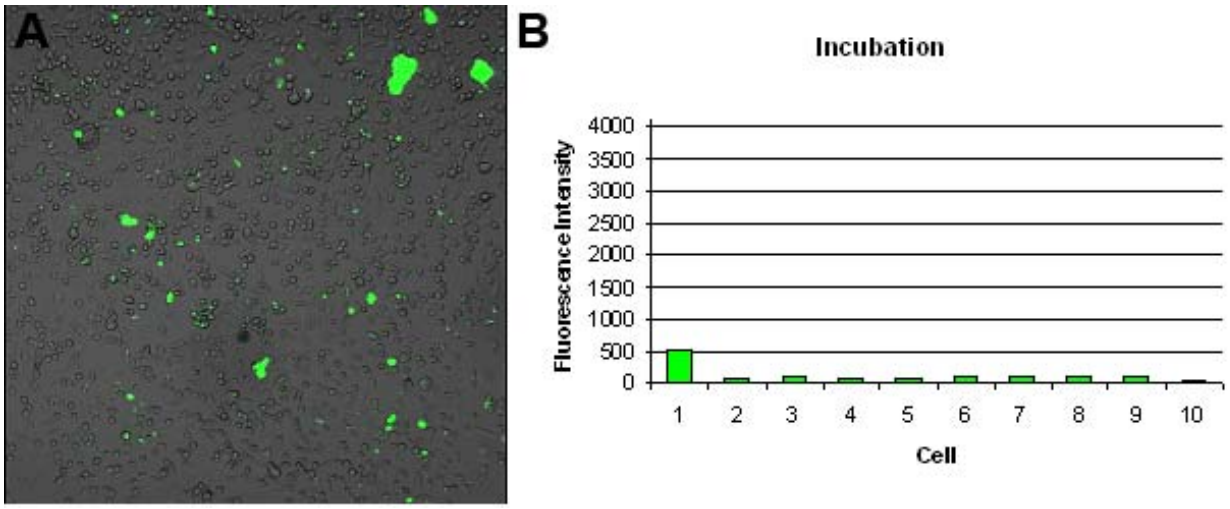

Figure 5-7. A) Fluorescence image of cells incubated with the fluorophore labeled DNA sequence for 1 hour. B) Plot of the average cell intensities of ten random cells incubated with the fluorophore labeled DNA.

Delivery Method Conclusions

In order to more effectively compare the different delivery methods, the average fluorescent intensities of the cells analyzed for each delivery method were calculated and plotted in Figure 5-8. Microinjection, reversible permeabilization, and the liposome based transfection all performed well with each method delivering experimentally significant amount of the fluorophore labeled DNA. The viral vector shows the potential for being a solid method for MB delivery although a great deal of work is still required to achieve that goal. Electroporation and incubation were both unsuccessful in delivering the fluorophore labeled DNA inside of the cells. However, in selecting a delivery method for future studies with DNA MBs, there were two main criteria established, one being that sufficient amounts of material can be delivered. The other criterion that is equally important is that any incubation must be less than 30 minutes. The two methods that achieved delivery in less than 30 minutes were microinjection and electroporation. The electroporation did not deliver sufficient material for use in the intracellular studies leaving microinjection as the only method left standing. However, when effective probes that are more

stable in the intracellular environment are used, delivery methods like the liposome transfection and reversible permeabilization should be very effective options for MB delivery assuming the similar delivery efficiencies with the non-standard MBs. The use of microinjection does create some additional problems. Certain problems like being low throughput and technically demanding are inherent to the method and cannot be effectively addressed. The variability that can be seen in the amount of probes delivered and other experimental variations can be addressed through different normalizations procedures. In particular, ratiometric analysis can be an effective tool in obtaining more reliable results from even technically demanding intracellular studies.

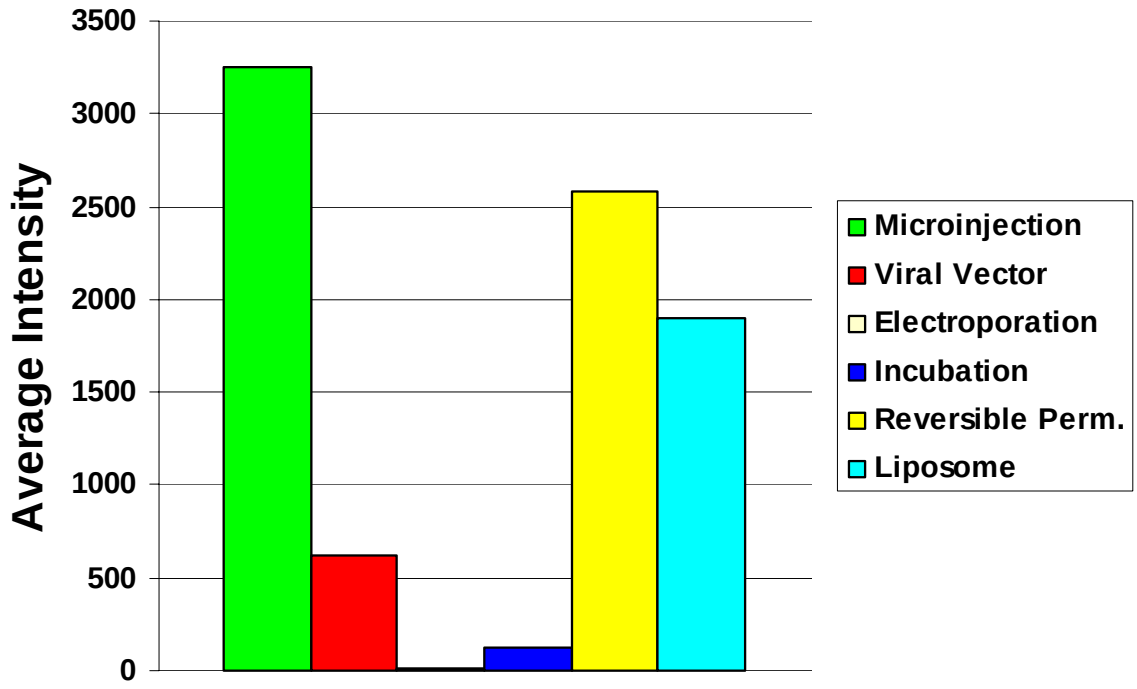

Figure 5-8. Average intensities from the cells for each DNA delivery method tested.

Ratiometric Analysis

The potential of using MBs to detect DNA and mRNA inside living cells has previously been demonstrated. However, such intracellular measurements have been based on measuring

the intensity of a single fluorescence signal. This fluorescence signal can be affected by signal changes from light scattering by the sample, excitation source fluctuations, variability in the intracellular delivery, and variability in the intracellular environment.[231,232] As a result, the use of MBs has been limited to visualization and not quantitation. Ratiometric analysis is one methodology that can address the problems posed by taking intensity measurement[231,233,234] since they normalize these effects by taking the ratio of the signal intensity caused by the specific probe for a target over the signal intensity produced by an unrelated reference probe that works as an internal standard. The ratio value is calculated by dividing the MB signal intensity by the signal intensity of the reference probe. Since the ratio between the two molecules stays constant change in the ratio only occurs when there is a change in the fluorescence intensity in one probe and not the other, like when the MB hybridizes to its target. The ratiometric analysis allows for the normalization of the fluorescence intensities from a myriad of experimental factors thus providing more reliable data.

To demonstrate the advantage of the ratiometric analysis used in future experiments a series of injections were made into the MDA-MB231 cells. For each injection the time duration of the injection was varied so that different amounts of material would be delivered to each cell. The probe solution consisted of 1μM concentrations of DNA labeled with either AF488 or AF647. The ratio of the DNA mixture was held constant. The cells were then monitored for nine minutes after injection and the fluorescent intensities of both probes were measured. Figure 5-9A shows the AF647 intensities of five cells injected with different amounts of fluorophore. This represents how the fluorescence intensity from experiment to experiment can altered in a controlled format as the cells showed dramatically different fluorescence intensities. However, when the same intensities are normalized through the ratiometric analysis, the result is a fairly

constant ratio as illustrated in Figure 5-9B. This allows for more reproducible results to be obtained in the intracellular experiments and for more reliable gene expression data.

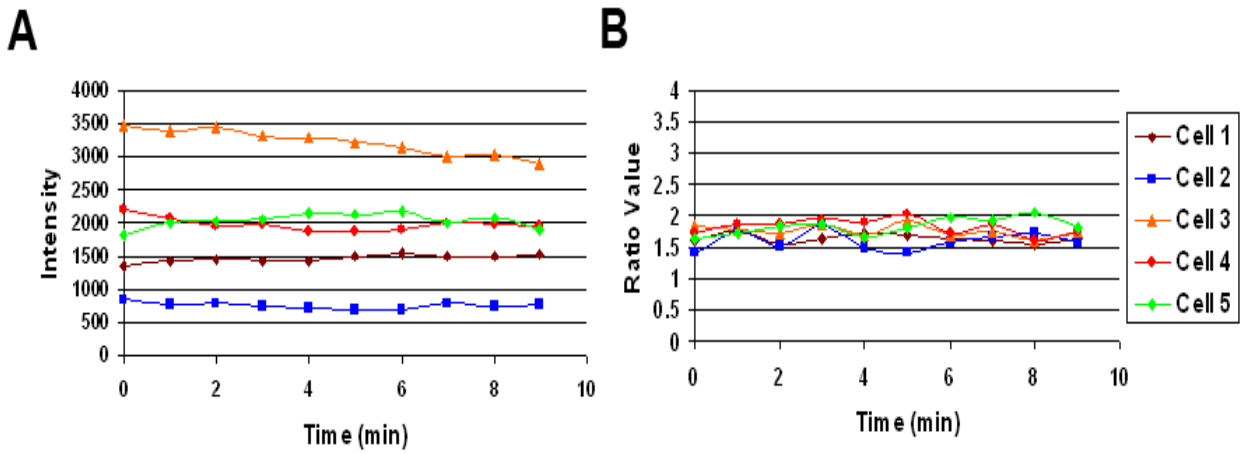

Figure 5-9. A) Fluorescent intensities over time for five cells injected with different amounts of fluorophore labeled DNA. B) The same cells after ratiometric analysis is used to normalize the fluorescent intensities.

In Vitro Testing of Molecular Beacons

In order to use the MBs for multiplexed studies, their individual performance for both *in vitro* and *in vivo* had to first be evaluated. The MBs were first tested in simple buffer experiments to confirm that they could hybridize selectively to their targets and that their signal enhancements were sufficient for intracellular analysis. Each MB that will be used in the subsequent intracellular experiments was first tested in buffer solution to verify its performance prior to intracellular demonstration. Each MB was diluted to a 1μM solution, each MB sample was then incubated with either buffer, 10μM target DNA, or 10μM random DNA. The signal intensities from the samples with target and random DNA were then divided by the closed MB intensity determined from the sample incubated with buffer. This ratio is referred to as the signal enhancement of the MB and the enhancements from the target and random DNA were plotted in Figure 5-10 for each MB sequence and fluorophore quencher pair.

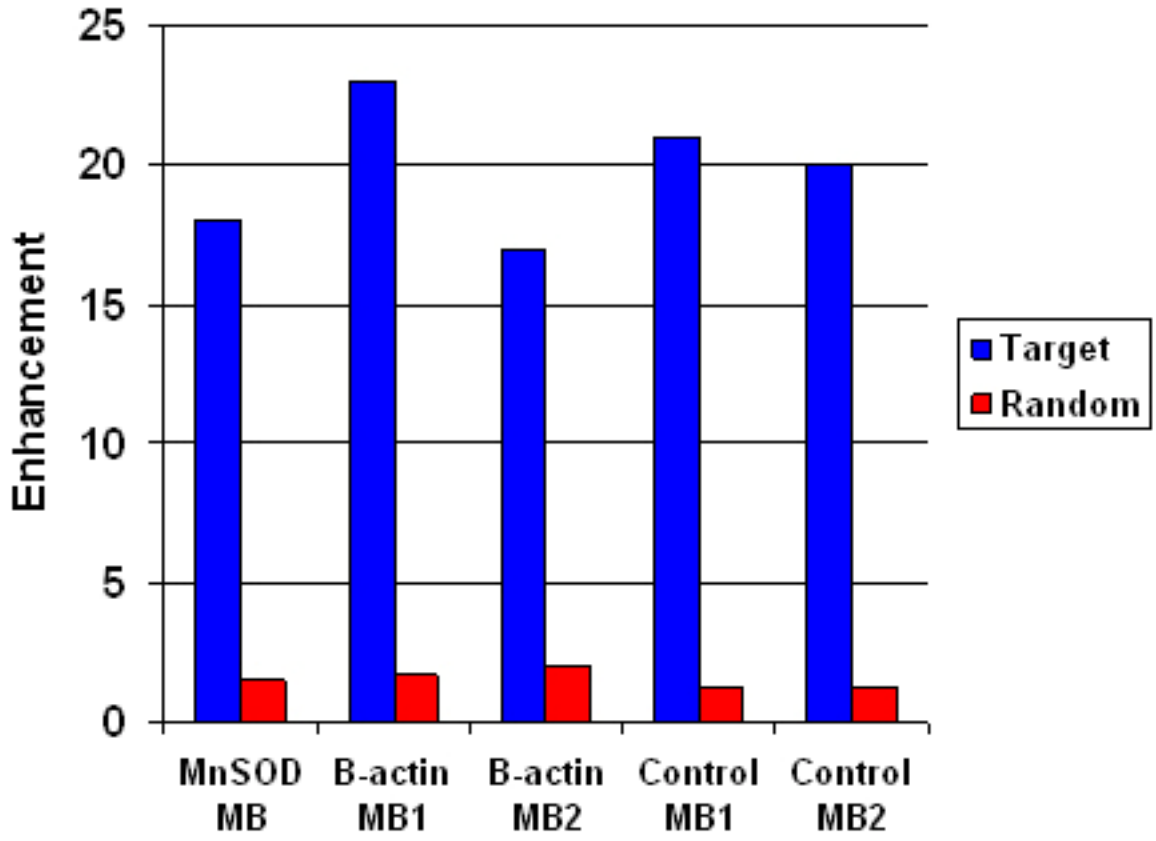

Figure 5-10. Signal enhancements in buffer solution for each MB utilized in the intracellular experiments.

The sequences and fluorophore quencher pairs for the MBs are listed in Table 5-1. The figure illustrates that each MB has excellent selectivity and a good signal enhancement of at least 15. The establishment of the 15 fold criteria simply indicates that the beacon undergoes a significant signal transduction upon binding to its target however the beacons were also assessed on their overall intensity as intracellular measurements require probes with very high signal intensities. Therefore, the beacons used in the subsequent two chapters were thoroughly and effectively evaluated prior to use.

Conclusions

Based on the results in this chapter, the optimal parameters for future intracellular experiments were determined. The sequences for the MBs were tested and the fluorophore and

quencher pairs were tested and optimized. The delivery methods for oligonucleotides were thoroughly evaluated leaving microinjection as the preferred method for DNA MB studies. The future application of this work is for the effective detection and monitoring of the MBs inside of single cells. The right selection of fluorophores and sequences with the most effective delivery method should allow for the sensitive detection of multiple mRNA sequences inside of a single cell. This would allow biological studies into how the expression levels of different genes are related and allow for new trends and correlations to be observed.

CHAPTER 6
STUDY OF CANCER CELLS THROUGH MULTIPLE GENE MONITORING

Introduction

A method in which the mRNA expression profile of a single cell can be collected and compared against another single cell would provide a powerful tool for many biological or medical applications that involve gene expression. In particular, the ability to monitor cytoplasmic mRNA expression of multiple genes would facilitate the study of cells to shed more light on disease processes and drug responses at the single cell level. In our research, we have sought to demonstrate the ability to monitor the mRNA expression of multiple genes and differentiate between different levels of mRNA expression. We have also sought to show that the data collected can be further analyzed to expose trends in multiple individual cells that would go unnoticed in single gene monitoring experiments. In these experiments, we used three separate molecular beacons with three unique fluorophores to measure the expression levels of different genes in the cytoplasm of a single cell. Along with the molecular beacons, a reference probe is also injected in order to conduct the ratiometric analysis. The molecular beacons were designed to be complementary to β-actin mRNA and manganese superoxide dismutase (MnSOD) mRNA, while a control molecular beacon was designed that has no complement inside of the cells. MDA-MB-231 breast carcinoma cells were used both at basal expression levels and after exposure to lipopolysaccharide (LPS), which is an inflammatory mediator involved in *E. coli* bacterial sepsis and is known to stimulate MnSOD mRNA expression in multiple mammalian cells. One of the limitations of molecular beacon's use for intracellular analysis has been the variability of the fluorescent signal inside of cells from an array of causes including light scattering in the sample, excitation source fluctuations, and variations in microinjection delivery of the molecular beacons into the cell. In an effort to achieve more reliable results for molecular

beacons, *in vivo* ratiometric analysis was conducted to compensate for the instrumental and experimental sources of these fluctuations. Ratiometric analysis involves injecting a reference probe along with the molecular beacons inside of the cell. The reference probe emits a stable constant fluorescence signal that acts as an internal standard for analyzing the signals from the molecular beacons. This technique thus allows the molecular beacon signals from different cells to be directly compared.

Methods and Materials

Cell Culture

MDA-MB-231 breast carcinoma cells (American Type Culture Collection, Manassas, VA) were maintained in Dulbecco's Modification of Eagle's Medium (DMEM, Fisher Scientific) with 10% fetal bovine serum (Invitrogen, Carlesbad, CA) and 0.5 mg/ml Gentamycin (Sigma, St. Louis, MO) at 37^{o}C in 5% CO_2/air. Cells were plated in 35mm glass bottom culture dishes and grown to 80% confluency (MatTek Corp., Ashland, MA) for 48 hours prior to injection. To stimulate MnSOD mRNA expression, cells were incubated in 1μg/ml LPS from *E. coli* serotype 055:B5 (Sigma, St. Louis, MO) for 4 hours prior to injection.

RNA Isolation and Northern Blot Analysis

MDA-MB-231 cells were grown as described on 100 mm tissue culture plates until 70-90% confluent prior to treatment with LPS concentrations of 0.1microgram/mL or 1 microgram/mL for 1, 2, and 4 hours. Total RNA was isolated by the acid guanidinium thiocyanate-phenol-chloroform extraction method described by Chomczynski and Sacchi[235] with modifications.[236] Twenty micrograms of total RNA was size-fractionated on a 1% agarose formaldehyde gel and electrotransferred to a charged nylon membrane (Zetabind, Cuno Laboratory Products, Cuno Inc., Meriden, CT) and UV covalently cross-linked. The membrane

was hybridized with ^{32}P-labeled human MnSOD or glyceraldehye-3-phosphate dehydrogenase (GAPDH) (as an RNA loading control) cDNAs and subjected to autoradiography.

Equipment

Fluorescence imaging was conducted with a confocal microscope setup consisting of an Olympus IX-81 inverted microscope with an Olympus Fluoview 500 confocal scanning system and three lasers, a tunable Argon Ion laser (458nm, 488nm, 514nm), a green HeNe laser (543nm), and a red HeNe laser (633nm) with three separate photomultiplier tubes (PMT) for detection. The cellular images were taken with a 60x 1.4 NA oil immersion objective. A Leiden microincubator with a TC-202A temperature controller (Harvard Apparatus, Holliston, MA) was used to keep the cells at 37^{o}C during injection and monitoring. An EXFO Burleigh PCS-6000-150 micromanipulator was used for positioning the injector tip. An Eppendorf Femtojet microinjector with 0.5μm Femtotips was used to inject the molecular beacons and reference probe into the cells. All analysis was conducted on the Fluoview 500 software, followed by processing of the data using Microsoft Excel.

Fluorescence Imaging

All cellular fluorescent images were collected using the confocal microscope setup. The confocal consists of an Olympus IX-81 automated fluorescence microscope with a Fluoview 500 confocal scanning unit. There are three lasers providing laser excitation at 458nm, 488nm, 514nm, 543nm, and 633nm. Alexa Fluor 488 based probes were excited at 488nm and collected at 520nm. The Alexa Fluor 555 based MBs were excited at 543nm and collected at 560nm. The Alexa Fluor 647 based MBs were excited at 633nm and collected at 660nm. RuBpy was excited at 458nm and the emission was collected at 610nm. Images were taken after a five to ten second period during which the instrument was focused to yield the highest intensity from the

fluorescence channels. The images were assigned color representations for clarity and are not indicative of the actual emission wavelengths.

Molecular Beacon Design for Multiple Gene Monitoring

One of the first issues confronting these experiments was selecting the appropriate fluorophores to use on the three molecular beacons and the reference probe to ensure that no crosstalk or fluorescence resonance energy transfer (FRET) was taking place. Due to their high quantum yields and separation of their emission and excitation wavelengths AF488, AF555, and AF647 were chosen for the fluorophores of the molecular beacons while RuBpy was chosen for its excitation wavelength which proved not to excite the molecular beacon fluorophores (data not shown). In addition, experiments were conducted to test the stability of each dye inside of the cell. Each dye including RuBpy was conjugated to a random oligonucleotide sequence and injected inside of a single cell. Those experiments showed that the fluorophores demonstrated excellent stability in a cellular environment for the length of the measurement (data not shown). The injections of dye labeled oligonucleotide also allowed the calibration of the channels since the dye labeled oligonucleotide would mimic the response of fully open molecular beacons inside of the cell and allowed for the optimization of the optics to use for each channel to eliminate cross-talk between the different channels in the confocal system. Experiments were also conducted to verify that each molecular beacon could function properly inside of the cell by itself before conducting any experiments with multiple molecular beacons (data not shown). Part of these experiments included monitoring the stability of the control molecular beacon inside of the cell to determine the lifetime of the probes inside of the cell. The control molecular beacon has no target inside of the cell and therefore any increase in signal from the molecular beacon is due to non-specific binding or degradation of the probe. We found that the molecular beacon was stable inside of the cell for 35 minutes after which there was an increase in the fluorescence.

This indicates the molecular beacons have a finite lifespan inside of the cell of approximately 30 minutes, after that the molecular beacon can no longer be considered functional inside of a cell.

Multiple Gene Monitoring

With the suitable control experiments completed, the next experiments involved the actual detection of mRNA inside of a single cell and monitoring its expression over a set amount of time. Figure 6-1 shows an image of each molecular beacon detection channel and the reference channel to demonstrate the stability of the reference probe over time and the basal expression of β-actin. In this experiment femtoliters of 1μM of each of the three molecular beacons and 20μM of the RuBpy reference probe were injected into a single human breast carcinoma cell. Using the signal from the reference probe, the instrument was focused to yield the highest fluorescence intensity in the reference channel. After an initial image is collected, the cell is monitored for 14 minutes with the fluorescent signal from each channel being measured every minute. This allows ample time for the molecular beacon to hybridize with its mRNA complement without the increase on fluorescence that may accompany the degradation of the molecular beacon after 30 minutes. The PMT for each channel was set to be able to measure the full enhancement of each molecular beacon as determined in the control experiments. The nucleus of the cell in each channel was discarded during analysis of the signal since nuclear uptake mechanisms exist that cause nucleic acids to be transferred to and non-specifically opened or degraded in the nucleus. This process can cause a false-positive signal, although it is unclear whether the signal is from degraded probes or simply the concentration of the fluorescent probes in the nucleus. Thus the analysis of the fluorescence signals from the cell cytoplasm is used to determine the mRNA expression levels.

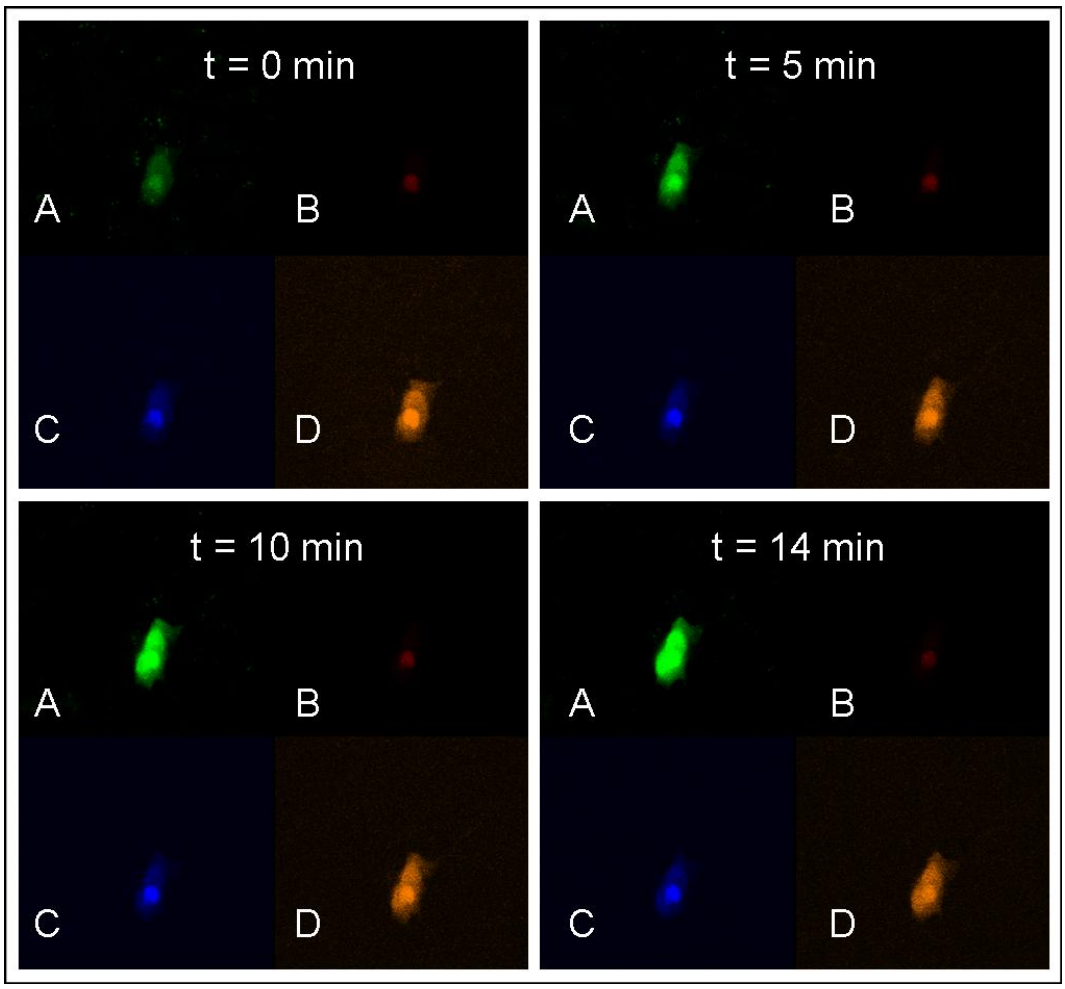

Figure 6-1. Time elapsed fluorescent images of each MB inside of a single MDA-MB-231 cell. A is the image of the β-actin MB (green), B is the image of the control MB (red), C is the image of the MnSOD MB (blue) , and D is the image of the RuBpy reference probe (orange).

In the channel B, the channel monitoring the control molecular beacon, there is a very small amount of background fluorescence from the molecular beacon, most likely from incomplete quenching of the fluorophore or some form of degradation. The signal however remains at a very low level throughout the monitoring period, even as the other molecular beacons show an increase in their fluorescence signal. Due to the overall low level of fluorescence and the lack of any increase of fluorescence, it appears the control molecular beacon remains closed inside of the cell over the monitoring period, which shows that the

molecular beacon is mostly stable and also represents the absence of its complement. The significance of the negative response of the control molecular beacon is that it indicates that the signal produced from the other molecular beacons inside of the cell is a result of the hybridization with its mRNA complement and not due to degradation of the probe inside of the cell. If degradation were taking place during the monitoring period, then the control molecular beacon as well as the MnSOD and β-actin molecular beacons should have been affected equally producing fluorescence.

In channel A, the channel monitoring the β-actin molecular beacon, the fluorescence signal starts at a barely detectable level and increases over time to a level in which the fluorescence saturates the PMT. The increase of fluorescence represents the hybridization of the molecular beacon and its target, the β-actin mRNA. This is consistent with the high expression anticipated for β-actin mRNA. The MnSOD molecular beacon monitored in channel C shows a slightly higher fluorescent signal than the control molecular beacon but not to the extent seen in the β-actin molecular beacon. This is consistent with basal levels of MnSOD mRNA, which are usually at a low expression level. From this experiment we have seen that it is possible to monitor more than one gene simultaneously inside a single living cell.

Monitoring Stimulated Gene Expression

The next goal was to demonstrate the method's ability to monitor gene expression changes in response to cellular treatment. For these experiments two groups of cells were used, one control group of human breast carcinoma cells and a second group where the gene expression of MnSOD had been induced by LPS stimulation. The inducible expression of MnSOD mRNA by LPS has been previously described[236] and was verified by Northern analysis prior to the cellular monitoring experiments. Northern analysis allows for the accurate determination of steady-state mRNA expression from a large number of cells. MDA-MB-231 cells were incubated with LPS

for time intervals of 1, 2, or 4 hours prior to total RNA isolation and northern analysis. The results shown in Figure 2 confirm that MnSOD mRNA expression is significantly increased after incubation with 0.1μg/ml or 1.0μg/ml LPS. During this short LPS-exposure experiment, the greatest increase in MnSOD mRNA expression was observed after a four hour incubation with 1.0μg/ml LPS.

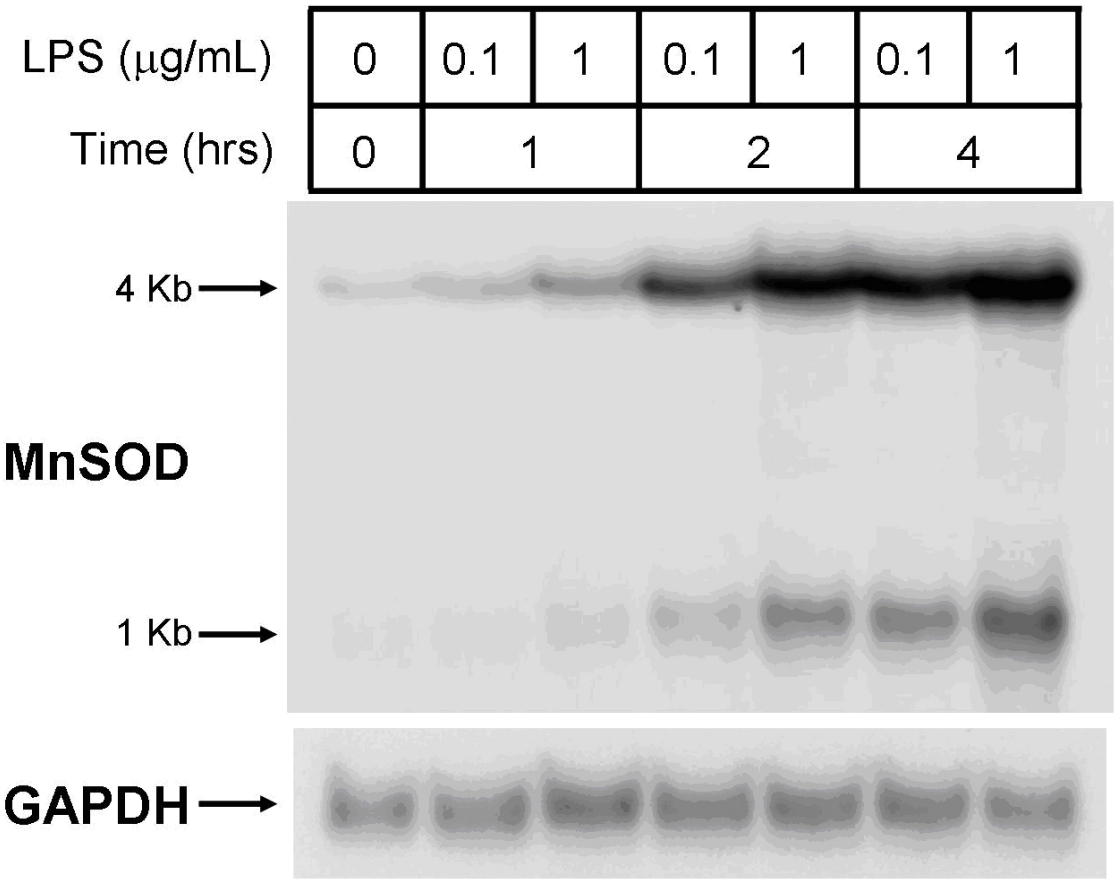

Figure 6-2. Northern analysis of LPS-inducible MnSOD mRNA expression in MDA-MB-231 cells.

Based on the ability of the cells to produce a significant increase in MnSOD mRNA production after a four hour incubation with LPS, the three molecular beacons and the reference probe were injected into a control and an induced human breast cancer cell in order to monitor a change in the MnSOD mRNA expression. The experimental parameters were similar to the

initial mRNA expression monitoring experiment with each molecular beacon at a concentration of 1μM and the RuBpy reference probe at a concentration of 25μM. Each cell was monitored for 14 minutes and the same signal collection and analysis protocols were observed as used in Figure 6-1. The signals from the cytoplasm were then measured along with those of the background. The background in each channel was subtracted from both the molecular beacon signal and the reference signal, after which the ratio values were calculated. The experiment was repeated multiple times and the results of a representative cell are shown in Figure 6-3.

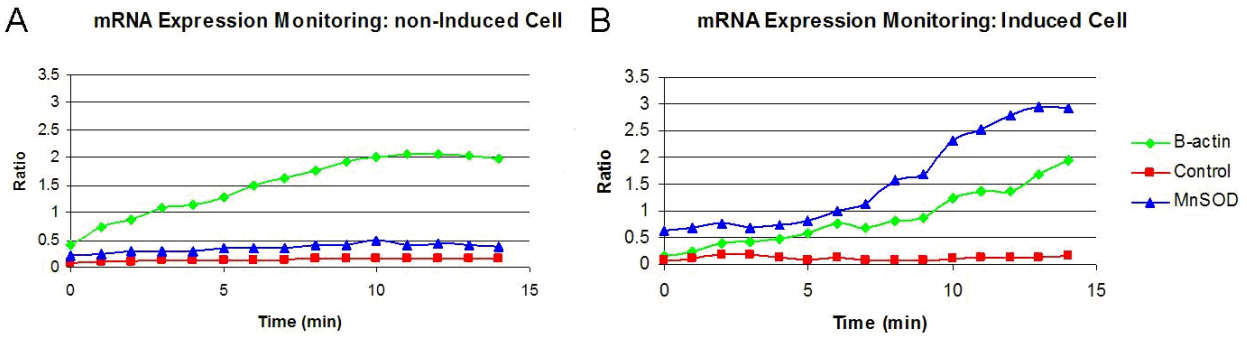

Figure 6-3. Ratiometric analysis of the real time monitoring of gene expression (A) Real-time monitoring of gene expression in a single control MDA-MB-231 cell. (B) Real-time monitoring of gene expression in a single LPS induced MDA-MB-231 cell.

In both cells the control molecular beacon exhibits the same constant low level of fluorescence. Since this molecular beacon shows no increase in signal and has no target inside of the cell it is believed that it remains closed during the monitoring time. Unlike the control molecular beacon, the β-actin molecular beacon shows an increase in fluorescence in both cells, using the same rationale as before it is believed that the β-actin molecular beacon is hybridizing with the β-actin mRNA. The level of β-actin is similar in both cells which is expected since LPS has not been shown to impact the expression of β-actin mRNA. The signal from the MnSOD molecular beacon however changes significantly in the induced cell when compared to the non-induced cell. Whereas no significant increase in the MnSOD molecular beacon signal is

observed in the control cell, there is a large increase in signal from the MnSOD molecular beacon in the induced cell. Based on the lack of change in the control and β-actin molecular beacon it is believed that this large increase in signal is due to the increased expression of MnSOD mRNA. This is consistent with the Northern analysis, which also showed a large increase in MnSOD mRNA expression in cells exposed to LPS. Thus the results from the Northern analysis correlate with the results obtained from the multiple gene monitoring by molecular beacon.

The gene expression profile was determined twenty times for both the control and LPS-induced cells, the average peak ratio for each molecular beacon was calculated as the average ratio value after the signal plateaued inside of the cell. This value is used as the final signal from each molecular beacon. Consistently in each of the cells measured, high expression levels of β-actin mRNA were measured along with constant low signals from the control molecular beacon. There was a degree of variation in both the LPS induced and non-induced cells that showed some variation in how highly β-actin mRNA was expressed. This is consistent with the findings of other investigators that there are cell to cell variations in gene expression.[237-239] In each induced cell there was a high expression level of MnSOD, which was far different from the control cells, which generally showed a very low expression level with the exception a few that showed a moderate level of MnSOD expression. The induced cells were consistent with our expectations based on the results of the Northern Blot. In agreement with the β-actin mRNA expression, the induced and non-induced MnSOD mRNA expression showed some variability which is again consistent with the belief that there is no average cell and that mRNA expression will vary from cell to cell.

In order to compare the results from all of the cells, the average peak signals from each cell were collected and plotted in a histogram in Figure 6-4. The histograms clearly show a shift in the MnSOD mRNA expression in the induced cells when compared to the non-induced cells. The average ratio of signals for each molecular beacon was found to be 1.8 for β-actin, 0.2 for the control MB, and 0.6 for MnSOD in the untreated control cells; and 2.1 for β-actin, 0.3 for the control MB, and 2.0 for MnSOD in the induced group of cells. Thus in each of the twenty induced cells there was a significant increase in the ratio of the MnSOD molecular beacon when compared to the control cells. The β-actin and control molecular beacons had relatively similar ratios in both the induced and control cell lines, throughout the entire series of experiments, although the β-actin expression showed a small increase in expression in the LPS-induced cells.

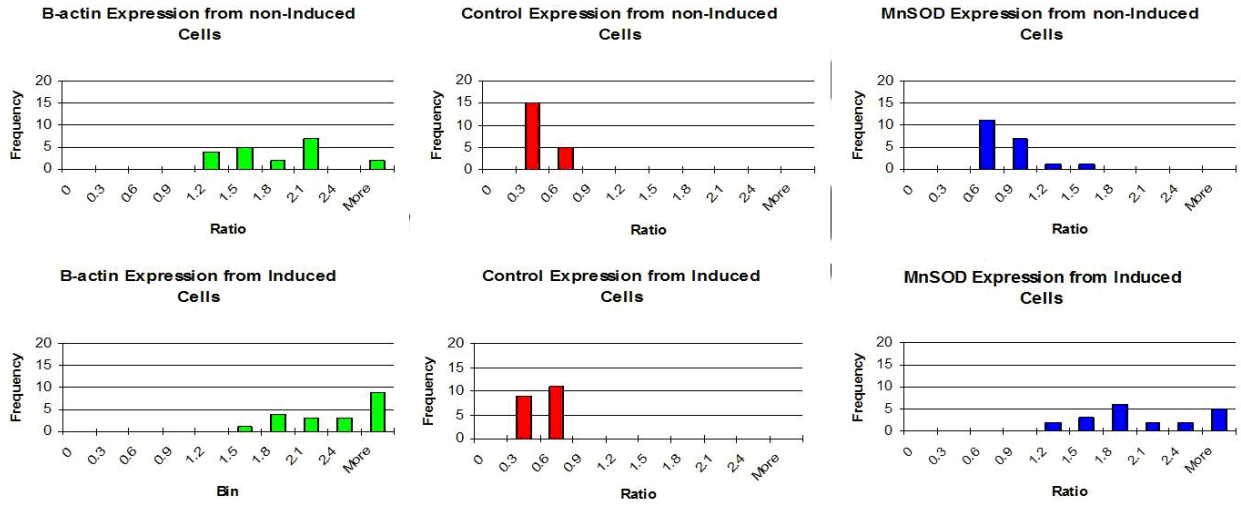

Figure 6-4. Histograms showing distribution of ratiometric responses for control and LPS induced MDA-MB-231 cells with control MB (red), MnSOD MB (blue) and β-actin MB (green) measured simultaneously in each cell.

Gene expression pattern comparison

Since we are able to detect and monitor the mRNA levels of different genes inside the same single cell, comparisons can be made at the single cell level and trends can be elucidated. In determining the gene expression profiles of both groups of cells, there were variations in the

levels of gene expression in both β-actin and MnSOD mRNA. Based on results we sought to determine if the variations formed a pattern of gene expression or were merely random fluctuations. It was unknown if any such pattern existed since no previous literature was found that compared the mRNA expression of multiple genes inside the same cell to expression levels inside of other single cells. In this comparison the MnSOD and β-actin mRNA expression levels were set relative to the control molecular beacon to compensate for any variances in the cellular environment that would cause the expression levels to appear artificially high or low. The relative ratios from each cell were then plotted against each other in Figure 6-5 to determine whether any pattern existed.

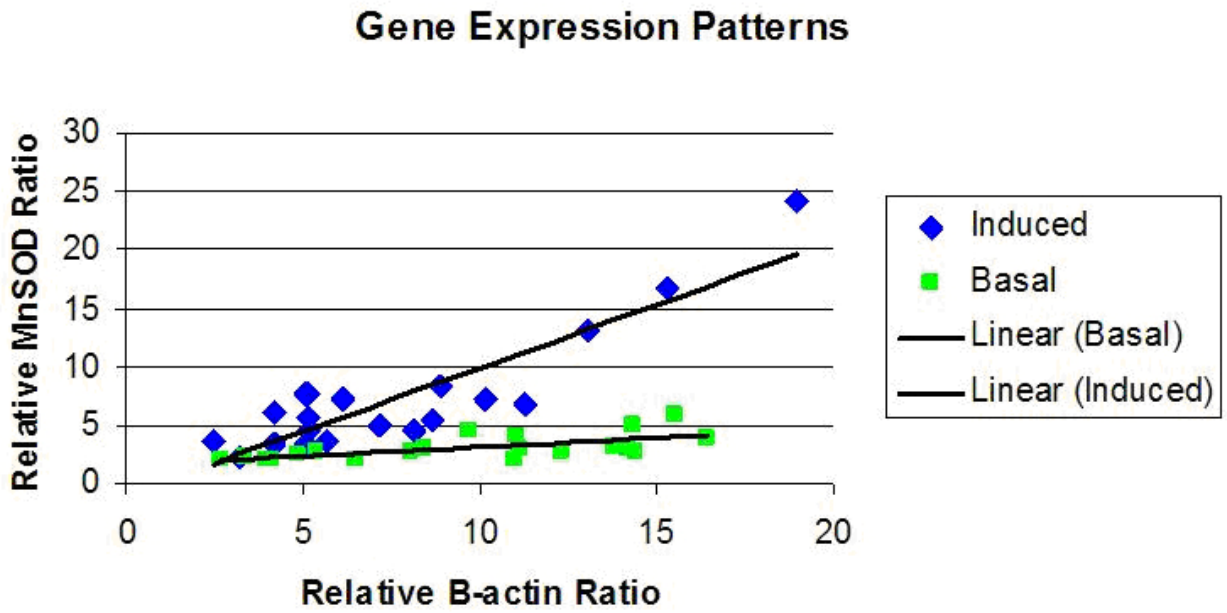

Figure 6-5. Plots showing the relationship between the relative β-actin mRNA expression and the relative MnSOD mRNA expression in both the LPS-induced and non-induced cells.

This analysis yielded a relationship between the expression levels of MnSOD and β-actin. In the plot this relationship based on R^2 values yielded a linear relationship but it is unknown whether this is truly representative. The line mainly serves as a guideline for comparison. The analysis does show that when the β-actin mRNA expression is high in comparison to other cells,

the basal and induced levels of MnSOD mRNA is also high. This correlation is possibly explained by effects of MnSOD expression on the cell cycle. Previous work on different cell lines indicates that high MnSOD expression retards the transition from the G_1 phase to the S phase.240 Further research has shown that β-actin expression is upregulated in the G_1 phase.[241] This indicated that a likely explanation for the trend is that the higher MnSOD expression causes the cell to remain in the G_1 cell cycle phase which also causes the upregulation of β-actin mRNA. On the other hand it is also possible that the trend is due to an artifact in the experimental method caused by biology phenomena such as differential transport into the nucleus or localization of the probes to different parts of the cell given their different sequences. Future studies will examine the uptake and transportation kinetics of the probes that may provide information to better distinguish between trends and artifacts. However, the observed relationship demonstrates the potential of the technique to explore the inner workings of cell by giving a more complete picture of processes involving mRNA expression by detecting the expression of multiple genes in single cells instead of focusing on merely a single mRNA expression.

Conclusions

We have demonstrated a novel method to monitor multiple molecular beacons simultaneously using confocal microscopy allowing determination of multiple genes' expression profiles within single human breast carcinoma cells. Once the suitable control experiments were conducted, the mRNA expression was measured in individual cells that expressed both basal and stimulated levels of mRNA. After satisfactory results were obtained, the method was reproduced on twenty control and LPS induced cells. The β-actin molecular beacon and the control molecular beacon demonstrated similar expression levels in the control and LPS induced cells however the MnSOD molecular beacon showed a significantly higher response when the

expression of MnSOD was induced with LPS. This trend agreed with the Northern analysis of LPS induced MDA-MB-231 cells (Figure 2). The individual cells in both the control and induced groups displayed variation in gene expression which is consistent with the varied expression profiles seen by other investigators using fixed cells [17,18,19]. We have demonstrated the ability to differentiate between basal and stimulated levels of mRNA expression. Furthermore we showed the ability draw correlations between the levels of mRNA expression on a single cell level. This methodology should also have a wide applicability since in theory any mRNA for which a molecular beacon can be designed can be studied along with controls or to simply monitor the expression of multiple genes inside of any single cell.

Future research in this area includes determining the effect of the cell cycle on the levels of mRNA measured, evaluating the toxicity of the probes on the cell, and measuring the kinetic parameters of the probes inside of the cell. These experiments will allow us to limit the cell to cell variability and allow for better distinctions to be made between cellular trends and artifacts of analysis. Future applications of this method involve applying it to disease states to study effects on gene expression. These include issues of medical relevance such as investigating the effects on gene expression in human breast carcinoma cells after treatment with chemotherapeutic drugs. Other issues of biological importance involve investigating multiple mRNA expression patterns in single neuron cells as a means of investigating the processes involved in memory and learning. Furthermore, plans to incorporate nuclease resistance into molecular beacons would allow extended measurements of molecular beacon fluorescence inside living cells to the order of hours or days and incorporating different types of analytes like ions and proteins, thus truly broadening the scope of future experiments. Ultimately, utilizing molecular beacons linked to cell-penetrating peptides may allow the delivery of multiple

molecular beacons to thousands of cells simultaneously. Development of such techniques might eventually permit clinical laboratories to utilize MBs in fluorescent plate readers for diagnostic and drug sensitivity assays in cells obtained from human biopsy specimens for a variety of disease states.

CHAPTER 7
STUDY OF CANCER CELLS BY MONITORING MULTIPLE ANALYTES

In the previous chapter, fluorescence microscopy was used to monitor multiple gene sequences inside of a single human breast cancer cell. However, only looking at a single analyte type only gives a partial look at the complex processes inside the cell as genes are only one important class of molecule inside of the cells. In most studies the detection and monitoring of analytes is restricted to a single type of analyte. By monitoring different types of analytes inside of the cell, more complex phenomena can be studied including different signaling pathways. By studying the different analytes at the single cell level, trends and correlations can be elucidated by comparing the signal levels inside of different groups of signal cells. In this way, the groups can be compared on a cell to cell instead of relying on the average responses of millions of cells. In addition to genes, molecules like ions have many vital functions inside of the cell. In particular Ca^{2+} is an important signaling molecule to help regulate muscle contraction, neurotransmitter release, cell migration, gene expression, and cytoskeleton manangement. In order to advance the utility of single cell studies, we propose using MBs and fluorescent Ca^{2+} indicators simultaneously in the same single cell. By combining these different types of fluorescent probes for intracellular analysis we can develop a more complete understanding of biological processes. The ability to detect and monitor these two very different types of analytes simultaneously will have far reaching applications from basic biological investigations to the study of diseases like cancer.

Methods and Materials

Fluorescent Probes

All MBs were designed in-house based on published mRNA sequences. The Alexa Fluor based MBs were synthesized by Genomechanix (Gainesville, FL) while the rest of the MBs were

synthesized in-house. The fluorophores Alexa Fluor 555 (AF555), and Alexa Fluor 647 (AF647) were purchased from Invitrogen (Carlsbad, California). All other reagents including Tetramethylrhodamine (TMR) and Cy5 fluorophores were purchased from Glen Research (Sterling, VA). The quenchers used for the MBs were Blackhole Quencher 2 (BHQ2) and Blackhole Quencher 3 (BHQ3). The sequences and fluorophore/quencher pair combinations used are listed in Table 1. The probe solution used for injections in the experiments contained 1μM of each MB and in 20 mM Tris, 50mM NaCl and 5mM Mg_2Cl_2 buffer. All MB sequences were tested *in vitro* prior to use and all exhibited enhancements greater than 15 fold upon target hybridization. Cell-permeant Fluo-4 Calcium ion indicator was purchased from Invitrogen (Carlsbad, California) and diluted in DMSO to a concentration of 5mM. The Fluo-4 was then further diluted to 1μM in cell media. The cells were incubated in the Fluo-4 media for one hour prior to injection of the MBs. All probes were first evaluated separately inside of the cells prior to any multiplexing experiments to verify and evaluate their performance.

Cells

MDA-MB-231 breast carcinoma cells (American Type Culture Collection, Manassas, VA) were maintained in Leibovitz's L-15 Medium (American Type Culture Collection, Manassas, VA) with 10% fetal bovine serum (Invitrogen, Carlesbad, CA) and 0.5 mg/ml Gentamycin (Sigma, St. Louis, MO) at 37^{o}C. Cells were plated in 35mm glass bottom culture dishes and grown to 80% confluency (MatTek Corp., Ashland, MA) for approximately 48 hours prior to any experiments. TSA exposed cells were incubated in 300ng/ml Trichostatin A from Streptomyces sp. (Sigma, St. Louis, MO) for 24 hours prior to injection.

Protein isolation and Western analysis

MDA-MB-231 cells were grown as described on 100 mm tissue culture plates until 70-90% confluent prior to treatment with a TSA concentrations 50, 100, and 300ng/mL for 24

hours. Total cellular protein was harvested utilizing CellLytic-M Mammalian Lysis Extraction Reagent (Sigma-Aldrich Co.) and Complete protease inhibitors (Roche Biochemicals). Protein concentrations were measured by modified Bradford assay (Pierce Biotechnology) and proteins (20 micrograms of total protein for each sample) were size fractionated on a 10% Tris-Glycine polyacrylamide gel (Invitrogen) and electro-transferred to a cellulose acetate membrane for western analysis. Rabbit anti-MnSOD antibody and mouse monoclonal anti-□-tubulin antibody (Stressgen Bioreagents Corp.) were incubated as primary antibodies followed by secondary horseradish peroxidase-linked IgG antibodies (Amersham Biosciences). Chemiluminescence detection of protein was performed using SuperSignal chemiluminescence substrate (Pierce Biotechnology) followed by autoradiography.

Equipment

Fluorescence imaging was conducted with a confocal microscope setup consisting of an Olympus IX-81 inverted microscope with an Olympus Fluoview 500 confocal scanning system. The cellular images were taken with a 40x 1.35 NA oil immersion objective. A Leiden microincubator with a TC-202A temperature controller (Harvard Apparatus, Holliston, MA) was used to keep the cells at 37^{o}C during injection and monitoring. An EXFO Burleigh PCS-6000-150 micromanipulator was used for positioning the injector tip. An Eppendorf Femtojet microinjector with 0.5μm Femtotips was used to inject the MBs into the cells.

Fluorescence Imaging

All cellular fluorescent images were collected using the confocal microscope setup. The Fluo-4 was excited at 488nm and collected at 520nm. The Alexa Fluor 555 and TMR based MBs were excited at 543nm and collected at 560nm. The Alexa Fluor 647 and Cy5 based MBs were excited at 633nm and collected at 660nm. Images were taken after a five to ten second period during which the instrument was focused to yield the highest intensity from the

fluorescence channels. The images were assigned color representations for clarity and are not indicative of the actual emission wavelengths.

Data Analysis

All data collected were analyzed using the Fluoview analysis software. Only the signal in the cytoplasm was used due to the nuclear uptake of the MBs. The same area of cytoplasm was analyzed in each channel for each measurement. The equilibrium state fluorescence for each probe was determined as the level where the probe fluorescence remained constant. Prior to further analysis, the background was subtracted from all of the probe intensities.

Simultaneous Detection of Ca^{2+} and Gene Expression inside of Single Cells

The first step to developing this methodology was determining the best loading methodologies for both the MB and the Fluo-4 Ca^{2+} indicator. From a conceptual standpoint, methods that used membrane pore formation such as electroporation or reversible permeabilization for the delivery of MBs were not considered. The pores allow passive diffusion in and out of the cells and therefore the ion concentrations may reach equilibrium with the cell media preventing their accurate measurement. Methods requiring incubation times of greater than 30 minutes were also discounted. It has been shown that inside of cells DNA based MBs remain viable for thirty minutes[191], therefore incubations needing longer than thirty minutes makes it difficult to determine whether the MB response is from specific hybridization or merely due to degradation from the cellular environment. Finally, microinjection was selected since it had neither of these limitations and it also is reproducible from injection to injection and applicable to all adherent cell types.

Next, the delivery of the indicator was investigated. Our first effort was to deliver the indicator using microinjection along with the MBs. However, the indicator suffered from very poor retention inside the cell even when conjugated to larger Dextran molecules (data not

shown). The poor retention time resulted in the Fluo-4 leaking from the cell prior to the MB signal reaching equilibrium. This would have prevented taking the measurements from the cells at the same time point possibly introducing a source of variation or error into the data. Instead, a two-step delivery mechanism, wherein cell permeable Fluo-4 indicator was incubated with the cells prior to injection of the MBs was utilized. Using this protocol the Fluo-4 exhibited very reproducible performance inside of the cell and excellent retention. The advantage of this two-step technique is that it can be applied to virtually any type of adherent cells without any prior alteration to the cells.

With a strategy in place, the first step was to validate the protocols using positive and negative controls. β-actin mRNA was chosen as a positive control due to its high intracellular expression at all points in the life cycle of the cell. The second MB chosen was a negative control MB that was designed to have no complementary target inside of human cells. The β-actin MB and the Control MB have spectrally distinct fluorophores that enable their simultaneous detection along with the Fluo-4 indicator. The similar fluorophores have been previously demonstrated to be spectrally compatible with our imaging equipment.[242] The MBs were injected into MD-MB-231 human breast carcinoma cells and all the fluorescent channels were monitored for 15 minutes with one image taken every minute. Figure 7-1a shows the time elapsed images from a representative cell.

As can be seen in the image, the Fluo-4 signal remains at a high level of fluorescence throughout the monitoring period. The high constant signal from the Fluo-4 indicates that it has reached equilibrium with the free Ca^{2+} prior to injection. Based on this constant signal, it was also concluded that the addition of the MB solution volume had a negligible effect on the concentration levels of the indicator and Ca^{2+}. If there had been an appreciable effect, a decrease

in the signal intensity of the indicator would have been observed, however no decrease was observed during the measurement or upon comparison of the signal obtained prior to injection.

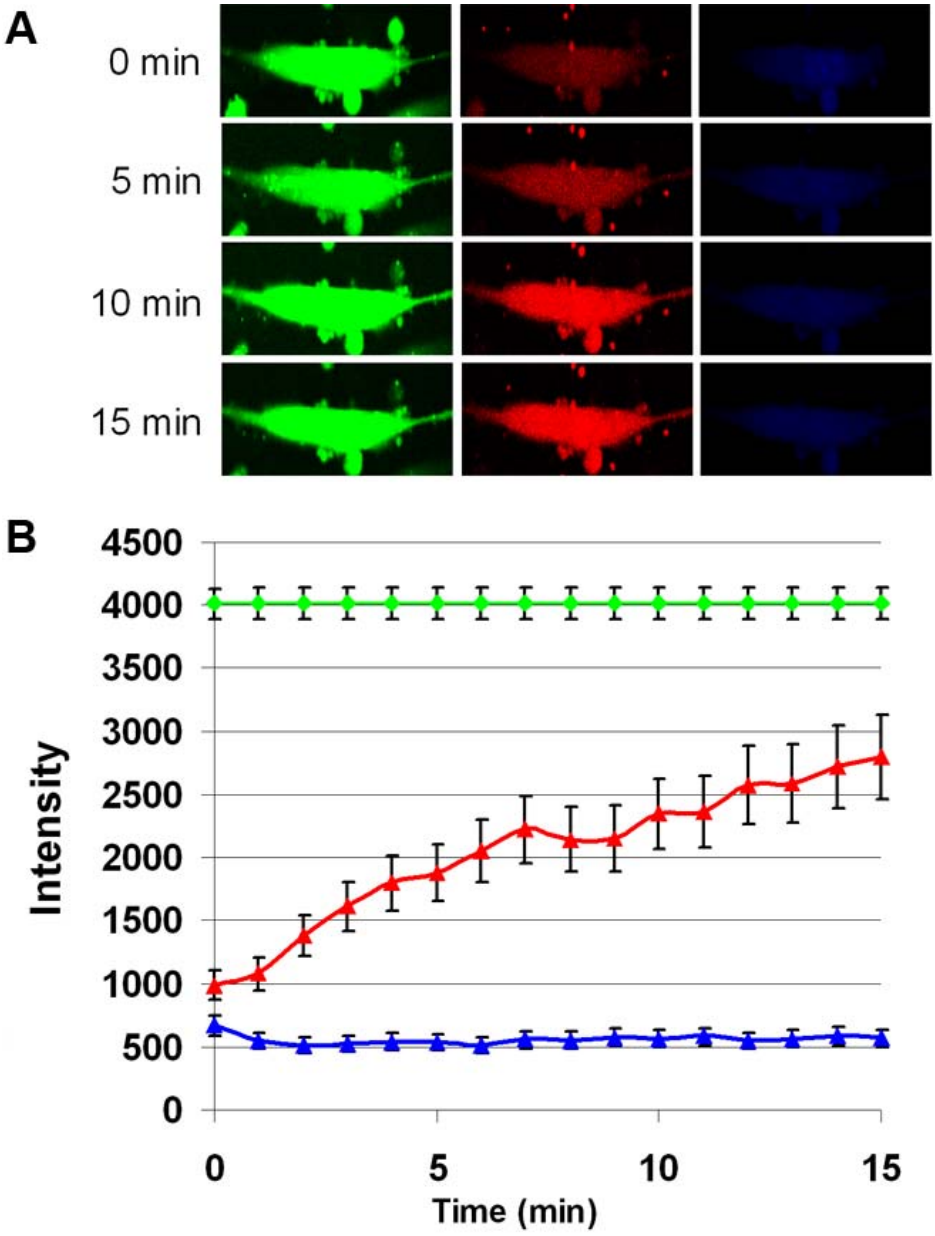

Figure 7-1. a) Time resolved fluorescence images from the Fluo-4 channel (green), β-actin MB (red), and the negative control MB (blue). b) Plots of the average intensities versus time for each probe for the ten cells being monitored.

The β-actin MB signal is at a low level of intensity during the first images but then increases steadily until plateauing after 10-12 minutes indicating an equilibrium occurring between the MB and the β-actin mRNA. The Control MB has no target inside of the MDA-MB-

231 cells and therefore remains at a low intensity level throughout the monitoring period. This is an important observation as it signifies that no nonspecific interactions are taking place during the monitoring period, which validates the increase of signal seen for the β-actin MB. If that increase had been due to a nonspecific interaction then the Control MB would have been similarly affected.

Studying the Effects of Trichostatin A on Ca^{2+} levels and Gene Expression

Histone deacetylase inhibitors such as Trichostatin A (TSA) have been shown to inhibit the proliferation of tumor cells in culture and *in vivo* by causing cell cycle arrest and/or apoptosis.[243] One of genes affected by TSA is Manganese Superoxide Dismutase (MnSOD). Superoxide dismutases like MnSOD scavenge superoxide anions and catalyze their conversion to H_2O_2. Decreased levels of superoxide anions and other reactive oxygen species (ROS) have been shown to be related to tumorigenesis in several experimental models and human cancers.[244,245] It has been reported that MnSOD over-expression in several cancer cell types restores a relatively normal phenotype,[246-248] and it has also been theorized that MnSOD could be considered an anti-oncogene.[249] The effect of TSA on MnSOD expression was verified using Western Blot analysis as illustrated in Figure 7-2e. MnSOD protein levels are dramatically increased after TSA exposure. Thus, TSA has been shown to affect both the MnSOD mRNA and protein expression in the MDA-MB-231 cells.

There have also been studies showing that Ca^{2+} concentrations are affected by ROS[250] and that intracellular ROS generation leads to an increase in the Ca^{2+} inside of cells.[251] These two phenomena then might be connected in that the increase in MnSOD would result in a decrease in ROS. The decrease in ROS may then result in the Ca^{2+} levels returning to normal. Therefore, we will use the methodology we developed to explore whether these intracellular events are linked as suggested or merely coincidental.

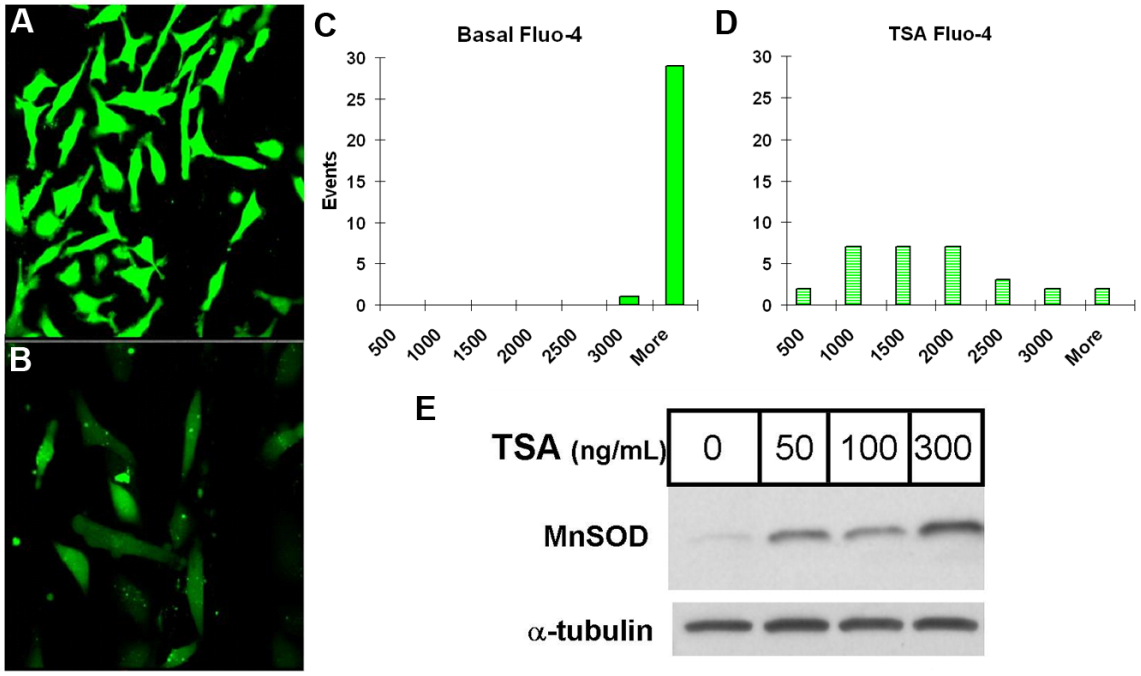

Figure 7-2. a) Fluorescence image of Fluo-4 in the basal cell group. b) Fluorescence image of Fluo-4 in the TSA exposed cell group. The fluorescence is significantly decreased upon exposure to TSA c) Histogram of the range of intensities of Fluo-4 in the basal cell group. d) Histogram of the range of intensities of Fluo-4 in the TSA exposed cell group. Each histogram contains from the signal intensities from thirty cells in each group. e) e) Western Analysis of the upregulation of MnSOD after exposure to TSA. The MnSOD protein is most upregulated after exposure to 300ng/ml of TSA. This concentration was then used for the further experiments involving TSA. α-Tubulin is used as the loading control.

As the effect of TSA on the Ca^{2+} levels inside the MDA-MB-231 cells has not yet been studied, the first step was to determine whether TSA can affect the Ca^{2+} concentration inside the cell. For this study two groups of cells were utilized. In the first group no changes were made to the cell media while in the second group 300ng/ml of TSA was added into the normal cell media. Figure 7-2a and 7-2b show fluorescence images of representative cells from the basal and TSA exposed group respectively. The images clearly show that the fluorescence intensity of the Fluo-4 indicator decreases after exposure to TSA. The fluorescent intensities of thirty cells from each group were then analyzed and plotted in a histogram in Figure 7-2c and 7-2d to illustrate the overall trend and to show the range of fluorescent intensities that are observed. These results

indicate that TSA exposure decreases the free Ca^{2+} concentration in the MDA-MB-231 cells. Thus, TSA has been shown to stimulate the MnSOD mRNA expression while decreasing the Ca^{2+} levels in the MDA-MB-231 cells. However, it is interesting to note that there is a wide variation in the observed Ca^{2+} levels even between neighboring cells in the TSA exposed group. If it could be shown that the lower Ca^{2+} levels correlate with higher MnSOD expression levels and vice versa, then there would be a strong argument that these two analytes would be closely linked inside of the cell.

To determine whether the increase in MnSOD is related to the decrease in Ca^{2+}, two groups of cells were utilized, one group at basal levels and another exposed to TSA. Each group of cells was then incubated with Fluo-4 for sixty minutes. Ten cells from each group were injected with MBs complementary for MnSOD and a negative control MB. Figure 7-3a shows a representative cell from each group 15 minutes after injection. In the basal cell, the Fluo-4 fluorescence is at a very high intensity indicating a high Ca^{2+} level, while the fluorescence from the Control MB and the MnSOD MB are at a much lower intensity. This indicates that the Control MB is functioning as expected, since no target is present, the MB should not open. The MnSOD MB also remains at a constant low fluorescence level indicating the MnSOD mRNA is below our detection limits. This is not unexpected as the MnSOD expression is significantly downregulated in the MDA-MB-231 cell line. In the TSA exposed cells the Fluo-4 signal is significantly decreased, indicating a decrease in the free Ca^{2+} concentration. The Control MB remains at the same low intensity as the basal cells as the MB has no target in either group of cells. The MnSOD MB however now shows an increase in it's intensity as the TSA upregulates the MnSOD expression inside of the cells. Again the negative control MB validates this result since any nonspecific event that would cause the MnSOD MB to open would also affect the

Control MB resulting in a similar increase in fluorescence. Since no increase in the Control MB is detected then the increase in the MnSOD MB must be due to a specific hybridization with its mRNA target.

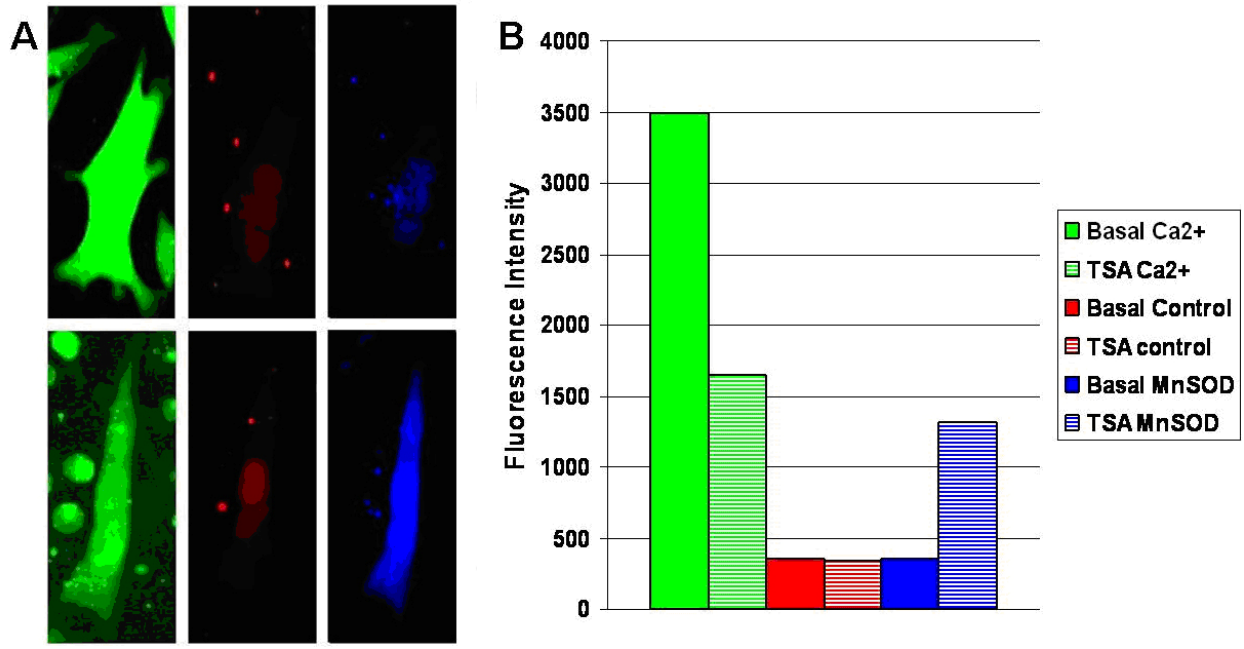

Figure 7-3: a) Fluorescence Images of Fluo-4 (green), the Control MB (red), and the MnSOD MB (blue) for both the basal group and TSA exposed group of cells. The images indicate that the Fluo-4 intensity decreases after exposure to TSA while the MnSOD MB intensity increases after exposure to TSA. The Control MB intensity does change from one group to the other. b) The average intensities of each probe in the two groups of cells. The averages show a significant decrease in the Fluo-4 signal after TSA incubation while the MnSOD expression increases. The control MB is not affected by the TSA exposure.

The average signals from ten cells of each group were then determined and plotted in Figure 7-3b. This is consistent with the overall trends observed initially in the Western Blot analysis and the Fluo-4 averaged results without injection of MBs. However no further information can be effectively determined from looking at the average values. To determine whether there were any patterns in the expression levels of the probes in the two groups, the equilibrium signals from each probe were plotted in histograms. The histograms also allow

observing the overall trends while utilizing the individual intensities so the distribution patterns can be studied. The histograms are shown in Figure 7-4.

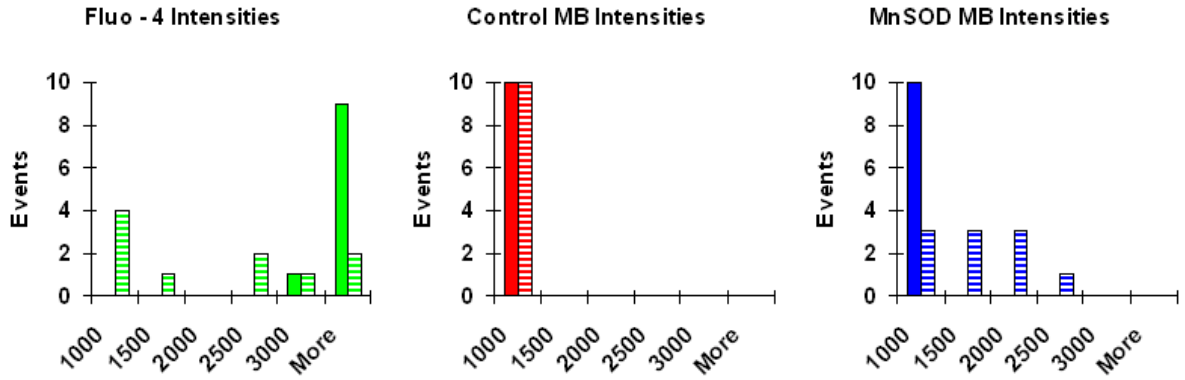

Figure 7-4. Histograms showing the distribution of intensities from each probe in the basal cell group (solid) and the TSA exposed cell group (striped). In addition to the distributions, the overall trends in each group of cells can be seen from the histograms such as the increase in the MnSOD levels and the decreases in the Ca^{2+} levels inside of the cell.

While the histograms show the same overall trends as observed in Figures 7-2 and 7-3, they also show the distribution patterns of the TSA exposed Fluo-4 and the MnSOD MB. The cells in this study exhibited a wide range of intensity levels in their Fluo-4 signal and cells with very high and low signals were chosen for further examination. If the Ca^{2+} and MnSOD levels were related one would expect them to exhibit a similar distribution pattern of intensities, such that cells with a high Fluo-4 intensity would have low MnSOD levels and those with low Fluo-4 signals would have a higher MnSOD expression. However, the Fluo-4 signals show a varying yet level range of intensities while the MnSOD distribution appears to be Gaussian. This indicates that perhaps the two analytes are not closely linked inside of the cell.

To further explore the differences between the distribution patterns, correlation plots of the signal levels were prepared. In the correlation plots, the signal intensities of two different probes in the same cell are plotted against each other. If the intensity levels form a pattern such as a line or an exponential curve, the analyte levels should share a similar relationship. For these plots the

R^2 value of the line indicates how well the analyte signals correspond to that relationship. Correlation plots for Fluo-4 and the Control MB against MnSOD expression are displayed in Figure 7-5.

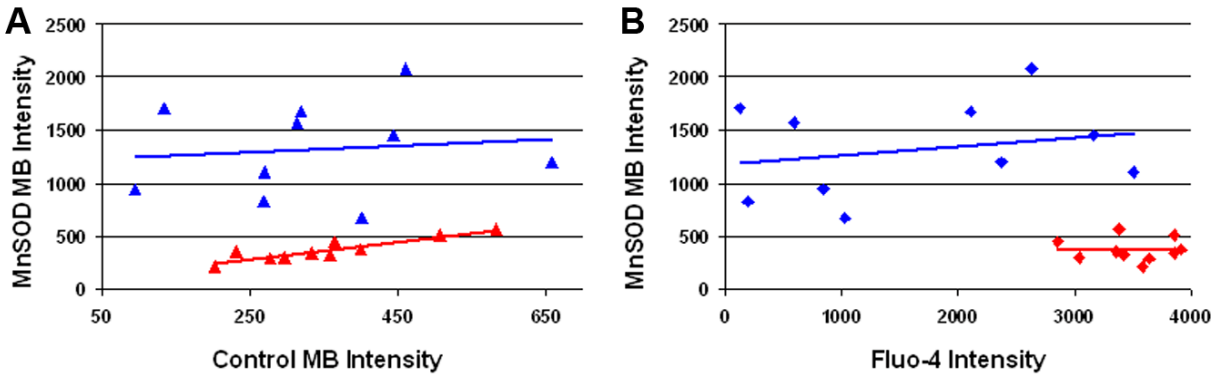

Figure 7-5. Correlation plots comparing the levels of MnSOD to the control and Fluo-4 levels. The degree of correlation is determined by fitting a trend line and using the R^2 value. a) The plot of the MnSOD MB signal versus the Control MB for the TSA exposed cells (blue) and the unexposed cells (red). b) The plot of the MnSOD MB intensity versus the Fluo-4 intensity for each group of cells.

In Figure 7-5a, when basal intensities of the Control and MnSOD MBs are compared against each other a strong linear relationship is observed between those probes with an R^2 value of higher than 0.900. Since the MnSOD levels are repressed in this cancer cell line, the basal expression of MnSOD is below the detection limit of the MB. Therefore the fluorescence measured from the channel corresponds to the background from the MB, just like the negative control MB. Since the intensities are based solely on the amount of the MBs injected there is a strong correlation between the intensities as the ratio of the injected probes remains constant. This relationship is no longer visible in the TSA exposed cells however as now the MnSOD MB fluorescence is based primarily on the amount of MnSOD mRNA inside of the cell, not simply on the amount injected into the cell. In Figure 7-5b, no patterns are observed for the basal and TSA exposed cells when trying to correlate the MnSOD and Ca^{2+} concentrations. R^2 values of

less than 0.100 are obtained for these plots indicating there is no correlation between these points.

Based on the histograms and the correlation plot there does not appear to be any connection between the levels of MnSOD mRNA and Ca^{2+} inside of the TSA exposed cells. Indeed further literature research into the known effects of TSA on the MDA-MB-231 cells reveals that TSA also upregulates the mRNA and protein expression of Gelsolin.[252] Gelsolin is an actin binding protein that has several Ca^{2+} binding motifs that are utilized when the protein binds to actin. Therefore, the decrease of the Ca^{2+} concentration inside of the TSA exposed cells could be due to the upregulation of Gelsolin. However further work must be completed before it is known whether this is the correct explanation or if the phenomena we observed is due to another process or protein altogether. Regardless, the technique has demonstrated its potential for aiding the understanding of biological phenomena and disease states.

Conclusion

Advancing the understanding of biological processes and disease states requires the development of more complex forms of analysis. In order to address this need we have developed a methodology that allows for the detection and monitoring of different types of analytes simultaneously inside of the same single cell. Our technique was first illustrated using positive and negative controls along with a basal concentration of Ca^{2+}. The demonstration convincingly showed that the detection of ion concentrations and mRNA expression were possible simultaneously. Also, it was done without any pretreatment of the cells and is readily applicable to almost any type of adherent cell. In addition, any gene expression system in theory could be studied by simply changing the MB sequences to different targeted mRNA.

To demonstrate the utility and the potential of this technique, it was applied to the study of the effects of an anti-cancer agent in human breast cancer cells. In this study we sought to

determine whether the levels of Ca^{2+} where related to the expression of MnSOD mRNA since the level of Ca^{2+} has been previously shown to be related to the levels of ROS inside of the cell. Despite the fact that no relationship was found between those levels, the study still provided valuable information into those biological processes. No other method exists for this level of biological analysis into single cells with the ability to compare and investigate such different biologically important analytes. This methodology will allow further investigation into a wide range of medically and biologically relevant systems that simply is not possible with other techniques.

The future of intracellular analysis in terms of single cell experiments is still largely unexplored. There are countless signaling pathways and other biological functions that can be studied by detecting multiple analytes on the single cell level. In particular studies using other ions such as ROS and gene expression could be particularly useful to study the effects of anticancer agents on different cell types. However, one area of intracellular analysis still needs more improvement. While the MBs can function very well inside of the cells for a short time, the MBs do not remain stable inside of the cells for longer than 30 minutes. This obviously limits the ability of the MBs for intracellular monitoring and requires that different groups of cells be used to study cellular processes through chemical stimulation. If more stable MBs were developed, this would enable monitoring for hours thus allowing the effects of chemical stimulation to be monitored in the same single cell. Therefore to address this limitation, the next chapter will focus on the integration of locked nucleic acid bases into the MB in an effort to improve the stability of the MBs for intracellular analysis.

CHAPTER 8
INTRACELLULAR APPLICATIONS OF LOCKED NUCLEIC ACID MOLECULAR BEACONS

Introduction

In the previous chapters, the potential for intracellular analysis using MBs was demonstrated. However, one of the problems with MBs is that they generate false-positive signals due to nuclease degradation and protein binding[253,254] leading a half life in complex biological systems like the inside of a cell of only 15 to 20 minutes.[255] Also, it's not only degradation that leads to the generation of false positive signals as even simple binding to entities like single strand binding proteins can disrupt the stem structure of the beacon leading to the restoration of fluorescence.[256]

In order to minimize the effect of the intracellular environment, nuclease-resistant backbones such as phosphorothioate and 2'-O-methyl RNA bases have been incorporated into molecular beacons. In addition, various groups have demonstrated neutral peptide nucleic acids (PNAs) for use in the MBs. While the backbone and sugar modifications have their advantages, the non-standard bases also possess different drawbacks depending on the base used.

For example, those that retain the repeating charge continue to behave like natural nucleic acids in their hybridizing properties, while introducing new problems such as the toxicity demonstrated by phosphorothioate-containing oligonucleotides.[257] Non-toxic modifications that more closely resemble natural nucleic acids can still be opened by intracellular DNA- and RNA-binding proteins, many of which recognize a repeating backbone negative charge to initiate binding to the oligonucleotide sequence. MBs with 2'-O-methyl RNA bases possess better nuclease resistance, higher affinity to DNA and RNA, increased specificity, and a superior ability to bind to structured targets compared to their DNA counterparts. However, 2'-O-methyl modified MBs still produce a fluorescence signal non-specifically in cells, most likely as a result

of protein binding.[258] With no repeating backbone charges, PNA is resistant to nucleases and binding proteins. In addition, their hybridization products with RNA are thermally more stable compared with DNA-RNA and RNA-RNA hybrids. It has also been reported that using PNA-MBs instead of DNA-MBs as *in situ* hybridization probes would benefit cell detection under a wide range of conditions.[259] However, the neutral backbone creates several new problems for using molecular inside of the cell. For instance, PNA has a tendency to aggregate in aqueous environments due to its neutral charge and even fold in ways that interfere with the hybridization of the probe to its target.[260] Also, the physical properties of PNA like solubility can change dramatically with small changes to the sequence of the strand.[261] Since the environmental conditions inside of a living cell can not be optimized for the solubility of PNA, intracellular applications of PNA are limited.

Locked nucleic acids (LNA) offer one possible solution to this quandary by possessing a negatively charged backbone with enough modification to disrupt protein binding.[262-265] LNA is a conformationally restricted nucleic acid analogue, that possesses a simple 2'-O, 4'-C methylene bridge locking the ribose ring into a rigid C3'-*end* conformation as illustrated in Figure 8-1A. LNA has many advantageous properties such as high binding affinity, excellent base mismatch discrimination capability, and decreased susceptibility to nuclease digestion. When LNA hybridizes to DNA or RNA, there is a large increase in melting temperature ranging from +3.0 to +9.6^{o}C per LNA modification compared to normal DNA duplexes. Furthermore, LNA oligonucleotides can be synthesized using conventional phosphoramidite chemistry allowing the automated synthesis of both fully modified LNA and mixed oligonucleotide sequences using combinations of LNA, DNA, and RNA. Other advantages of LNA stemming from its close structural resemblance to native nucleic acids, include good solubility and no toxicity in

physiological conditions. This allows the LNA based probes to be used for intracellular applications utilizing any of the previous established delivery mechanisms. The combination of these properties give LNA a great deal of potential for intracellular applications.

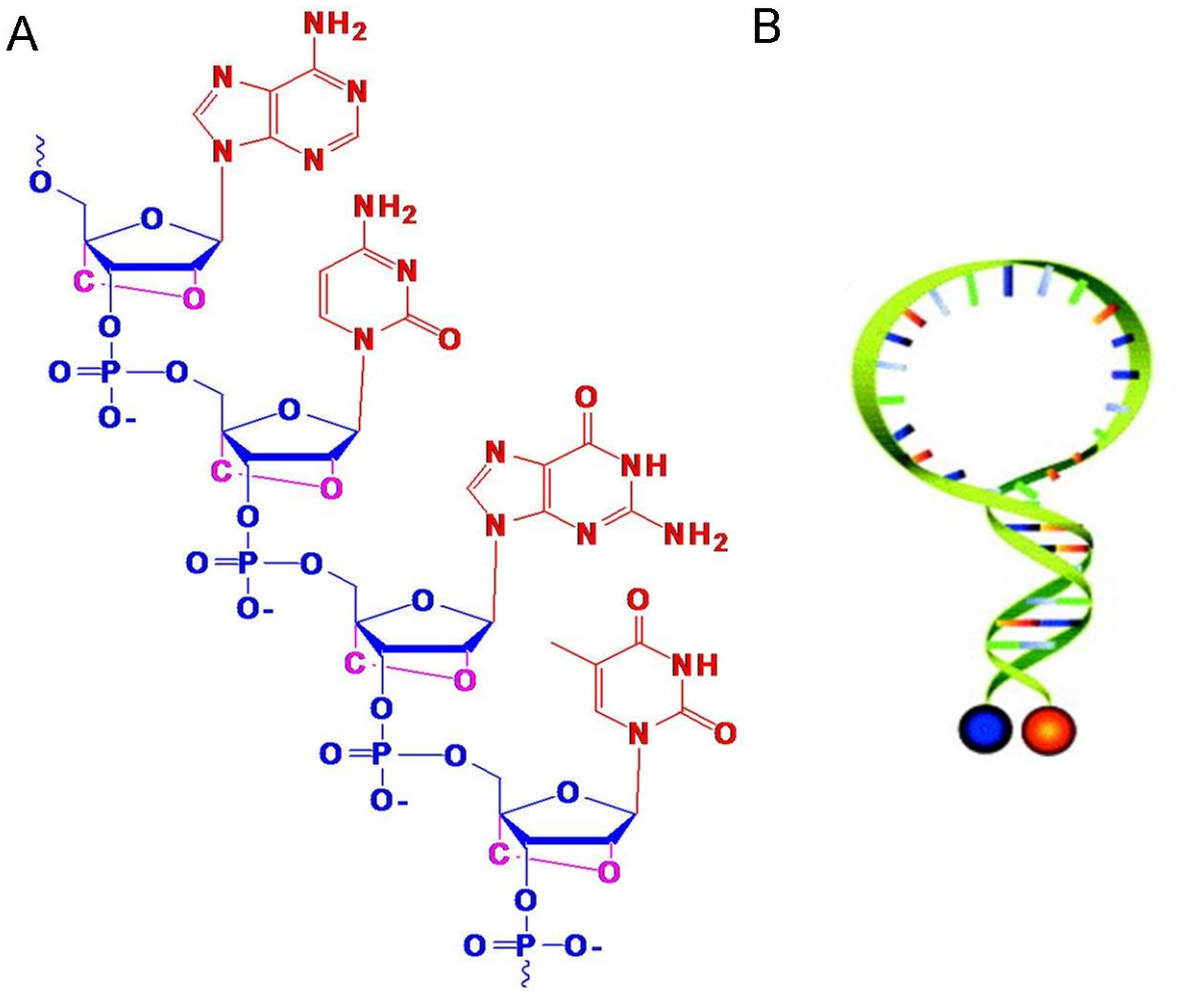

Figure 8-1. A) Illustration of the structure of the Locked Nucleic Acid bases. B)Illustration of a molecular beacon.

Methods and Materials

Equipment

An ABI3400 DNA/RNA synthesizer (Applied Biosystems, Foster City, CA) was used for target DNA synthesis and MB probe preparation. Probe purification was performed with a

ProStar HPLC (Varian, Walnut Creek, CA) where a C18 column (Econosil, 5u, 250×4.6 mm) from Alltech (Deerfield, IL) was used. UV-Vis measurements were performed with a Cary Bio-300 UV spectrometer (Varian, Walnut Creek, CA) for probe quantitation. Fluorescence measurements were performed on a Fluorolog-Tau-3 spectrofluorometer (Jobin Yvon, Inc., Edison, NJ). Fluorescence imaging was conducted with a confocal microscope setup consisting of an Olympus IX-81 inverted microscope with an Olympus Fluoview 500 confocal scanning system and three lasers, a tunable Argon Ion laser (458nm, 488nm, 514nm), a green HeNe laser (543nm), and a red HeNe laser (633nm) with three separate photomultiplier tubes (PMT) for detection. The cellular images were taken with a 60x 1.4 NA oil immersion objective. A Leiden microincubator with a TC-202A temperature controller (Harvard Apparatus, Holliston, MA) was used to keep the cells at 37^{o}C during injection and monitoring. An EXFO Burleigh PCS-6000-150 micromanipulator was used for positioning the injector tip. An Eppendorf Femtojet microinjector with 0.5μm Femtotips was used to inject the molecular beacons and reference probe into the cells. All image analysis was conducted on the Fluoview 500 software, followed by processing of the data using Microsoft Excel.

Molecular Beacon Synthesis

Molecular Beacons possessing locked nucleic acid bases were synthesized on an Applied Biosystem 3400 DNA/RNA synthesizer by using locked nucleic acid phorsphoramidites. The controlled-pore glass columns used for these syntheses introduced a DABCYL (4-(4-(dimethylamino) phenylazo) benzoic acid) molecule at the 3' ends of the oligonucleotides. FAM (6-carboxyfluorescein) phosphoramidite was used to couple FAM to the 5' ends of the sequence. The complete MB sequences were then deprotected in concentrated ammonia overnight at 65°C and purified by high-pressure liquid chromatography. The collection from the first HPLC

separation was then vacuum dried, incubated in 200 µl 80% acetic acid for 15 min, incubated with 200 µl ethanol and vacuum dried before the second round of HPLC.

Hybridization Study

Unless otherwise indicated, hybridization experiments were conducted with 100 nM MBs, 500 nM complimentary target sequences in a total volume of 200 µL. All experiments were conducted in 20 mM Tris-HCl (pH 7.5) buffer containing 5 mM $MgCl_2$ and 50 mM NaCl.

DNase I Sensitivity

To test the nuclease sensitivity of MBs, the fluorescence of a 200 µl solution containing 20 mM Tris-HCl (pH 7.5), 5 mM $MgCl_2$, 50 mM NaCl and 100 nM MBs was measured as a function of time at room temperature. One unit of ribonuclease-free DNase I was added, and the subsequent change in fluorescence was recorded.

Cell Culture

MDA-MB-231 breast carcinoma cells (American Type Culture Collection, Manassas, VA) were maintained in Dulbecco's Modification of Eagle's Medium (DMEM, Fisher Scientific) with 10% fetal bovine serum (Invitrogen, Carlesbad, CA) and 0.5 mg/ml Gentamycin (Sigma, St. Louis, MO) at 37^{o}C in 5% CO_2/air. Cells were plated in 35mm glass bottom culture dishes and grown to 80% confluency (MatTek Corp., Ashland, MA) for 48 hours prior to injection. To stimulate MnSOD mRNA expression, cells were incubated in 1µg/ml LPS from *E. coli* serotype 055:B5 (Sigma, St. Louis, MO) for 4 hours prior to injection.

Fluorescence Imaging

All cellular fluorescent images were collected using the confocal microscope setup. The confocal consists of an Olympus IX-81 automated fluorescence microscope with a Fluoview 500 confocal scanning unit. The TMR based MBs were excited at 543nm and collected at 560nm. The Alexa Fluor 647 based MBs were excited at 633nm and collected at 660nm. The Alexa

Fluor 488 reference probe was excited at 488nm and its emission was detected at 520nm. Images were taken after a five to ten second period during which the instrument was focused to yield the highest intensity from the fluorescence channels. The images were assigned color representations for clarity and are not indicative of the actual emission wavelengths.

Results and Discussion

While the LNA MB has demonstrated impressive performances in buffer solutions the true measure of the intracellular potential of LNA MB can only be evaluated inside of living cells. As a first test of the LNA MB its intracellular background and signal enhancement were tested inside living MDA-MB-231 cells. In these experiments, the LNA MB was compared directly against a normal DNA MB counterpart. Both beacons possessed the Control MB sequence with a TMR/BHQ2 fluorophore/quencher pair. The beacons were injected into the cell at 1μM concentrations with and without a pre-incubation with 10μM target DNA. The microscope settings were kept constant to allow a fair comparison between the two probes. A 1μM AF488 reference probe was injected along with the beacons to allow ratiometric analysis to be performed. This minimizes any experimental fluctuations that might have influenced the results of the experiment. A representative fluorescence image for each sample is shown in Figure 8-2.

When comparing the two beacons, the DNA MB has a higher fluorescence intensity after the incubation with target DNA although the signal from the LNA counterpart is still high. The most pronounced difference between the two probes however is in the unhybridized state. The LNA MB has a much lower fluorescence background than the DNA MB. This is mostly likely due to decreased thermodynamic fluctuations in stem since the LNA has a much higher binding affinity. Degradation of the probe is unlikely as a suspect as the images were taken less than a minute after injection of the probe mixtures.

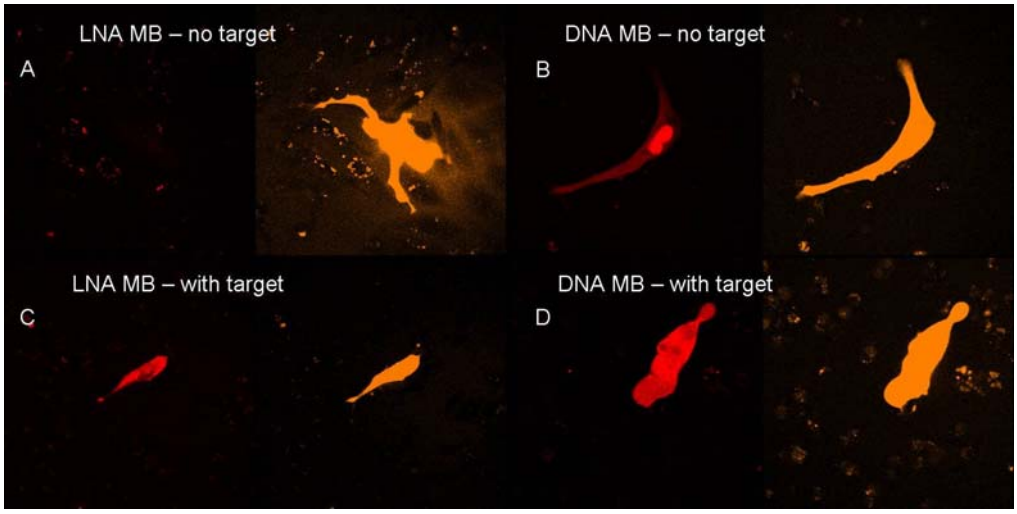

Figure 8-2. A) Fluorescence image of cell injected with and LNA MB (red) and the reference probe (orange) without target. B) Fluorescence image of cell injected with and DNA MB (red) and the reference probe (orange) without target. C) Fluorescence image of cell injected with and LNA MB (red) and the reference probe (orange) with target. D) Fluorescence image of cell injected with and DNA MB (red) and the reference probe (orange) with target.

The probe mixtures were injected in a total of three cells for each sample. The signals obtained for each MB were then divided by the reference probe intensity, averaged, and then plotted in Figure 8-3. The plot illustrates that the low background and also the superior signal enhancement of the LNA MB. Thus the LNA MB seems to have outperformed the DNA MB based on the criteria of the lower fluorescence background and the better signal enhancement.

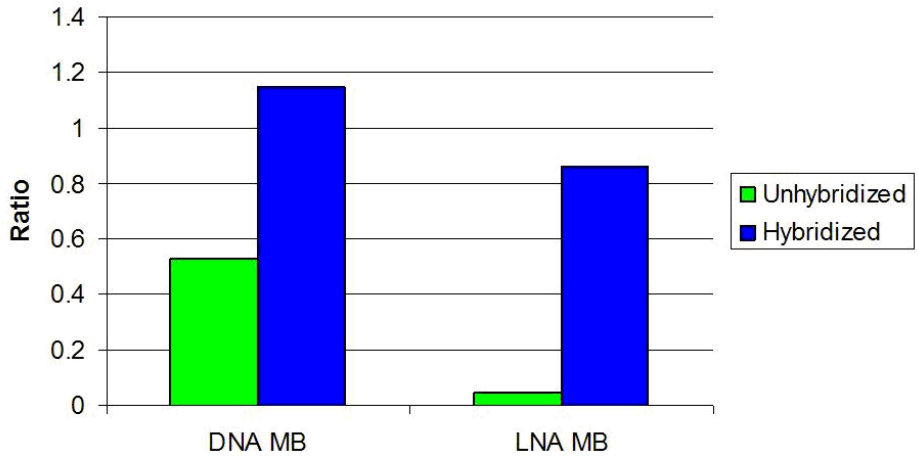

Figure 8-3. Comparison of the LNA and DNA MBs with and without target inside of living cells.

The next test for the LNA MB was to determine whether it had better stability inside of the cell compared to the DNA MB. In these experiments, one of the major disadvantages of the MB design actually becomes beneficial. A problem with the MBs is that when the MB is degraded, the fluorescence signal is restored just like when the MB hybridizes to its target. Normally, this is a problem as there is no way to distinguish between target hybridization and degradation. In these experiments however, MBs with no target inside of the cells can be used and the fluorescence intensity can be measured to monitor the degradation of the MB. As no target is present, any increase in the fluorescence signal must be due to the degradation of the probe. For these experiments, 1μM of the LNA or DNA MB was injected into the cell along with 1μM of the reference probe. The signals from each cell were monitored for one hour with the results from three cells from each probe being plotted in Figure 8-4. The results show that after 30 minutes the fluorescence from the DNA MBs increases despite a lack of target. This indicates that the probe is being degraded inside of the cell. This is in stark contrast to the LNA MB which in addition to exhibiting a lower background signal, remains at the same constant low level throughout the monitoring period. Therefore, the LNA MB seems to possess better stability in the cellular environment than normal DNA MBs.

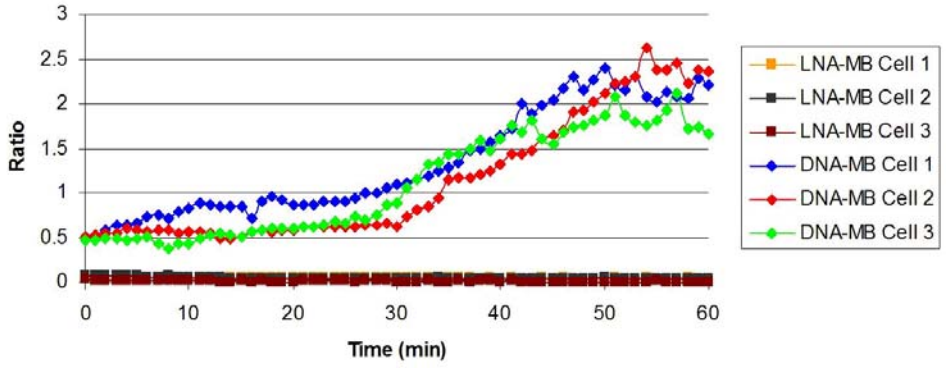

Figure 8-4. Plots of the monitoring of the ratiometric values of the probes inside of cells depicting the degradation of the probes.

While the LNA MB has many advantages, through the course of these experiments one glaring weakness of the LNA MB was made clear. This is that slow hybridization kinetics of the MB prevent it from being used for most applications. In order for the LNA MB to produce a comparable hybridized signal to the DNA MB it required an incubation time of 24 hours. That length of time makes the LNA MB unsuitable for most applications especially intracellular experiments where real time measurements and the actual lifetime of the cell are critical parameters.

LNA MB Optimization

In order to render the LNA MB useful for widespread applications, its hybridization kinetics need to be drastically improved. However, the beneficial aspects of the LNA MB also need to be conserved like its biostability. While its possible many strategies could accomplish this aim the following research focused on lowering the energy barrier of the opening of the stem. In theory, in order for the MB to open and generate a signal, two processes must occur; the hybridization of the loop to the target sequence and the dehybridization or melting of the stem. As the LNA has a higher affinity for DNA than the DNA has for itself the problem is not likely to be the hybridization of the loop. The higher binding affinity of the LNA however could cause the dehybridization or melting of the stem region to be much slower as the thermodynamic energy barrier of the process may be higher. In pursuing this line of reasoning, the major modification to the LNA MB were tested is the incorporation DNA bases along with the LNA in the MB sequence. This should partially destabilize the stem allowing for faster hybridization kinetics without sacrificing the improved biostability of the probes.

Solution Experiments

The first step in determining the optimal strategy for the beacon composition was using different ratios of DNA to LNA and determining in solution whether the change in composition

had a sufficient effect on the hybridization rate. In this experiment, the different molecular beacons were monitored in their closed state briefly to target addition. After target was added the increase in fluorescence was monitored for each beacon. All signals were normalized to the closed molecular beacon signal intensity to directly compare the hybridization rates for each in order to show the data on the same scale so they can be accurately compared. These are plotted in Figure 8-5.

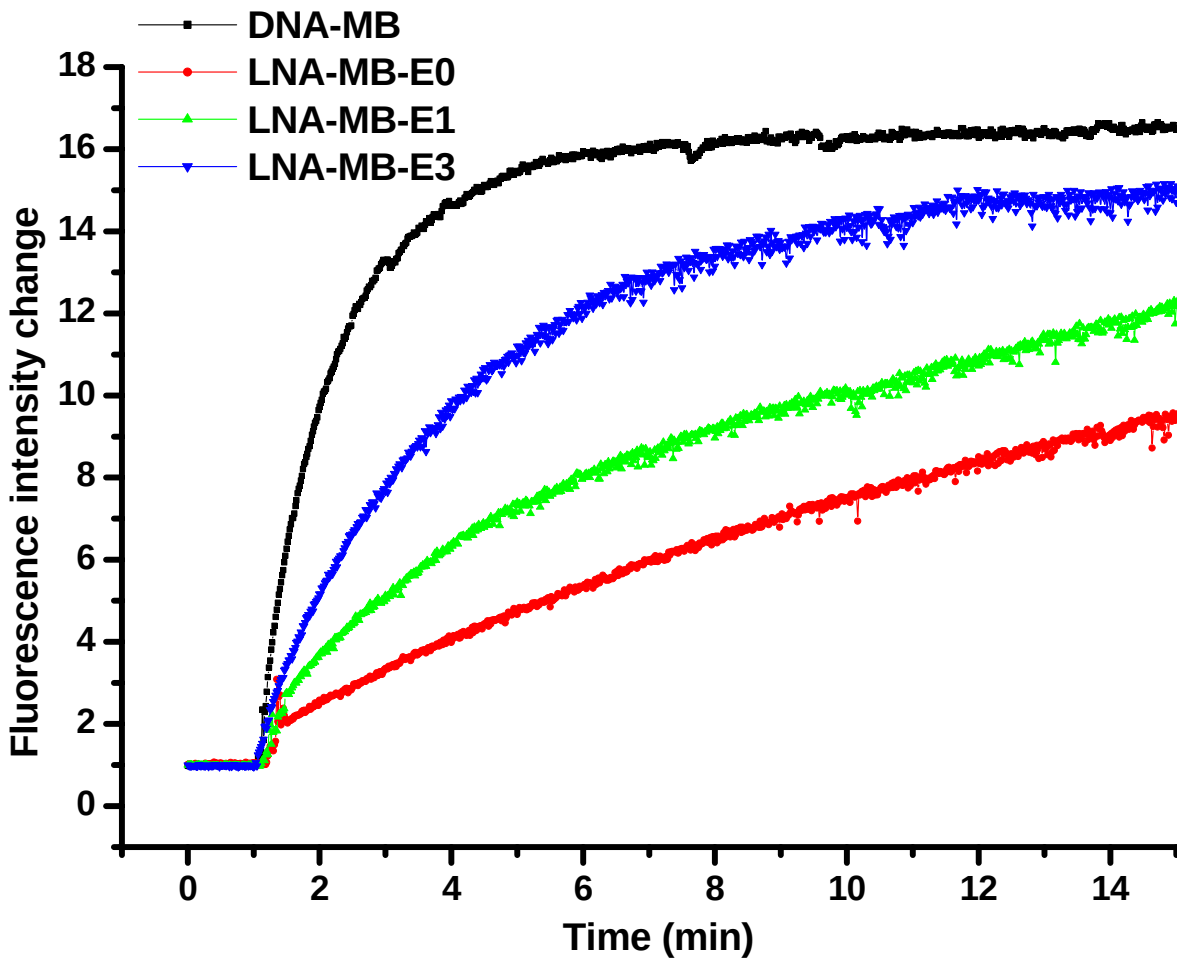

Figure 8-5. Hybridization rates of the different molecular beacon compositions. The data shows the full DNA MB has the fastest hybridization rate, while each hybridization rate slows as more LNA is substituted into the sequence.

The full DNA molecular beacon clearly has the fastest hybridization rate reaching equilibrium after 5 to 6 minutes. The LNA-MB-E3 that possesses a DNA to LNA ratio of 3:1

had the next fastest hybridization rate reaching equilibrium after 12 to 13 minutes. The full LNA sequence designated LNA-MB-E1 and the LNA-MB-E1 sequence containing 50% LNA had slower hybridization rates both taking longer than the 15 minutes in the plot to reach equilibrium. The LNA-MB-E1 required approximately one hour to reach equilibrium while the LNA-MB-E0 required over 24 hours to reach equilibrium. While this MB appears to reach a decent level of fluorescence quite quickly based on the figure, it is important to understand that this is the signal enhancement being monitored which is a ratio between the hybridized and unhybridized fluorescence intensities. Therefore despite reaching a signal enhancement of roughly half of the DNA MB, the actual intensity of the beacon at this point is at a very intensity due to the extremely low background of the LNA MB. However, both the LNA-MBE1 and LNA-MBE3 had higher intensities making them adequate for intracellular analysis based on their hybridization rates.

The next set of experiments was to determine whether the LNA/DNA beacons could still withstand nuclease degradation. This is an important determination as the primary rationale for the modified MBs is to make them more stable in a biological environment. If the optimized probe can no longer resist DNAse cleavage then further experiments with that sequence would prove fruitless as it would have the same limitations as DNA based probes along with slower hybridization rates. In these experiments each probe was incubated with DNase I and the fluorescence intensity was monitored. It is important to note that the degradation of the MB by a nuclease causes the cleaving of the bases that make up the probe. This results in the spatial separation of the fluorophore and quencher and restoring the fluorescence emission of the fluorophore. Thus degradation of the probes can be monitored just like the hybridization of the probes.

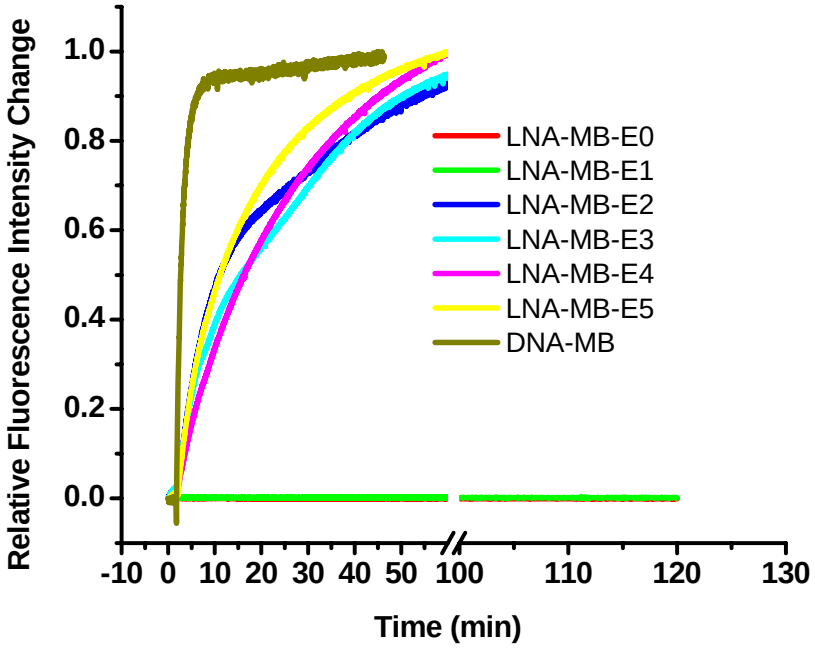

Figure 8-6. Plot showing the response of the different MB compositions to the addition of DNase I that causes the degradation of the probes.

The response for each probe to DNase I is illustrated in Figure 8-6. Of all the compositions tested only two were sufficiently stable in the presence of DNase I, the probe with all LNA and the probe with 50% LNA. None of the other compositions exhibited any resistance to the LNA indicating that the only the LNA-MB-E1 had the potential for intracellular analysis based on biostability and hybridization kinetics. Therefore, the LNA MB-E1 sequence was further evaluated inside of the cell.

Neuron Imaging

To thoroughly evaluate the performance of the LNA-MB-E1 sequence, it was tested inside of neurons from *Aplysia Californica*. *Aplysia Californica* is a type of marine sea slug with a comparatively simple nervous system that is often used as a model for studies trying to elucidate the foundations of learning and memory. In order to truly evaluate the potential of the LNA-MB-E1 composition however, different sequences were required. For these experiments

the same LNA percentage and composition as the LNA-MB-E1 were applied to sequences that were more suitable for use in the *Aplysia Californica* neurons. One sequence was complementary for B-tubulin mRNA, a highly expressed gene in all of the neurons while the other sequence did not have a complement in the known Aplysia genome. Each sequence was injected inside a single Aplysia neuron and monitored for six hours. Representative images for one cell with each probe is shown in Figure 8-7.

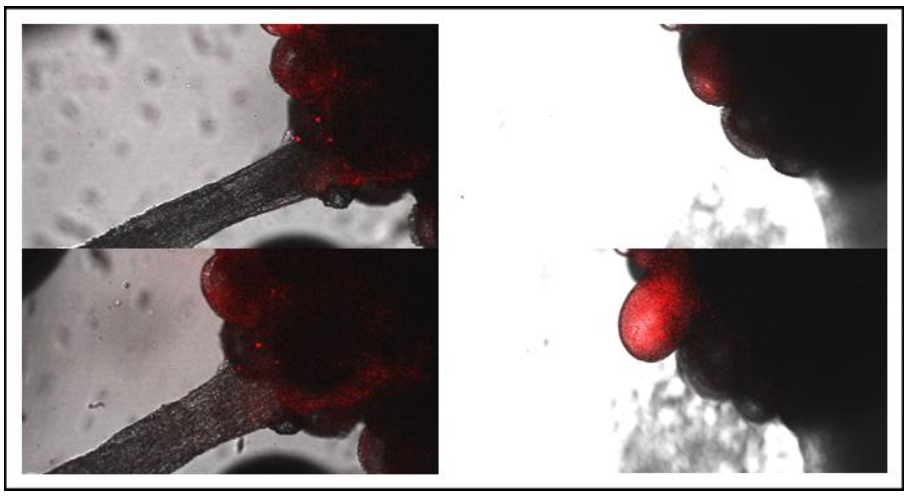

Figure 8-7. Representative images for neurons injected with the negative control sequence (left) and the B-tubulin sequence (right) directly after the injection (top) and after six hours (bottom).

The images indicate that the negative control sequence remained closed throughout the monitoring period with no increase in the fluorescence intensity of the probe. The cell with the B-tubulin sequence however displayed a significant increase in intensity. This is due to high expression of the B-tubulin mRNA in side of the Aplysia neuron. This experiment was repeated once more for each probe. Additional neurons were not directly available which prevented further experiments from being conducted. The fluorescence intensities versus time for each neuron injected is plotted in Figure 8-8. The plot reinforces the images in that each negative

control cell remains at a level low intensity for the duration of the monitoring. However, the signal from the B-tubulin probe increases gradually over the monitoring period.

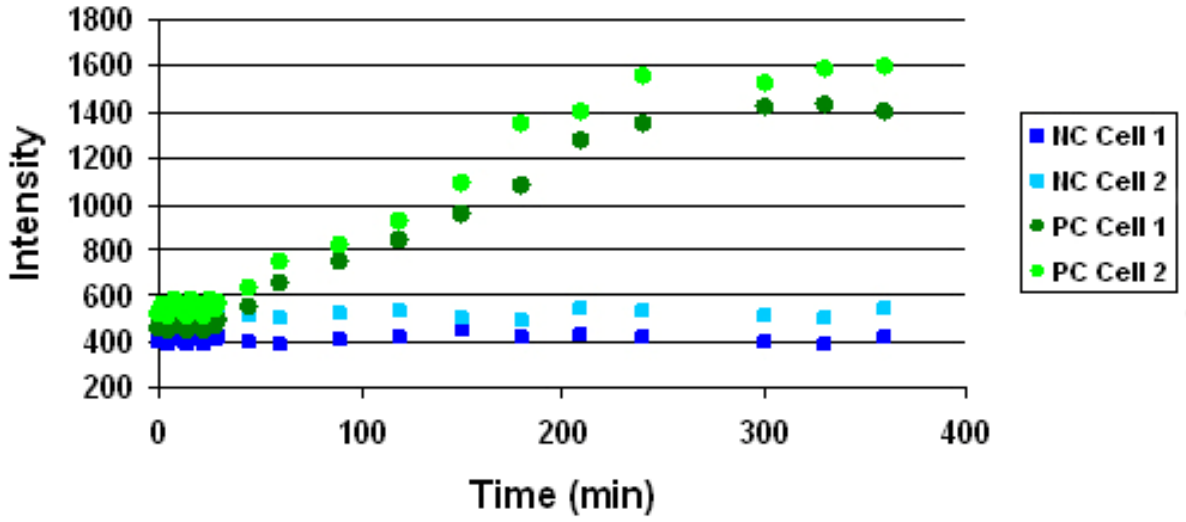

Figure 8-8. Plots showing the fluorescence intensity versus time for each neuron injected with the alternating LNA/DNA molecular beacon.

While successful the experiments indicate a problem with sequences used. The problem is that the hybridization kinetics are still not fast enough as the probe requires approximately four hours to reach equilibrium. This indicates that additional steps will be required before the LNA MBs will be suitable for routine intracellular analysis. Most likely this will involve further steps to destabilize the stem such as using fewer bases or more DNA bases in the stem while conserving the alternating or full LNA modification of the loop region of the probe.

LIST OF REFERENCES

1. Faderl, S.; Kantarjian, H. M.; Talpaz, M.; Estrov, Z. *Blood* **1998**, *91* (11) 3995-4019.

2. Grabstald, H. *CA Cancer J Clin* **1965**, *15*, 134-138.

3. Paredes-Aguilera, R.; Romero-Guzman, L.; Lopez-Santiago, N.; Burbano- Ceron, L.; Camacho-Del Monte, O.; Nieto-Martinez S. *Amer. J. Hematol.* **2001**, *68*, 69-74.

4. Ghossein, R.A. Bhattacharya, S. *European Journal of Cancer* **2000**, *36*, 1681-1694.

5. Iinuma, H.; Okimaga, K.; Adachi, M.; Suda, K.; Sekine, T.; Sakagawa, K.; Baba, Y.; Tamura, J.; Kumagai, H.; and Ida, A. *Int. J. Cancer* **2000**, *89*, 337-344.

6. Zhao, X.; Tapec-Dytioco, R.; Tan, W. *J. Am. Chem. Soc.* **2003**, *125*, 11474-11475.

7. Simard, J.; Briggs, C.; Boal, A. K.; Rotello, V. M. *Chem. Commun.* **2000**, 1943-1944.

8. Schvedova, A.; Kisin, E.; Mercer, R.; Murray, A.; Johnson, V.; Potapovich, A.; Tyurina, Y.; Gorelik, O.; Arepalli, S.; Schwegler-Berry, D. *Am. J. Physiol. Lung. Cell Mol. Physiol.* **2005**, *289*, L698-L708.

9. Stepanov, A.L.; Krenn, J.R; Difbacher, H.; Hohenau, A.; Steinberger, B.; Leitner, A.; Aussenegg, F.R. *Optics Letters* **2005**, *30* (12) 1524-1526.

10. Tan, M.Q.; Wang, G.L.; Hai, X.D.; Ye, Z.Q.; Yuan, J.L.; *J. Mater. Chem.* **2004**, *14*, 2896-2901.

11. Zhu, M.Q.; Chang, E.; Sun, J.; Drezek, R.A.; *J. Mater. Chem.* **2007**, *17*, 800-805.

12. Takafuji, M.; Ide, S.; Ihara, H.; Xu, Z.; *Chem. Mater.* **2004**,*16*, 1977-1981.

13. Bohren, C.F.; Huffman, D.R. *Absorption and Scattering of Light by Small Particles*; Wiley: New York. **1983**.

14. Kerker, M.; J. *Colloid Interface Sci.* **1985**, *105*, 297-314.

15. Moskovits, M.; Suh, J.S.; *J. Phys. Chem.* **1984**, *88*, 5526-5530.

16. Faraday, M. *Philos. Trans.* **1857**, *147*, 145-181.

17. Savage, G. *Glass and Glassware*; Octopus Book: London, **1975**.

18. Kunckels, J. Nuetliche *Observationes oder Anmerkungen von Auro und Argento Potabili; Schutzens*: Hamburg, **1676**.

19. Turkevitch, J.; Stevenson, P. C.; Hillier, J. *Discuss. Faraday Soc.* **1951**, *11*, 55-75.

20. Grabar, K.C.; Freeman, R.G.; Hommer, M.B.; Natan, M..J. *Anal. Chem.* **1995**, *67*, 735–743.

21. Grabar, K.C.; Brown, K.R.; Keating, C.D.; Stranick, S.J.; Tang, S.L.; Natan, M.J. *Anal. Chem.* **1997**, *69*, 471–477.

22. Franzen, S.; Folmer, J.C.W.; Glomm, W.R.; O'Neal, R. *J. Phys. Chem. A* **2002**, *106*, 6533–6540.

23. Simard, J.; Briggs, C.; Boal, A.K.; Rotello, V.M. *Chem. Commun.* **2000**, 1943–1944.

24. Storhoff, J.J.; Mirkin, C.A. *Chem. Rev.* **1999**, *99*, 1849–1862.

25. Storhoff, J.J.; Elghanian, R.; Mucic, R.C.; Mirkin, C.A.; Letsinger, R.L. *J. Am. Chem. Soc.* **1998**, *120*, 1959–1964.

26. Storhoff, J.J.; Lazarides, A.A.; Mucic, R.C.; Mirkin, C.A.; Letsinger, R.L.; Schatz, G.C. *J. Am. Chem. Soc.* **2000**, *122*, 4640-4650.

27. Wang, G.L.; Zhang, J.; Murray, R.W. *Anal. Chem.* **2002**, *74*, 4320-4327.

28. Park, S.J.; Taton, T.A.; Mirkin, C.A. *Science* **2002**, *295*, 1503-1506.

29. Taton, T.A.; Mirkin, C.A.; Letsinger, R.L. *Science* **2000**, *289*, 1757-1760.

30. Demers, L.M.; Mirkin, C.A.; Mucic, R.C., Reynolds, R.A.; Letsinger, R.L.; Elghanian, R.; Viswanadham, G. *Anal. Chem.* **2000**, *72*, 5535–5541.

31. Elghanian, R.; Storhoff, J.J.; Mucic, R.C.; Letsinger, R.L.; Mirkin, C.A. *Science* **1997**, *277*, 1078–1081.

32. Mirkin, C.A. *Inorg. Chem.* **2000**, *39*, 2258-2272.

33. Gomez, S.; Philippot, K.; Colliere, V.; Chaudret, B.; Senocq, F.; Lecante, P. *Chem. Commun.* **2000**, 1945–1946.

34. Hayat, M.A. *Colloidal Gold: Principles, Methods and Applications*; New York: Academic Press; **1989**, Vol. 1.

35. Tkachenko, A.G.; Xie, H., Coleman, D.; Glomm, W.; Ryan, J.; Anderson, M.F.; Franzen, S.; Feldheim, D.L. *J. Am. Chem. Soc.* **2003**, *125*, 4700–4701.

36. Xie, H.; Tkachenko, A.G.; Glomm, W.R.; Ryan, J.A.; Brennaman, M.K.; Papanikolas, J.M.; Franzen, S.; Feldheim, D.L. *Anal. Chem.* **2003**, *75*, 5797–5805.

37. Templeton, A.C.; Chen, S.W.; Gross, S.M.; Murray, R.W. *Langmuir* **1999**, *15*, 66–76.

38. Faulk, W.P.; Taylor, G.M. *Immunochemistry* **1971**, *8*, 1081.

39. Wang, B.L., Scopsi, L., Nielsen, M.H., and Larsson, L.I. *Histochemistry* **1985**, *83*, 109–115.

40. Mentlein, R.; Buchholz, C.; Krisch, B. *Cell Tissue Res.* **1990**, *262*, 431-443.

41. Krisch, B.; Buchholz, C.; Mentlein, R.; Turzynski, A. *Cell Tissue Res.* **1993**, *272*, 523–531.

42. Krisch, B.; Feindt, J.; Mentlein, R. J. *Histochem. Cytochem.* **1998**, *46*, 1233–1242.

43. Niemeyer, C.M. and Mirkin, C.A. *Nanobiotechnology: Concepts, Applications and Perspectives*, Weinheim: Wiley-VCH, Verlag, **2004**.

44. Gribnau, T.C.J., Leuvering, J.H.W., and Vanhell, H. *J. Chromatogr.* **1986**, *376*, 175–189.

45. Brust, M.; Kiely, C.J. *Colloid Surf. A Physicochem. Eng. Asp.* **2002**, *202*, 175–186.

46. Kreibig, U.; Genzel, L. *Surf. Sci.* **1985**, *156*, 678–700.

47. Mirkin, C.A.; Letsinger, R.L.; Mucic, R.C.; Storhoff, J.J. *Nature* **1996**, *382*, 607–609.

48. Reynolds, R.A.; Mirkin, C.A.; Letsinger, R.L. *J. Am. Chem. Soc*. **2000**, *122*, 3795–3796.

49. Chikazumi, S.; Taketomi, S.; Ukita, M.; Mizukami, M.; Miyajima, H.; Setogawa, M.; Kurihara, Y. *J. Magn. Magn. Mater.* **1987**, *65*, 245.

50. Lu, A.H.; Schmidt, W.; Matoussevitch, N.; Bonnermann, H.; Spliethoff, B.; Tesche, B.; Bill, E.; Kiefer, W.; Schuth F. *Angew. Chem.* **2004**, *116*, 4403.

51. Tsang, S.C.; Caps, V.; Paraskevas, I.; Chadwick, D.; Thompsett, D. *Angew. Chem.* **2004**, *116*, 5763.

52. Gupta, A.K.; Gupta, M. *Biomaterials* **2005**, *26*, 3995.

53. Mornet, S.; Vasseur, S.; Grasset, F.; Verveka, P.; Goglio, G.; Demourgues, A.;Portier, J.; Pollert, E.; Duguet, E. *Prog. Solid State Chem.* **2006**, *34*, 237.

54. Li, Z.; Wei, L.; Gao, M.Y.; Lei, H. *Adv. Mater.* **2005**, *17*, 1001.

55. Hyeon, T. *Chem. Commun.* **2003**, 927.

56. Elliott, D.W.; Zhang, W.X. *Environ. Sci. Technol.* **2001**, *35*, 4922.

57. Takafuji, M.; Ide, S.; Ihara, H.; Xu, Z. *Chem. Mater.* **2004**, *16*, 1977.

58. Neveu, S.; Bee, A.; Robineau, M.; Talbot, D. *J. Colloid Interface Sci.* **2002**, *255*, 293.

59. Park, S.J.; Kim, S.; Lee, S.; Khim, Z.; Char, K.; Hyeon, T.; *J. Am. Chem. Soc*. **2000**, *122*, 8581.

60. Puntes, V. F. ; Krishan, K. M. ; Alivisatos, A. P. *Science* **2001**, *291*, 2115.

61. Chen, Q.; Rondinone, A.J.; Chakoumakos, B.C.; Zhang, Z.J. *Magn. Magn. Mater.* **1999**, *194*, 1.

62. Park, J.; An, K.; Hwang, Y.; Park, J.G.; Noh, H.J.; Kim, J.Y.; Park, J.H., Hwang, N.M.; Hyeon, T. *Nat. Mater.* **2004**, *3*, 891.

63. Bonnemann, H.; Brijoux, W.; Brinkmann, R.; Matoussevitch, N.; Waldoefner, N.; Palina, N.; Modrow, H. *Inorg. Chim. Acta.* **2003**, *350*, 617.

64. Sun, S.; Murray, C.B.; Weller, D.; Folks, L.; Moser, A. *Science* **2000**, *287*, 1989.

65. Shevchenko, E. V.; Talapin, D.V.; Rogach, A.L.; Kornowski, A.; Haase, M.; Weller, H. *J. Am. Chem. Soc.* **2002**, *124*, 11480.

66. Grasset, F.; Labhsetwar, N.; Li, D.; Park, D.C.; Saito, N.; Haneda, H.; Cador, O.; Roisnel, T.; Mornet, S.; Duguet, E.; Portier, J.; Etourneau, J. *Langmuir* 2002, *18*, 8209.

67. Bee, A.; Massart, R.; Neveu, S. *J. Magn. Magn. Mater.* **1995**, *149*, 6.

68. Lee, J.; Isobe, T.; Senna, M. *Colloids Surf. A* **1996**, *109*, 121.

69. Cornell, R.M.; Schindler, P.W. *Colloid Polym. Sci.* **1980**, *258*, 1171.

70. Willis, A.L.; Turro, N.J.; O'Brien, S. *Chem. Mater.* **2005**, *17*, 5970.

71. Murray, C.B.; Norris, D.J.; Bawendi, M.G. *J. Am. Chem. Soc.* **1993**, *115*, 8706.

72. Peng, X.; Wickman, J.; Alivisatos, P. *J. Am. Chem. Soc.* **1998**, *120*, 5343.

73. O'Brien, S.; Brus, L.; Murray, C.B. *J. Am. Chem. Soc.* **2001**, *123*, 12085.

74. Farrell, D.; Majetich, S.A.; Wilcoxon, J.P. *J. Phys. Chem. B* **2003**, *107*, 11022.

75. Jana, R.J.; Chen, Y.; Peng, X.; *Chem. Mater.* **2004**, *16*, 3931.

76. Samia, A.C.S.; Hyzer, K.; Schlueter, J.A.; Qin, C.J.; Jiang, J.S.; Bader, S.D.; Lin, X.M. *J. Am. Chem. Soc.* **2005**, *127*, 4126.

77. Li, Y.; Afzaal, P.; O'Brien, J. *J. Mater. Chem.* **2006**, *16*, 2175.

78. Yamada, Y.; Suzuki, T.; Abarra, E.N. *IEEE Trans. Magn.* **1998**, *34*, 343.

79. Tegus, O.; Bruck, E.; Buschow, K.H.J.; de Boer, F.R. *Nature* **2002**, *415*, 150.

80. Song, Q.; Zhang, Z.J. *J. Am. Chem. Soc.* **2004**, *126*, 6164.

81. Langevin, D. *Annu. Rev. Phys. Chem.* **1992**, *43*, 341.

82. Carpenter, E.E.; Seip, C.T.; O'Connor, C.J. *J. Appl. Phys.* **1999**, *85*, 5184.

83. Liu, C.; Zou, B.; Rondinone, A.J.; Zhang, Z.J. *J. Phys. Chem. B* **2000**, *104*, 1141.

84. Wang, X.; Zhuang, J.; Peng, Q.; Li, Y. *Nature* **2005**, *437*, 121.

85. Deng, H.; Li, X.; Peng, Q.; Wang, X.; Chen, J.; Li, Y. *Angew. Chem. Int. Ed.* **2005**, *44*, 2782.

86. Euliss, L.E.; Grancharov, S.G.; O'Brien, S.; Deming, T.J.; Stucky G.D.; Murray, C.B.; Held, G.A. *Nano. Lett.* **2003**, *3*, 1489.

87. Kobayashi, Y.; Horie, M.; Konno, M.; Rodriguez-Gonzalez, B.; Liz-Marzan, L.M. *J. Phys. Chem. B* **2003**, *107*, 7420.

88. Liu, Q.; Xu, Z.; Finch, J.A.; Egerton, R. *Chem. Mater.* **1998**, *10*, 3936.

89. Jiles, D.C. *Acta Mater.* **2003**, *51*, 5907.

90. Salata, O.V. *J. Nanobiotechnol.* **2004**, *2*, 3.

91. Barratt, G. *Cell. Mol. Life Sci.* **2003**, *60*, 21.

92. Neuberger, T.; Schopf, B.; Hofmann, H.; Hofmann, M.; von Rechenberg, B. *J. Magn. Magn. Mater.* **2005**, *293*, 483.

93. Berry, C.C. *J. Mater. Chem.* **2005**, *15*, 543.

94. Tartaj, P.; del Puerto Morales, M.; Veintemillas-Verdaguer, S.; Gonzalez-Carreno, T.; Serna, C.J. *J. Phys. D* **2003**, *36*, R182.

95. Gu, H.; Xu, K.; XU, C.; Xu, B. *Chem. Commun.* **2006**, 941.

96. Kalambar, V.S.; Han, B.; Hammer, B.E.; Shield, T.W.; Bischof, J.C. *Nanotechnology* **2005**, *16*, 1221.

97. Huber, D.L. *Small* **2005**, *1*, 482.

98. Batlle, X.; Labarta, A. *J. Phys. D* **2002**, *35*, R15.

99. C. M. Sorensen, *Magnetism in Nanoscale Materials in Chemistry*, Wiley-Interscience Publication, New York, **2001**.

100. Iwaki T.; Kakihara, Y.; Toda,T.; Abdullah, M.; Okuyama,K. *J Appl. Phys.* **2003**, *94*, 6807.

101. Henglein, A. *Chem. Rev.***1989**, *89*, 1861-1873.

102. Schmid, G. *Chem. Rev*. **1992**, *92*, 1709-1727.

103. Alivisatos, A.P. *Science* **1996**, *271*, 933-937.

104. Nirmal, M.; Brus, L.E. *Acc Chem Res* **1999**, *32*, 407-414.

105. Murray, C.B.; Norris, D.J.; Bawendi, M.G. *J. Am. Chem. Soc.* **1993**, *115*, 8706-8715.

106. Han, M.Y.; Gao, X.; Su, J.Z.; Nie, S.M. *Nat. Biotechnol.* **2001**, *19*, 631-635.

107. Dabbousi, B.O.; Rodriguez-Viejo, J.; Mikulec, F.V.; Heine, J.R.; Mattoussi, H.; Ober, R.; Jensen, K.F.; Bawendi, M.G. *J. Phys. Chem. B* **1997**, *101*, 9463-9475.

108. Peng, X.G.; Schlamp, M.C.; Kadavanich, A.V.; Alivisatos, A.P. *J. Am. Chem. Soc.* **1997**, *119*, 7019-7029.

109. Hines, M.A.; Guyot-Sionnest, P. *J. Phys. Chem. B* **1996**, *100*, 468-471.

110. Peng, X.G.; Wickham, J.; Alivisatos, A.P.; *J. Am. Chem. Soc.* **1998**, *120*, 5343-5344.

111. Desmet, Y.; Deriemaeker, L.; Parloo, E.; Finsy, R. *Langmuir* **1999**, *15*, 2327-2332.

112. Dahan, M.; Laurence, T.; Schumacher, A.; Chemla, D.S.; Alivisatos, A.P.; Sauer, M.; Weiss S. *Biophys J.* **2000**, *78*, 2270.

113. Dahan, M.; Laurence, T.; Pinaud, F.; Chemla, D.S.; Alivisatos, A.P.; Sauer, M.; Weiss, S. *Opt. Lett.* **2001**, *26*, 825-827.

114. Hines, M.A.; Guyot-Sionnest, P. *J. Phys. Chem. B* **1998**, *102*, 3655-3657.

115. Guzelian, A.A.; Katari, J.E.B.; Kadavanich, A.V.; Banin, U.; Hamad, K.; Juban, E.; Alivisatos, A.P.; Wolters, R.H.; Arnold, C.C.; Heath, J.R. *J. Phys. Chem.* **1996**, *100*, 7212-7219.

116. Prieto, J.A.; Armelles, G.; Groenen, J.; Cales, R. *Appl. Phys. Lett.* **1999**, *74*, 99-101.

117. Micic, O.I.; Cheong, H.M.; Fu, H.; Zunger, A.; Sprague, J.R.; Mascarenhas, A.; Nozik, A.J. *J. Phys. Chem. B* **1997**, *101*, 4904-4912.

118. Katari, J.E.B.; Colvin, V.L.; Alivisatos, A.P. *J. Phys. Chem.* **1994**, *98*, 4109-4117.

119. O'Neil, M.; Marohn, J.; McLendon, G. *J. Phys. Chem.* **1990**, *94*, 4356-4363.

120. Alivisatos, A.P.; Johnsson, K.P.; Peng, X.; Wilson, T.E.; Loweth, C.J.; Bruchez, M.P. Jr.; Schultz, P.G.; *Nature* **1996**, *382*, 609-611.

121. Peng, X.G.; Wickham, J.; Alivisatos, A.P. *J. Am. Chem. Soc.* **1998**, *120*, 5343-5344.

122. Winter, J.O.; Liu, T.Y.; Korgel, B.A.; Schmidt, C.E. *Adv. Mater.* **2001**, *13*, 1673.

123. Jaiswal, J.K.; Mattoussi, H.; Mauro, J.M.; Simon, S.M. *Nature Biotechnol*. **2003**, *21*, 47.

124. Lidke D.S.; Nagy, P.; Heintzmann, R.; Arndt-Jovin, D.J.; Post, J.N.; Grecco, H.E.; Jares-Erijman, E.A.; Jovin, T.M. *Nature Biotechnol*. **2004**, *22*, 198.

125. Derfus, A.M.; Chan, W.C.W.; Bhatia, S.N. *Nano Lett.* **2004**, *4*, 11.

126. Rosenthal, S.J.; Tomlinson, I.; Adkins, E.M.; Schroeter, S.; Adams, S.; Swafford, L.; McBride, J.; Wang, Y.; DeFelice, L.J.; Blakely, R.D. *J. Am. Chem. Soc.* **2002**, *124*, 4586-4594.

127. Winter, J.O.; Liu, T.Y.; Korgel, B.A.; Schmidt, C.E. *Adv. Mater.* **2001**, *13*, 1673.

128. Pinaud, F.; King, D.; Moore, H.P.; Weiss, S. *J. Am. Chem. Soc.* **2004**, *126*, 6115.

129. Larson D.; Zipfel, W.R.; Williams, R.M.; Clark, S.W.; Bruchez, M.P.; Wise, F.W.; Webb, W.W. *Science* **2003**, *300*, 1434-1436.

130. Kim, S.; Lim, Y.T.; Soltesz, E.G.; De Grand, A.M.; Lee, J.; Nakayama, A.; Parker, J.A.; Mihaljevic, T.; Laurence, R.G.; Dor, D.M.; Cohn, L.H.; Bawendi, M.G.; Frangioni, J.V. *Nature Biotechnol.* **2004**, *22*, 93-97.

131. Xiao, Y.; Barker, P.E. *Nucleic Acids Res.* **2004**, *32*, 28E.

132. Hoshino, A.; Hanaki, K.; Suzuki, K.; Yamamoto, K. *Biochem. Biophys. Res. Commun.* **2004**, *314*, 46–53.

133. Derfus, A. M.; Chan, W. C. W.; Bhatia, S. N. *Nano Lett.* **2004**, *4* (1), 11–18.

134. van Blaaderen, A.; Imhof, A.; Hage, W.; Vrij, A. *Langmuir* **1992**, *8*, 1514–1517.

135. Yamauchi, H.; Ishikawa, T.; Kondo, S. *J. Colloids Surf.* **1989**, *37*, 71–80.

136. Schmidt, J.; Guesdon C.; Schomäcker R. *J. Nanoparticle Res.* **1999**, *1*, 267–276.

137. Zhao, X. J.; Bagwe, R. P.; Tan, W. H. *Adv. Mater.* **2004**, *16*, 173–176.

138. van Blaaderen, A.; Vrij, A. *Langmuir* **1992**, *8*, 2921–2931.

139. Verhaegh, A. M. N.; van Blaaderen, A. *Langmuir* **1994**, *10*, 1427–1438.

140. Deng, G.; Markowitz, M. A.; Kust, P. R.; Gaber B. P. *Mater. Sci. Eng.* **2000**, *11*, 165–172.

141. Santra, S.; Yang, H.; Stanley, J. T.; Holloway, P. H.; Tan, W. H.; Moudgil, B. M.; Mericle, R. A. *Chem. Commun.* **2004**, *24*, 2810–2811.

142. Santra, S.; Xu, J. S.; Wang, K. M.; Tan, W. H. J. *Nanosci. Nanotechnol.* **2004**, *4*, 590–599.

143. Ohno, T.; Takeshi, M.; Hisao, S.; Masayuki, F. *Adv. Powder Tech.* **2006**, *17*(2) 167-179.

144. Roy, I.; Ohulchanskyy, T.Y.; Bharali, D.J.; Pudavar, H.E.; Mistretta, R.A.; Kaur, N.; Prasad, P.N. *Proc. Nat. Aca. Sci.* **2005**, *102* (2), 279-284.

145. Hermanson, G. T. *Bioconjugate Techniques*. Academic Press: San Diego, CA, **1996.**

146. Gerion, D.; Pinard, F.; William, S. C.; Parak, W. J.; Zanchet, D.; Weiss, S.; Alivisatos, A P. *J. Phys. Chem. B* **2001**, *105*, 8861–8871.

147. Tapec, R.; Zhao, X.J.; Tan, W. *J Nanosci Nanotechnol.* **2002**, *2*(4), 405-409.

148. Giri, S.; Trewyn, B. G.; Stellmaker, M. P.; Lin, V. S. Y.; *Angew. Chem. Int.* **2005**, *44*, 5038–5044.

149. Brehm-Stecher, B.; Johnson, E.; *Microbiol Mol Biol Rev* **2004**, *68*(3), 538-59.

150. Williams, N. *Methods Cell Biol* **2000**, *62*, 449-53.

151. Kurien, B.; Scofield, R. *Methods* **2006**, *38* (4), 283-93.

152. Scanziani, E. *Methods Mol Biol* **2001**, *104*, 133-40.

153. Gold, L. *J. Biol. Chem.* **1995**, *270*, 13581-13584.

154. Famulok, M.; Mayer, G. *Curr. Top. in Microbiol. and Immun.* **1999**, *243*,123-136.

155. Brody, E. N.; Gold, L. *Rev. Mol. Biotechnol.* **2000**, *74*, 5-13.

156. Conrad, R.; Keranen, L.M.; Ellington, A.D.; Newton, A.C. *J Biol Chem.* **1994**, *269*, 32051-32054.

157. Hirao, I.; Spingola, M.; Peabody, D.; Ellington, A.D. *Mol Divers* **1998**, *4*, 75-89.

158. Macaya, R. F.; Schultze, P.; Smith, F. W.; Roe, J. A.; Feigon, J. *Proc. Nat. Acad. Sci.* **1993**, *90*, 3745-3749.

159. Kelly, J. A.; Feigon, J.; Yeates, T.O. *J. Mol. Biol.* **1996**, *256*, 417-422.

160. Gold, L.; Polisky, B.; Uhlenbeck, O.; Yarus, M. *Annu. Rev. Biochem.* **1995**, *64*, 763-797.

161. White, R.R.; Sullenger, B.A.; Rusconi, C.P. *J. Clin. Invest.* **2000**, *106*, 929-934.

162. Bock, L.C.; Griffin, L.C.; Latham, J.A.; Vermaas, E.H.; Toole, J.J. *Nature* **1992**, *355*, 564-566.

163. Hicke, B.J.; Marion, C.; Chang, Y.F.; Gould, T.; Lynott, C.K.; Parma, D.; Schmidt, P.G.; Warren, S. *J. Biol. Chem.* **2001**, *276*, 48644-48654.

164. Daniels, D.A.; Chen, H.; Hicke, B.J.; Seiderek, K.M.; Gold, L. *Proc. Nat. Acad. Sci.* **2003**, *100* (26), 15416-15421.

165. Wang, C.; Zhang, M.; Yang, G.; Zhang, D.; Ding, H.; Wang, H.; Fan, M.; Shen, B.; Shao, N. *J. Biotechnol.* **2003**, *102*, 15-22.

166. Morris, K.N.; Jensen, K.B.; Julin, C.M.; Weil, M.; Gold, L. *Proc. Nat. Acad. Sci.* **1998**, *95*, 2902-2907.

167. Homann, M.; Goringer, H.U. *Nucleic Acids Res.* **1999**, *27*, 2006-2014.

168. Blank, M.; Weinschenk, T.; Priemer, M.; Schluesener, H. *J. Biol. Chem.* **2001**, *276*, 16464-16468.

169. Li, J.; Fang,, X. H.; Tan, W. *Biochem. Biophys. Res. Commun.* **2002**, *292*, 31-40.

170. Knox, K.K.; Brewer, J.H.; Henry, J.M.; Harrington D.J.; Carrigan, D.R. *Clin. Infectious Diseases* **2000**, *31* (4), 894-903.

171. Cerchia, L.; Hamm, J.; Libri, D.; Tavitian, B.; Franciscis, V. *FEBS Letters* **2002**, *528*, 12-16.

172. Hermann, T.; Patel, D.J. *Science* **2000**, *287*, 820-825.

173. Harding, J. D.; MacDonald, R. J.; Przybyla, A. E.; Chirgwin, J. M.; Pictet, R. L.; Rutter, W. J. *J. Biol. Chem.* **1977**, *252*, 7391-7397.

174. Hallick, R. B.; Chelm, B. K.; Gray, P. W.; Orozco, E. M., Jr. *Nucl. Acids Res.* **1977**, *4*, 3055-3064.

175. Velculescu, V. E.; Zhang, L.; Vogelstein, B.; Kinzler, K. W. *Science* **1995**, *270*, 484-487.

176. Lockhart, D. J.; Dong, H.; Byrne, M. C.; Follettie, M. T.; Gallo, M. V.; Chee, M. S.; Mittmann, M.; Wang, C.; Kobayashi, M.; Norton, H.; Brown, E. L. *Nature Biotechnology* **1996**, *14*, 1675-1680.

177. Schena, M.; Shalon, D.; Davis, R. W.; Brown, P. O. *Science* **1995**, *270*, 467-470.

178. Drake, T. J.; Zhao, X. J.; Tan, W. *Nanobiotechnology* **2004**, 444-457.

179. Eberwine, J.; Belt, B.; Kacharmina, J. E.; Miyashiro, K. *Neurochemical Research* **2002**, *27*, 1065-1077.

180. Eberwine, J. H.; Spencer, C.; Newell, D.; Hoffman, A. R. *Microscopy Research and Technique* **1993**, *25*, 19-28.

181. Spencer, C. M.; Eberwine, J. *DNA and Cell Biology* **1999**, *18*, 39-49.

182. Dirks, R. W.; Molenaar, C.; Tanke, H. J. *Histochemistry and Cell Biology* **2001**, *115*, 3-11.

183. Drake, T.J.; Medley, C.D.; Rogers R.J.; Tan W. *ChemBioChem* **2005**, *6*, 2041-2047.

184. Perlette, J.; Tan,W. *Anal.Chem.* **2001**, *73*, 5544-5550.

185. Bratu,D.P.; Cha,B.J.; Mhlanga,M.M.; Kramer,F.R.; Tyagi,S. *Proc. Natl. Acad. Sci. U.S.A.* **2003**, *100*, 13308-13313.

186. Santangelo, P.J.; Nix, B.; Tsourkas, A.; Bao, G. *Nucleic Acids Res.* **2004**, *32* (6), e57/1-e57/9.

187. Tsourkas, A.; Behlke, M.A.; Bao, G. *Nucleic Acids Res.* **2002**, *30* (23), 5168-5174.

188. Ono, T.; Scalf, M.; Smith, L.M. *Nucleic Acids Res*. **1997**, *25* (22), 4581-4588.

189. Ortiz, E.; Estrada, G.; Lizardi, P.M. *Mol. Cell. Probes*, **1998**, *12* (4), 219-26.

190. Braasch, D. A.; Corey, D. R. *Chem. Biol.* **2001**, *8*, 1.

191. Wang, L.; Yang, C.J.; Medley, C.D.; Benner, S.A.; Tan, W. *J. Am. Chem. Soc.* **2005**, *127* (45), 15664-15665.

192. Dubertret, B.; Calame, M.; Libchaber, A.J. *Nature Biotechnology* **2001**, *19* (4), 365-370.

193. Maxwell, D.J.; Taylor, J.R.; Nie, S. *J. Am. Chem. Soc.* **2002**, *124* (32), 9606-9612.

194. Yang, C.J.; Lin, H.; Tan, W. *J. Am. Chem. Soc.* **2005**, *127* (37), 12772-12773.

195. Yang, C.J.; Pinto, M.; Schanze, K.; Tan, W. *Angew.Chemie Int. Ed.* **2005**, *44* (17), 2572-2576.

196. Kim, J.H.; Morikis, D.; Ozkan, M. *Sensors and Actuators, B: Chemical* **2004**, *B102* (2), 315-319.

197. Tomita, N.; Morishita, R.; Kaneda, Y.; Higaki, J.; Ogihara, T. *Drug News Perspect.* **2000**, *13*, 206.

198. Gryaznov, S.M.; Banait, N.S. *Expert Opin. Ther. Pat.* **2002**, *12*, 543.

199. Hayakawa, Y. *Bull. Chem. Soc. Jpn.*, **2001**, *74*, 1547.

200. Verma, S.; Eckstein, F. *Annu. Rev. Biochem.*, **1998**, *67*, 99.

201. Stanciu, L.A.; Shute, J.; Holgate, S.T.; Djukanovic, R. *J. Immun. Methods* **1996**, *189*, 107-115.

202. Benez, A.; Geiselhart, A.; Handgretinger, R.; Schiebel, U.; Fierlbeck, G. J. *Clin. Lab. Analysis* **1999**, *13*, 229-233.

203. Sandrock, M. L.; Foss, C. A., Jr. *J. Phys. Chem. B* **1999**, *103*, 11398-11406.

204. Storhoff, J. J.; Lazarides, A. A.; Mucic, R. C.; Mirkin, C. A.; Letsinger, R. L.; Schatz, G. C. *J. Am. Chem. Soc.* **2000**, *122*, 4640-4650.

205. Park, S.-J.; Lazarides, A. A.; Mirkin, C. A.; Letsinger, R. L. *Angew. Chem. Int. Ed.* **2001**, *40*, 2909-2912.

206. Norsten, T. B.; Frankamp, B. L.; Rotello, V. M. *Nano Lett.* **2002**, *2*, 1345-1348.

207. Jain, P.K.; Lee, K.S.; El-Sayed, I.H.; El-Sayed, M.A. *J. Phys. Chem. B* **2006**, *110*, 7238-7248.

208. Tyagi, S.; Kramer, F.R.. *Nature Biotechnology* **1996**, *14* (3), 303.

209. Tan, W., K. Wang and T. Drake. *Current Opinion in Chemical Biology* **2004**, *8* (5), 547-553.

210. Piatek, A.S.; Tyagi, S.; Pol, S.C.; Telenti, A.;Miller, L.P.; Kramer, F.R.; Alland, D. *Nature Biotechnology* **1998**, *16*(4), 359-363.

211. Sokol, D.L.; Zhang, X.; Lu, P.; Gewirtz, A.M. *Proc. Nat. Acad. Sci.***1998**, *95* (20), 11538.

212. Marras, S. A. E.; Kramer, F. R.; Tyagi, S. *Nucl. Acids Res.* **2002**, *30*, art-e122.

213. Crockett, A. O.; Wittwer, C. T. *Analytical Biochemistry* **2001**, *290*, 89-97.

214. Seidel, C. A. M.; Schulz, A.; Sauer, M. H. M. *Journal of Physical Chemistry* **1996**, *100*, 5541-5553.

215. Tyagi, S.; Bratu, D. P.; Kramer, F. R. *Nature Biotechnology* **1998**, *16*, 49-53.

216. Dirks, R.W.; Molenaar, C.; Tanke, H.J. *Methods* **2003**, *29*, 51-57.

217. Golzio, M.; Rols, M.P.; Teissie, J. *Methods* **2004**, *33*, 126-135.

218. Nitin, N.; Santangelo, P.J.; Kim, G.; Nie, S.; Bao, G. *Nucleic Acids Res.* **2004**, *32* (6), e58/1-e58/8.

219. Santangelo, P.J.; Nitin, N.; Bao, G. *J. Biomedical Optics* **2005**, *10* (4), 044025 1-6.

220. Santangelo, P.J.; Nix, B.; Tsourkas, A.; Bao, G. *Nucleic Acids Res.* **2004**, *32* (6), e57/1- e57/9.

221. Faria, M. et al. *Nat. Biotechnol.* **2001**, *19*, 40-44.

222. Samulski, R. J.; Berns, K. I.; Tan, M.; Muzyczka, N. *Proc. Natl. Acad. Sci.* **1982**, *79*, 2077–2081.

223. Carter, B. J. *Hum. Gene Ther.* **2005**, *16*, 541–550.

224. McCarty, D. M.; Monahan, P. E.; Samulski, R. J. *Gene Ther.* **2001**, *8*, 1248–1254.

225. Wang, Z.; Ma, H.I.; Li, J.; Sun, L.; Zhang, J.; Xiao, X. *Gene Ther*. **2003**, *10*, 2105–2111.

226. McCarty, D.M.; Fu, H.; Monahan, P.E.; Toulson, C.E.; Naik, P.; Samulski, R. J. *Gene Ther.* **2003**, *10*, 2112–2118.

227. Fu, H.; Muenzer, J.; Samulski, R.J.; Breese, G.; Sifford, J.; Zeng, X.; McCarty, D.M. *Mol. Ther.* **2003**, *8*, 911–917.

228. Yang, G. S.; Schmidt, M.; Yan, Z.; Lindbloom, J. D.; Harding, T. C.; Donahue, B. A.; Engelhardt, J. F.; Kotin, R.; Davidson, B. L. *J. Virol.* **2002**, *76*, 7651–7660.

229. Xu, D.; McCarty, D.; Fernandes, A.; Fisher, M.; Samulski, R.J.; Juliano, R.L. *Mol. Ther.* **2005**, *11*, 523–530.

230. Lakowicz, J. R.; Editor. *Topics in Fluorescence Spectroscopy*; Plenum Press: New York, **1994**.

231. Perlette, J.; Tan, W. H. *Anal. Chem.* **2001**, *73*, 5544-5550.

232. Barker, S. L.; Clark, H. A.; Swallen, S. F.; Kopelman, R.; Tsang, A. W.; Swanson, J. A. *Anal. Chem.* **1999**, *71*, 1767-1772.

233. Tan, W.; Shi, Z. Y.; Smith, S.; Birnbaum, D.; Kopelman, R. *Science* **1992**, *258*, 778-781.

234. Chomczynski, P.; Sacchi, N. *Anal. Biochem.* **1987**, *162*, 156-159.

235. Visner, G.A., Dougall, W.C.; Wilson, J.M.; Burr, I.A.; Nick, H.S. *J. Biol. Chem.* **1990** *265*, 2856-2864.

236. Elowitz, M.B., Levine, A.J.; Siggia, E.D.; Swain, P.S. *Science* **2002**, *297*, 1183-1186.

237. Levsky, J.M.; Singer, R.H. *Trends in Cell Biology* **2002**, *13*, 4-6.

238. Zak, D.E., Gonye, G.E.; Schwaber, J.S.; Doyle, F.J. *Genome Research* **2003**, *13*, 2396-2405.

239. Venkataraman, S.; Jiang, X.; Weydert, C.; Zhang, Y.; Zhang, H.J.; Goswami, P.C.; Ritchie, J.M.; Oberley, L.W.; Buettner, G.R. *Oncogene* **2005**, *24*, 77-89.

240. Spellman, P.T.; Sherlock, G.; Zhang, M.Q.; Iyer, V.R.; Anders, K.; Eisen, M.B.; Brown, P.O.; Botstein, D.; Futcher, B. *Molecular Biology of the Cell* **1998**, *9*, 3273-3297.

241. Medley, C.D.; Drake, T.J.; Tomasini, J.M.; Rogers, R.J.; Tan, W. *Anal. Chem.* **2005**, *77*(15), 4713-4718.

242. Yoshida, M.; Horinouchi, S.; Beppu, T. *Bioessays* **1995,** *17*, 423–30.

243. Galeotti, T.; Wohlrab, H.; Borrello, S.; Deleo, M.E. *Biochem. Biophys. Res. Commun.* **1989,** *165*, 581-589.

244. Sun, Y. *Free Radical Biol. Med.* **1990,** *8,* 583-599.

245. Bravard, A.; Hoffschir, F.; Sabatier, L.; Ricoul, M.; Pinton, A.; Cassingena, R.; Estrade, S.; Luccioni, C.; Dutrillaux, B. *Int. J. Cancer* **1992,** *52*, 797-801.

246. Bravard, A.; Petridis, F.; Luccioni, C. *Free Radical Biology and Medicine* **1999,** *26*, 1027-1033.

247. Li, N.; Oberley, T.D.; Oberley, L.W.; Zhong, W.X. *Prostate* **1998,** *35*, 221-233.

248. Bravard A.; Sabatier L.; Hoffschir F.; Ricoul M.; Luccioni C.; Dutrillaux B. *Int. J. Cancer* **1992,** *51*, 476-480.

249. Goldman, R.; Moshonov, S.; Zor, U. *Arch. Biochem. Biophys.* **1998,** *350*,10-18.

250. Alexandratou, E.; Yova, D.; Loukas, S. *Free Radical Biol. Med.* **2005,** *39*, 1119-1127.

251. Mielnicki, L.M.; Ying A. M.; Head, K.L.; Asch, H.L.; Asch, B.B. *Exp.Cell Res.* **1999,** *249*, 161–176.

252. Li, J.; Fang, X.H.; Schuster, S. M.; Tan, W. H. *Angewandte Chemie-International Edition* **2000**, *39*, 1049.

253. Tan, W. H.; Fang, X. H.; Li, J.; Liu, X. J. *Chemistry-A European Journal* **2000**, *6*, 1107-1111.

254. Uchiyama, H.; Hirano, K.; KashiwasakeJibu, M.; Taira, K. *J. Biol. Chem.* **1996**, *271*, 380-384.

255. Fang, X. H.; Li, J. J.; Tan, W. H. *Anal. Chem.* **2000**, *72*, 3280-3285.

256. Braasch, D. A.; Corey, D. R. *Chemistry & Biology* **2001**, *8*, 1-7.

257. Tsourkas, A.; Behlke, M. A.; Bao, G. *Nucleic Acids Res.* **2002**, *30*, 5168-5174.

258. Xi, C. W.; Balberg, M.; Boppart, S. A.; Raskin, L. *Appl. Environ. Microbiol.* **2003**, *69*, 5673-5678.

259. Dueholm, K. L.; Egholm, M.; Behrens, C.; Christensen, L.; Hansen, H. F.; Vulpius, T.; Petersen, K. H.; Berg, R. H.; Nielsen, P. E.; Buchardt, O. *J. Org. Chem.* **1994**, *59*, 5767-5773.

260. Gildea, B. D.; Casey, S.; MacNeill, J.; Perry-O'Keefe; H., Sorensen, D.; Coull, J. M. *Tetrahedron Lett.* **1998**, *39*, 7255-7258.

261. Koshkin, A. A.; Rajwanshi, V. K.; Wengel, J. *Tetrahedron Lett.* **1998**, *39*, 4381-4384.

262. Koshkin, A. A.; Nielsen, P.; Meldgaard, M.; Rajwanshi, V. K.; Singh, S. K.; Wengel, J. *J. Am. Chem. Soc.* **1998**, *120*, 13252-13253.

263. Wengel, J. *Acc. Chem. Res.* **1999**, *32*, 301-310.

264. Vester, B.; Wengel, J. *Biochemistry (Mosc).* **2004**, *43*, 13233-13241.

265. Faulds, K.; Smith, E.W.; Graham, D. *Anal. Chem.* **2004**, 76, 412-417.

BIOGRAPHICAL SKETCH

Colin D. Medley was born in Toledo, OH in 1979. He completed his undergraduate carrer at the University of Tennessee in Knoxville under the research direction of S. Douglass Gilman graduating Magna Cum Laude in 2003. He continued his education at the University of Florida under Weihong Tan graduating in 2007.